Geochemistry Geophysics Geosystems G3
AN ELECTRONIC JOURNAL OF THE EARTH SCIENCES
Published by AGU and the Geochemical Society

Article
Volume 9, Number 5
15 May 2008
Q05014, doi:10.1029/2007GC001645
ISSN: 1525-2027

Plutonic foundation of a slow-spreading ridge segment: Oceanic core complex at Kane Megamullion, 23°30′N, 45°20′W

Henry J. B. Dick, Maurice A. Tivey, and Brian E. Tucholke

Department of Geology and Geophysics, Woods Hole Oceanographic Institution, Woods Hole, Massachusetts, USA (hdick@whoi.edu)

[1] We mapped the Kane megamullion, an oceanic core complex on the west flank of the Mid-Atlantic Ridge exposing the plutonic foundation of a ~50 km long, second-order ridge segment. The complex was exhumed by long-lived slip on a normal-sense detachment fault at the base of the rift valley wall from ~3.3 to 2.1 Ma (Williams, 2007). Mantle peridotites, gabbros, and diabase dikes are exposed in the detachment footwall and in outward facing high-angle normal fault scarps and slide-scar headwalls that cut through the detachment. These rocks directly constrain crustal architecture and the pattern of melt flow from the mantle to and within the lower crust. In addition, the volcanic carapace that originally overlay the complex is preserved intact on the conjugate African plate, so the complete internal and external architecture of the paleoridge segment can be studied. Seafloor spreading during formation of the core complex was highly asymmetric, and crustal accretion occurred largely in the footwall of the detachment fault exposing the core complex. Because additions to the footwall, both magmatic and amagmatic, are nonconservative, oceanic detachment faults are plutonic growth faults. A local volcano and fissure eruptions partially cover the northwestern quarter of the complex. This volcanism is associated with outward facing normal faults and possible, intersecting transform-parallel faults that formed during exhumation of the megamullion, suggesting the volcanics erupted off-axis. We find a zone of late-stage vertical melt transport through the mantle to the crust in the southern part of the segment marked by a ~10 km wide zone of dunites that likely fed a large gabbro and troctolite intrusion intercalated with dikes. This zone correlates with the midpoint of a lineated axial volcanic high of the same age on the conjugate African plate. In the central region of the segment, however, primitive gabbro is rare, massive depleted peridotite tectonites abundant, and dunites nearly absent, which indicate that little melt crossed the crust-mantle boundary there. Greenschist facies diabase and pillow basalt hanging wall debris are scattered over the detachment surface. The diabase indicates lateral melt transport in dikes that fed the volcanic carapace away from the magmatic centers. At the northern edge of the complex (southern wall of the Kane transform) is a second magmatic center marked by olivine gabbro and minor troctolite intruded into mantle peridotite tectonite. This center varied substantially in size with time, consistent with waxing and waning volcanism near the transform as is also inferred from volcanic abyssal-hill relief on the conjugate African plate. Our results indicate that melt flow from the mantle focuses to local magmatic centers and creates plutonic complexes within the ridge segment whose position varies in space and time rather than fixed at a single central point. Distal to and between these complexes there may not be continuous gabbroic crust, but only a thin carapace of pillow lavas overlying dike complexes laterally fed from the magmatic centers. This is consistent with plate-driven flow that engenders local, stochastically distributed transient instabilities at depth in the partially molten mantle that fed the magmatic centers. Fixed boundaries, such as large-offset fracture zones, or relatively short segment lengths, however, may help to focus episodes of repeated melt extraction in the same location. While no previous model for ocean crust is like that inferred here, our observations do not invalidate them but rather extend the known diversity of ridge architecture.

Components: 25,949 words, 16 figures, 4 tables.

Keywords: mid-ocean ridge processes.

Index Terms: 3035 Marine Geology and Geophysics: Midocean ridge processes; 3075 Marine Geology and Geophysics: Submarine tectonics and volcanism; 3039 Marine Geology and Geophysics: Oceanic transform and fracture zone processes.

Received 26 March 2007; **Revised** 12 February 2008; **Accepted** 14 February 2008; **Published** 15 May 2008.

Dick, H. J. B., M. A. Tivey, and B. E. Tucholke (2008), Plutonic foundation of a slow-spreading ridge segment: Oceanic core complex at Kane Megamullion, 23°30′N, 45°20′W, *Geochem. Geophys. Geosyst.*, *9*, Q05014, doi:10.1029/2007GC001645.

1. Introduction

[2] Creation and destruction of ocean crust is the major dynamic process affecting the Earth's surface, and the associated exchanges of heat, mass, and volatiles are central to understanding the global geochemical cycle. The basic unit of accretion at ocean ridges is the second-order magmatic ridge segment, which reflects inherent patterns of mantle flow, melting, and melt delivery, and their interplay with brittle and plastic deformation at the plate boundary. While first-order segmentation is defined by the spacing of large offset fracture zones, second-order segments are defined by smaller offsets that range from <10 to ~30 km and vary in age offset from 0.5 to approximately 2.0 ma [*Grindlay et al.*, 1991] and appear to persist for many millions of years with characteristic length scales that vary with spreading rate [e.g., *Whitehead et al.*, 1984]. Thus a specific knowledge of how crustal thickness and architecture vary across the ocean basins at the segment scale is essential.

[3] While the external character of magmatic ridge segments is well characterized, their internal architecture, particularly that of the lower crust, is known largely by analogy to ophiolites and from seismic imaging. Although ophiolites, fossil ocean crust emplaced on land, have long been used to investigate the internal architecture of the ocean crust, most are believed to have originated in young rifts and backarc or forearc environments, limiting their usefulness as analogs for crust at mature ocean ridges. In addition, there has been little success in using seismic methods to identify variations in the internal architecture of the crust, and correlations of lithologic boundaries with seismic reflection and velocity boundaries are controversial [*Christeson et al.*, 2007; *Detrick et al.*, 1993a; *Muller et al.*, 1997]. There is now an emerging consensus that the ocean crust is heterogeneous within and between individual segments, with a structure that varies with spreading rate, ridge geometry, and proximity to transforms and mantle hot spots [e.g., *Dick et al.*, 2006]. This then requires a more detailed examination of the ocean crust across the spectrum of ridge environments.

[4] In the 1970s and 1980s the Penrose ophiolite model, a simple layer cake structure of pillow lavas, sheeted dikes, and gabbro overlying mantle peridotite tectonite, was widely accepted [*Conference Participants*, 1973]. Important observations supported this model. First and foremost, seismic refraction showed nearly uniform 6 to 7 km thick crust in the oceans [e.g., *Purdy and Ewing*, 1986; *White et al.*, 1992] with a low-velocity sediment layer underlain by seismic layers 2a, 2b, and 3 and ending at the Mohorovicic discontinuity (Moho), which was interpreted as the crust-mantle boundary. Seismic velocities of these layers are consistent with basalt, diabase, and gabbro, respectively. All these lithologies are abundant at oceanic transform faults and are found in sequence in the layered stratigraphy of large "intact" ophiolite complexes such as the Bay of Islands, Oman, and Troodos.

[5] Although the Penrose model is generally viewed as applicable to fast spreading crust, this is no longer the case for slow- and ultraslow-spreading ridges. Gabbro, equivalent to seismic layer 3, is often rare or missing in deep crustal sections exposed on the walls of transform valleys at the latter. At the same time peridotite residues of high degrees of mantle melting are abundant at transforms, but the associated basalts are too differentiated to represent primary mantle melts. Moreover, dunite, produced by focused melt flow through the mantle, is scarce near transforms. For example, dunite constitutes only 2.3% of 5002 kg of peridotites described from 72 dredges from 17 Atlantic and Indian Ocean fracture zones [*Dick*, 1989]. Thus, there is little evidence for melt transport directly to the crust from the mantle near transforms, and the gabbroic cumulates that precipitated to form the differentiated basalts from mantle melts that

could represent seismic layer 3 are missing. Seismic refraction studies [*Cormier and Detrick*, 1984; *Detrick et al.*, 1982, 1993b; *Purdy and Detrick*, 1986; *Purdy and Ewing*, 1986; *White et al.*, 1984] and observations of negative residual mantle Bouguer (RMBA) gravity anomalies centered in ridge segments [*Kuo and Forsyth*, 1988; *Lin and Phipps Morgan*, 1992; *Tolstoy et al.*, 1993] indicate thicker crust toward the midpoints of slow-spreading ridge segments. All the above observations have led to a modified Penrose model where melt and/or mantle flow are focused toward the midpoints of magmatic ridge segments, and then the melt is intruded along-axis to form the crust. This effectively creates ribbons of thick and thin crust in the spreading direction at slow-spreading ridges [*Dick*, 1989; *Whitehead et al.*, 1984].

[6] Cannat and coworkers [*Cannat*, 1993a, 1996; *Cannat et al.*, 1997b], however, proposed that slow-spread lower ocean crust might consist of local gabbro plugs intruded between partially serpentinized mantle screens, with overlying dikes and a carapace of lavas. Although there are no detailed geologic studies of a large, intact section of the lower crust on the Mid-Atlantic Ridge (MAR), numerous studies of partial crustal sections at transform and rift valley walls appear to support the Cannat model [e.g., *Auzende et al.*, 1989a, 1989b, 1993, 1994; *Bonatti and Seyler*, 1987; *Cannat*, 1993, 1996; *Cannat et al.*, 1992, 1997b, 1995b; *Fox et al.*, 1976; *Karson and Dick*, 1983, 1984; *Karson and Fox*, 1986; *Karson et al.*, 1984; *Karson and Lawrence*, 1997; *Karson and Rona*, 1990; *Karson and Winters*, 1992; *Lagabrielle et al.*, 1998, 1992; *Mamaloukas-Frangoulis et al.*, 1991; *Mével et al.*, 1991; *Fox et al.*, 1985; *OTTER (Oceanographer Tectonic Research Team)*, 1984; *Stroup and Fox*, 1981]. This viewpoint is well laid out by *Lagabrielle et al.* [1998] and *Karson* [1998]. They infer that the ophiolite-based Penrose model may not be correct for large regions of slow-spreading ocean crust and further suggest that even sheeted dikes may be only intermittently developed.

[7] The above "gabbro-pudding model" is buttressed by ODP Leg 209 which drilled 19 holes at eight sites over a ~100 km N–S distance along the MAR and across the 15°20′ fracture zone (FZ) [*Shipboard Scientific Party*, 2004]. The holes were situated on low-angle fault surfaces bounding the rift valley that expose massive blocks of peridotite and gabbro, while a thin veneer of pillow basalts appears on the rift valley floor. A cumulative 1.5 km of hole was drilled, and peridotite intruded by gabbro was found at Sites 1268, 1271, 1272, and 1274, while peridotite only and gabbro only were drilled at Site 1273 and 1275, respectively. Excluding Site 1275, the proportion of gabbro (~25%) is similar to dredge results from the region, appearing to confirm the Cannat model [*Cannat*, 1993, 1996; *Cannat et al.*, 1997b; *Escartin and Cannat*, 1999].

[8] However, these apparent consistencies may be misleading as the Fifteen-Twenty FZ region is bathymetrically, geologically, and geochemically anomalous. The rift-valley walls expose largely peridotite, not basalt as in other MAR regions. Moreover, the abyssal peridotites show the highest degree of mantle melting of any yet found [*Bonatti et al.*, 1992], which suggests that significant magmatic crust should be present, yet gravity data and geologic mapping indicate that the crust is thin or absent over large regions [e.g., *Casey et al.*, 1998]. This contrasts with the general correlation of Atlantic and Indian abyssal basalt and peridotite compositions that may reflect increasing extents of mantle melting [*Dick et al.*, 1984] and increasing crustal thickness [*Klein and Langmuir*, 1987] near mantle hot spots.

[9] The geology of the Southwest Indian Ridge Atlantis Bank core complex contrasts sharply with the results in the Fifteen-Twenty FZ region and better fits the Penrose model as modified by *Whitehead et al.* [1984] and *Dick* [1989]. The bank exposes a 400-km^2 gabbro massif exhumed by a long-lived detachment fault [*Dick et al.*, 1999b]. The 1.5 km-deep ODP Hole 735B [*Dick et al.*, 2000; *Natland et al.*, 2002] and a 158 m-deep Hole 1105A [*Shipboard Scientific Party*, 1999] were drilled into massive gabbro in the center of the massif with no serpentinite screens and only two dikes in the upper 500 m.

[10] The Hole 735B gabbros are similar to evolved high-level gabbros in ophiolites, although they differ by having significantly coarser grain size and a great abundance of foliated oxide gabbro that indicates deformation in the presence of melt. The foliated oxide gabbros are most abundant in the upper 500 m and indicate that the detachment fault exposing the complex rooted in partially molten gabbro [*Dick et al.*, 1991a, 1991b, 1999b, 2000, *Natland*, 2002; *Natland and Dick*, 2001]. Numerous isolated dikes cut the gabbros across Atlantis Bank, and there are local inliers of the dike-gabbro transition with sheeted dikes at several locations [*Dick et al.*, 1999b]. This demonstrates that the fault rooted through a zone of active dike intrusion into partially molten gabbro and that an overlying

sheeted dike complex was removed in the hanging wall.

[11] At the MAR south of the Kane FZ (MARK area) at 23°N, the section sampled and observed by submersible at the eastern inside-corner high is generally used to support the gabbro-pudding model. However, in many respects this section resembles that at Atlantis Bank. MARK gabbros drilled during ODP Leg 153 include abundant coarse-grained oxide gabbro, that often show intense deformation in the presence of melt [*Agar et al.*, 1997; *Agar and Lloyd*, 1997; *Cannat et al.*, 1997a], and lack serpentine intercalations [*Cannat et al.*, 1995a]. The large number of drill holes (eight) and cumulative penetration (367.8 m) suggests a significant body of gabbro like that at Atlantis Bank. Numerous dikes intercalated with gabbro were also observed, suggesting removal of an overlying dike complex by faulting. In addition, there is a large volcanic edifice on the conjugate outside-corner high, indicating that there was robust magmatism when the inside corner high developed.

[12] All these results highlight the lithologic variability of slow-spreading crust and emphasize the need to study deep crustal architecture at the full-segment scale. Oceanic core complexes (OCCs) provide the opportunity to directly map and sample the plutonic foundation of ridge segments on ridge-parallel, large-offset detachment faults. In the present study, we explored one such exposure during Knorr Cruise 180, Leg 2 (November to December 2004) at the Kane Megamullion extending for ~80% of the length of a second-order ridge segment. It is located at 23°30′N, 45°20′W, ~30 km west of the MAR axis and just south of Kane FZ (Figure 1). Our results suggest focused melt flow from the mantle to local magmatic centers creates local plutonic complexes within the ridge segment whose position varies in space and time. Between and away from these, the crust may consist of a thin carapace of pillow lavas and dikes fed laterally from the magmatic centers. The architecture of the MAR crust at 23°N, then, appears to be a response to plate-driven flow that engenders local, stochastically distributed transient instabilities in the partially molten mantle beneath longer segments that feed individual magmatic centers.

2. Oceanic Core Complexes and Megamullions

[13] Oceanic core complexes are exposures of subvolcanic lithosphere exposed on low-angle normal faults at mid-ocean ridges [*Dick*, 1989; *Dick et al.*, 1981, 1991b; *Karson*, 1990]. While these faults typically dip 23 ± 8° where they break the seafloor [*Tucholke et al.*, 1998], their orientation at depth is unknown. Where they are exceptionally long-lived (≥1 ma), these "detachment" faults create a class of OCC termed megamullions, characterized by domed shapes resulting from footwall rollover and by well-defined flow line parallel corrugations (mullions) across their surfaces [*Tucholke et al.*, 1998]. Kane Megamullion is one of more than three dozen found on the Mid-Atlantic Ridge (MAR) [*Cann et al.*, 1997; *Casey et al.*, 1998; *Reston et al.*, 2002; *Tucholke et al.*, 1996, 1998], the Southwest and Southeast Indian Ridges [*Dick et al.*, 1999b; *Fujimoto et al.*, 1998; *Mitchell et al.*, 1998; *Searle et al.*, 1998], the Chile Ridge [*Karsten et al.*, 1999], and in the Parece Vela basin [*Ohara et al.*, 2001]. Megamullions typically have along- and across-isochron dimensions up to 20–30 km, and there are examples extending 50–125 km along flow lines [*Ohara et al.*, 2001; *Okino et al.*, 2004]. They generally form at inside-corner highs at transform and nontransform offsets and extend variable distances along the ridge axis within the spreading segment. As megamullions are exhumed, the volcanic carapace is largely carried away in the hanging wall on the conjugate plate [*Dick et al.*, 1981, 1991b; *Tucholke and Lin*, 1994].

[14] Megamullions provide a unique opportunity to study the emplacement and evolution of lower ocean crust and shallow mantle at mid-ocean ridges. It is important to keep in mind, however, that such crust has a deformation history different from that of an undisrupted section of oceanic crust. In addition, normal lithologic relations may not be fully developed in the subvolcanic section because as a megamullion is unroofed it cools more rapidly and at shallower depth than intact crust.

3. Geologic Setting

3.1. Segmentation Structure

[15] The Kane Megamullion exhibits a set of uplifted, corrugated domes beginning ~30 km west of the eastern ridge-transform intersection of the Kane FZ that extend WNW for ~23–24 km in the plate-spreading direction and for up to ~40 km SSW along isochrons (Figure 1). To the north the megamullion is bounded by the Kane transform fault, a ~150-km long, left-lateral offset of the

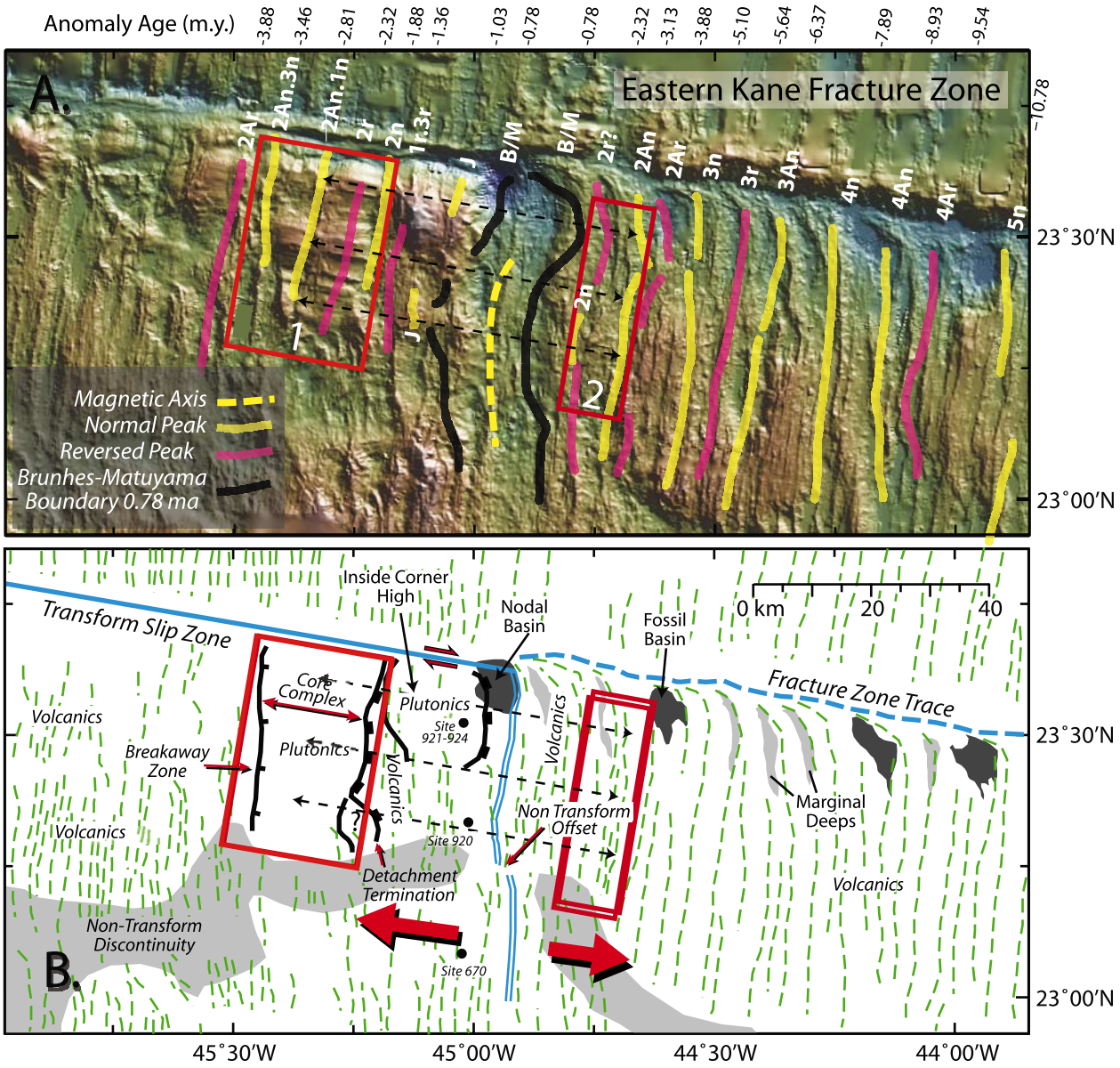

Figure 1. (a) Shaded-relief bathymetry (illuminated from the northeast) made using the online GeoMapAp 2 database at Lamont-Doherty Earth Observatory for the eastern ridge-transform intersection of the Kane FZ (MARK area). Box 1 Outlines Kane Megamullion and box 2 shows same-age conjugate crust on the African Plate. The southern dashed line connects the Adam and Eve gabbro complex on a flow line to a conjugate, paleo-axial volcanic high, while the middle and upper lines connect the Cain and Abel peridotites, and the Babel gabbro-peridotite complex, to corresponding conjugate volcanic terrains. Magnetic anomaly identifications based on the GPTS2004 timescale. (b) Tectonic map with dotted green lines tracing volcanic ridges and associated fault sets. Solid black lines indicate core complex breakaway zones and detachment fault terminations. Black dots show ODP Site 670 (serpentinites), Site 920 (serpentinites) and Sites 921–924 (gabbros and dikes) locations. Light gray shaded bands show the traces of the non-transform discontinuity at the southern end of the spreading segment enclosing Kane Megamullion, from *Cannat et al.* [1995b]. Dark shading shows present-day and older fossil nodal basins, while lighter shading shows captured marginal deeps that flanked axial highs at the ridge-transform intersection.

MAR within a ~4.5 km deep valley. The southern end of the spreading segment that encompasses the megamullion is a nontransform discontinuity ~50 km south of the fracture zone (Figure 1b). This discontinuity has marked the segment's southern limit from 10 Ma to present [*Pockalny et al.*, 1995; *Tucholke and Schouten*, 1988]. *Cannat et al.* [1995b] showed that the southern boundary mostly

correlates with elevated RMBA gravity (i.e., thin crust) and peridotite exposures, while basalts are more common in the central part of the spreading segment. They concluded that the segment consists of a single magmatic cell, underlain by a central, massive ~4 km thick gabbro body that thins rapidly at the segment ends.

3.2. Spreading History

[16] The anomalous crust consisting of mullioned domes flanking the south side of Kane FZ actually extends for about 90 km west of the present inside corner high, forming a triangular region that narrows westward and terminates at about 46°W (Figure 1a). This zone likely represents episodic exhumation of crystalline basement by a series of moderately long-lived faults that sequentially jumped toward the ridge axis, all rooting in a single long-lived shear zone beneath the rift valley over the last ~6.5 ma. This created a series of breakaway zones, one of which is at the western boundary of Kane Megamullion (Figures 1b and 2). At the latter, a relatively linear ridge up to several hundred meters high is interpreted as a breakaway where an eastward fault jump captured a block of volcanic crust from the hanging wall (rift valley floor) before the Kane Megamullion began to be exhumed. Farther east, the exhumed footwall comprising the megamullion ends in an isochron-parallel valley, and this termination sinuously follows corrugations in the detachment surface (Figure 2). On the basis of magnetic-anomaly identifications, the breakaway zone is in 3.3 Ma crust, and the detachment termination is at ~2.1 Ma, about the time of Chron 2r [*Williams*, 2007].

[17] A large block of volcanic crust, >10 km across isochrons and extending ~30–40 km south of Kane FZ, lies east of the megamullion termination. This block overlies the down-dip projection of the detachment fault (Figure 2) and exhibits hummocky topography with north–south trending ridges characteristic of lineated axial volcanic terrains. Dive KAN 9 (Figure 2) mapped the northern end of the block on the transform wall. It stepped upward from 3500 m depth across a series of steep normal faults, sampling pillow basalt, basalt, and hyaloclastite, and from 2800 m to 2000 m pillow basalt cut by N–S trending dikes [*Auzende et al.*, 1993, 1994]. SSW of this dive, ~10 km from the transform axis, there is a local high at ~23°34′N with a lineated ridge sloping down to the south at ~3° for 20 km. We believe this is a remnant of an axial volcanic center located near the transform where magmas were intruded laterally to the north and south. This block is interpreted as a hanging wall remnant stranded on the North American plate when Kane Megamullion detachment fault was abandoned. The detachment was replaced by a new fault farther to the east, creating another imbrication connecting to the long-lived shear zone beneath the rift valley.

[18] The NUVEL-1A model gives a present-day full spreading rate of 24.3 mm/a for the MAR in this area [*DeMets et al.*, 1990]. Over the past 10 ma, however, the MAR south of the fracture zone has been spreading at an average of 14.4 mm/a to the west and 9 mm/a to the east [*Williams*, 2007]. This asymmetry incorporates recent eastward ridge jumps [*Schulz et al.*, 1988; *Williams*, 2007] and resulted in a compressed magnetic polarity sequence on the eastern side of the MAR relative to the western flank. During formation of the Kane Megamullion between chrons 2 and 2A, spreading was even more asymmetric: ~17.9 mm/a to the west and 7.6 mm/a to the east. Chron 2An appears as a single peak on the eastern flank rather than as the usual double-peaked anomaly that is present on the western flank. In younger crust, anomaly 1r.3r is entirely absent on the eastern flank but is present on the west flank. These asymmetries are best explained by eastward fault jumps that captured large blocks of the rift-valley floor and isolated them on the North American plate (cf. Figures 1 and 2). At the time of anomaly 1r.3r, such jumps resulted in a 100% instantaneous local spreading asymmetry.

3.3. The 23°N MAR Rift Valley and Conjugate Crust (MARK Area)

[19] The MAR at 23°N is a typical slow-spreading rift valley with a lineated axial volcanic ridge and

Figure 2. Shaded-relief bathymetric map (illuminated from the southeast) and simplified tectonic interpretation of Kane Megamullion based on SeaBeam bathymetry from Knorr Cruise 180–2. Contour interval is 100 m. Larger pie diagrams show lithologic proportions by weight in dredge and dive collections from the Knorr and Kanaut expeditions; smaller pie diagrams indicate lithologies reported in the literature where proportions are not available (unpublished data from *Ghose* [1997]). Tracks of Jason II dives 110–117 and Nautile dives KAN 9 to 17 are shown in red, as are dredge locations. Small colored circles show lithology at Nautile sample locations. Dredge, Jason, and Nautile dive numbers are labeled. Shaded regions indicate areas of possible off-axis volcanism. Thin black lines show the positions of the cross sections in Figure 13 (which extend beyond the limits of this figure).

numerous small volcanic cones. Abundant plutonic rocks are described from the western rift valley wall [*Auzende et al.*, 1994; *Dick et al.*, 1981; *Karson and Dick*, 1983; *Karson and Winters*, 1992]. Massive gabbro and diabase exposed by normal faults were mapped and drilled at ODP Sites 921 to 924 ~2–3 km apart on the inside-corner high (Figure 1b). The cores [*Karson et al.*,

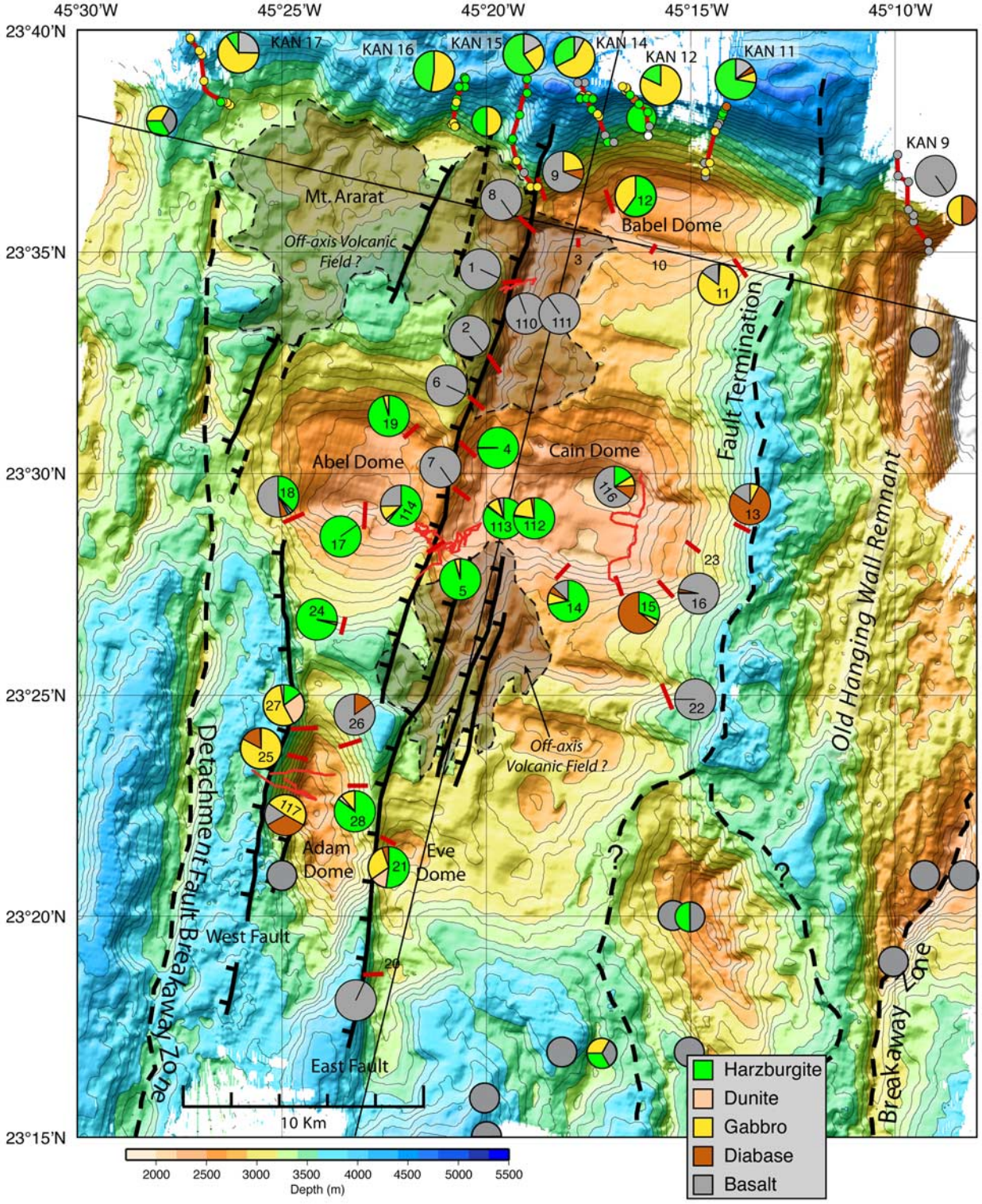

Figure 2

1997] have the petrologic and structural aspects of the Atlantis Bank gabbros, supporting the past presence of a magmatic complex near the transform.

[20] Near the base of the northeast corner of the inside-corner high, submersible Dive KAN 4 sampled highly sheared serpentinite at 3981 m, and Dive KAN 5 sampled less deformed serpentinite ~4 km upslope to the southwest at 2795 and 2779 m [*Auzende et al.*, 1993]. The serpentinites are associated with amphibolitized gabbro mylonites, greenschist facies undeformed and deformed diabase dikes, and weathered basalts. It is unclear whether the serpentinites are autochthonous or if they were emplaced by intrusion along a shear zone from some distance away (see section 7.3). The KAN 4 and 5 dive results appear to be anomalous in that diabase and pillow lavas were sampled lower on the wall than gabbro, an inversion of the expected lithologic sequence. A simplifying interpretation, however, is that the pillow basalts and possibly the diabase are hanging wall debris left on the gabbroic footwall as it was exposed by faulting (see also sections 6.1 and 6.2).

[21] At ODP Site 920, 22 km south of Site 921, serpentinized peridotite was drilled on the western rift valley wall to a depth of 201 m below seafloor (mbsf) (Figure 1) [*Cannat et al.*, 1995a]. This is close to the nontransform offset at the southern end of the spreading segment, so the crust is expected to be thin. Nineteen kilometers farther south, near the northern end of the adjacent spreading segment, serpentinites were again drilled on the rift-valley wall to a depth of 90 mbsf at Site 670 [*Cannat et al.*, 1995a].

[22] The present neovolcanic zone near Kane FZ is subdued compared to the robust volcanic tracts associated with former neovolcanic zones that are now captured in the abyssal hills on the African plate to the east (Figure 1). Near the transform the neovolcanic zone is a long, low linear ridge that slopes ~1.3° from ~3700 m at 23°23′N to ~5000 m at 23°35′N where it terminates on the eastern wall of the nodal deep. The low relief gives the impression that volcanism near the transform has been rather anemic and is fed along fissures from a magmatic center beneath the present axial high ~20 km to the south. In contrast, the eastern rift valley wall contains a prominent, uplifted volcanic ridge that parallels the present axial high; this ridge slopes only ~0.5° over the same distance, deepening just ~550 m from ~3200 m at the segment center down to its northern end. There it curves around the eastern edge of the nodal basin into the paleotransform trace, forming a prominent hooked ridge abutting the northern transform wall [*Karson and Dick*, 1983]. Formation of the hooked ridge was in part synchronous with the formation of the gabbro and diabase exposed at the inside-corner high and again indicates robust volcanism near the transform at the time.

[23] Hooked ridges are a repeated feature east of the ridge-transform intersection [*Karson and Dick*, 1983; *Tucholke and Schouten*, 1988], and often rise independently of old axial volcanic ridges farther south (Figures 1a and 1b). This implies that they emanated from separate magmatic centers in the rift valley close to the transform. Along the south wall of the fracture-zone valley there are a series of elongate marginal deeps formed between old axial volcanic ridges and rift valley walls, whose morphology was accentuated by back tilting as the crust was uplifted into the rift mountains (Figure 1b). There are also three prominent deeps that appear to be fossil nodal basins, located at 44°36′W, 44°12′W, and 43°58′W. These suggest significant magma deficits and thus periods of reduced volcanism, similar to that observed in the modern nodal basin. Elevated topography along the same isochrons to the south, however, indicates robust coeval volcanism, which again implies that separate magmatic centers were active along the MAR axis within the confines of this second-order ridge segment. The overall patterns of elevated ridges and depressed basins suggest a roughly 2–3 ma cycle of waxing and waning volcanism near the transform, similar to the period of magmatic cycles suggested elsewhere along the MAR by RMBA gravity variations [*Tucholke and Lin*, 1994].

3.4. Geophysical and Morphological Characteristics of Kane Megamullion

[24] Although Kane Megamullion heretofore has not been the subject of a focused study, it was well surveyed with surface-ship multibeam bathymetry, gravity, and magnetics [*Fujimoto et al.*, 1996; *Gente et al.*, 1995; *Maia and Gente*, 1998; *Morris and Detrick*, 1991; *Pockalny et al.*, 1988, 1995; *Schulz et al.*, 1988]. RMBA gravity anomalies are elevated over the megamullion compared to the fossil hanging wall to the east; suggesting densities greater than in a normal crustal section. The highest gravity values are over the older half of the megamullion (see also section 7.7). Magnetic anomalies C2r and C2An are well developed across the main part of the OCC (Figure 1).

[25] In a north–south direction, Kane Megamullion consists of three main domes, each with WNW–ESE oriented corrugations with amplitudes of up to ~400 m (Figures 1 and 2). The latter are interpreted as mullions, and they clearly delineate the exposed surface of the detachment fault. The detachment surface dips up to ~25° east near the fault termination, but up to 10° west close to the breakaway, presumably reflecting rollover of the footwall. The three main domes are cut by two major west-facing, high-angle normal faults (West and East Faults) that likely formed in response to footwall bending during exhumation [e.g., *Manning and Bartley*, 1994; *Tucholke et al.*, 1998]. Mullions are not well developed between the interpreted breakaway and West Fault (Figure 2), possibly because of extensive, fine-scale faulting and mass wasting in the brittle upper lithosphere first exhumed by the detachment [*Tucholke et al.*, 2001] and because disjointed hanging wall fragments may be stranded on the footwall near the breakaway zone.

[26] The main northern dome (Babel) extends ~12 km along a flow line adjacent to Kane FZ and is bounded to the west by East Fault, a steep outward facing, isochron-parallel fault scarp ~400 m high (Figure 2). Babel Dome features prominent corrugations that include a ~200 m deep trough down its axis and two adjacent ridges. Farther west, mullion structures are difficult to detect, and hummocky topography suggests that a volcanic carapace covers the area (Mt. Ararat). Just north of Mt. Ararat, major slide scars heavily dissect the transform wall and obscure the presumed original detachment fault.

[27] In the center of Kane Megamullion, a large domed region extends ~23–24 km along flow lines. The southward extension of East Fault separates it into two smaller domes Cain and Abel. These have mullion structures that continue across the fault despite an intervening ~150 m deep trough.

[28] Near the southern end of the megamullion, an elevated area exhibits several small domes and extends ~15 km along flow lines. In this area, Adam and Eve domes are separated by a southward apparently en-echelon extension of East Fault. Adam Dome is uplifted ~700 m on West Fault and is back-tilted 18° to the east. West Fault, or an en-echelon extension of the fault, may continue north to cut the southwestern edge of Abel Dome, although the offset there is minor. Both West and East Faults exhibit slide scars where large (100 s of meters) sections of the high-angle fault surfaces have failed. The slide-scar headwalls provide excellent windows into the detachment footwall, thus avoiding potential complications that are inherent in interpreting rocks from the fault surfaces themselves.

[29] The northern wall of Kane Megamullion (southern wall of Kane transform) was studied by submersible below Babel Dome and Mt. Ararat [*Auzende et al.*, 1994; *Ghose et al.*, 1996] and by a deep-tow side scan survey that extended 40 km west of the ridge-transform intersection [*Gao et al.*, 1998; *Karson et al.*, 1992]. As discussed later, this wall is an extension of the detachment fault surface, and it probably connects directly to the transform fault within the transform valley.

4. Sampling and Analysis: Knorr Cruise 180–2

[30] We extensively sampled Kane Megamullion using the remotely operated vehicle (ROV) Jason II and dredges (Figure 2; Tables 1–4). In several locations, Jason II dives were preceded by high-resolution (1–2 m contours), near-bottom SM2000 multibeam bathymetric surveys using the autonomous vehicle ABE. ROV and dredge samples were collected from the detachment fault surface and from the intersecting scarps and slide-scar headwalls along East and West faults. East and West faults are among the largest high-angle offsets of a detachment surface known at any oceanic core complex, and they provide a unique opportunity to access the interior of the core complex beneath the detachment footwall at numerous locations along the length of the spreading segment and far from a transform fault. The Jason II dives focused on traversing these scarps where they cut Babel Dome (Dives 110, 111), Cain Dome (Dives 112, 113) and Adam Dome (Dive 117). Jason II Dive 116 crossed over the detachment fault surface at Cain Dome, and Dive 114 investigated the headwall of a large slide scar in the detachment surface on Abel Dome.

[31] We recovered 1207 kg of rock with Jason II and 1459 kg of rock in 25 dredges (Figure 2). We described 756 dredge samples and 386 Jason II samples during the cruise, following procedures used on ODP Leg 176 [*Dick et al.*, 1999a]. Rock names follow IUGS nomenclature, with modifiers that are useful for abyssal assemblages. Using semiquantitative scales, we recorded the nature and extent of alteration of each mineral, the brittle

Table 1. Knorr Cruise 180, Leg 2 Dredges[a]

Dredge	Contents	Wt. (kg)	Number of Pieces Logged	Location	Pinger Over			On Bottom			Off Bottom				
					Deg. N	Deg. W	Ship Depth	Ship Depth	Wire Out	MAPR Depth	Deg. N	Deg. W	Ship Depth	Wire Out	MAPR Depth
1	17.4 kg pillow basalt, 1.6 kg basalt	19.0	12	Ridge on East Fault between Babel and Cain Domes	23.572	45.328	2997	2985	3105	N/A	23.573	45.320	2443	2498	N/A
2	8.3 kg pillow basalt +0.4 kg in bags	8.7	21	Ridge on East Fault, northern edge of Cain Dome	23.545	45.333	3065	2973	3083	2978	23.538	45.328	2415	2550	2495
3	Empty	0.0	0	South of ridge on Babel Dome	23.585	45.297	2585	2593	2670	2528	23.589	45.297	2480	N/A	2427
4	37 kg peridotite, 0.1 kg dunite	38.8	3	East Fault, northern edge of Cain Dome	23.513	45.345	2601	2780	2820	2716	23.507	45.338	2374	2574	2488
5	64.2 kg peridotite, 3 kg gabbro, 0.1 kg carbonate with basalt shards	67.3	31	East Fault, southern edge of Cain Dome	23.471	45.358	2827	2751	2870	2763	23.475	45.351	2467	2582	2506
6	1.85 kg haloclastite & pillow basalt, 15.4 kg basalt, 2.4 kg carbonates	19.7	7	Ridge on East Fault, at northern edge of Cain Dome	23.530	45.341	3016	3027	3108	2989	23.525	45.335	2612	N/A	2594
7	23.2 kg pillow basalt, 0.4 kg carbonate clasts	23.6	6	East Fault, central Cain Dome	23.495	45.347	2637	2620	2725	2609	23.491	45.341	2350	N/A	2299
8	59.0 kg pillow basalt & hyaloclastite breccia, 32.6 kg basalt, 0.3 kg coral	91.9	31	Northern end of ridge at East Fault	23.597	45.321	2902	2850	2925	2798	23.591	45.314	2330	2375	2297
9	16.5 kg gabbro, 22.5 kg basalt & basalt breccia, 27.0 kg pillow basalt & pillow basalt breccia, 5.2 kg polymict breccia, 6.2 kg diabase	77.4	39	Slide scar headwall, northwest corner Babel Dome	23.612	45.313	3380	3328	3458	N/A	23.603	45.310	2789	2820	N/A
10	Empty	0.0	0	South flank of Babel Dome	23.583	45.267	2630	2630	2723	N/A	23.587	45.265	2481	2460	N/A
11	57.7 kg gabbro, 10.1 kg pillow basalt & palagonite breccia, 0.7 kg soapstone & peridotite, 2.8 kg gravel & mudstone	71.8	7	South flank Babel Dome near footwall termination	23.574	45.228	3142	3150	3224	3105	23.581	45.233	2775	2740	2664
12	3.9 kg harzburgite & soapstone, 2.6 kg gabbro, & a few bits of coral	6.5	16	Northwest slope of Babel Dome	23.607	45.286	2659	2660	2714	2615	23.598	45.282	2498	2715	2282

Table 1. (continued)

Dredge	Contents	Wt. (kg)	Number of Pieces Logged	Location	Pinger Over			On Bottom			Off Bottom				
					Deg. N	Deg. W	Ship Depth	Ship Depth	Wire Out	MAPR Depth	Deg. N	Deg. W	Ship Depth	Wire Out	MAPR Depth
13	19.1 kg diabase, 1.9 kg gabbro, 2 kg pillow basalt & 1.9 kg basalt, 8 kg polymict cataclastic breccia, 0.1 kg lithified chalky ooze, 1.6 kg pebbles	37.3	56	Near core complex termination, east slope of Cain Dome	23.479	45.227	3586	3552	3652	N/A	23.482	45.233	3201	3200	N/A
14	99.4 kg harzburgite, 13.4 kg gabbro, 16.4 kg pillow basalt, 1.7 kg basalt, 7.2 kg diabase, 0.3 polymict breccia, 9.8 kg gravel	148.2	71	South slope of Cain Dome	23.461	45.306	2568	2574	2640	2543	23.467	45.300	2182	2245	2453
15	13.2 kg harzburgite, 28 kg diabase, 1.9 kg gabbro, 1.4 kg carbonate.	44.5	41	South slope of Cain Dome	23.455	45.279	2678	2650	2742	2635	23.462	45.282	2315	2364	2284
16	7.9 kg pillow basalt, 0.2 kg basalt, 0.2 kg diabase, 0.1 kg soapstone, 3.2 kg Fe-Mg crusts, 12.6 kg oolitic chalk, 0.1 kg coal slag.	24.3	28	South slope of Cain Dome	23.454	45.258	2910	2891	2980	2865	23.460	45.264	2578	2657	2569
17	33 kg harzburgite, 0.3 kg coral, 1.4 kg assorted pebbles.	35.0	18	Slide-scar headwall, south slope of Abel Dome	23.480	45.384	2496	N/A	2535	2438	23.490	45.383	2293	2290	2128
18	26.7 kg pillow basalt, 7.1 kg basalt, 4 kg diabase, 1.5 kg gabbro, 1.5 kg dunite, 24.4 kg harzburgite, 6 kg pebbles.	70.6	42	Southwest corner of Abel Dome	23.482	45.417	2980	2950	3055	2957	23.486	45.408	2540	2622	2538
19	1.6 kg gabbro, 34.9 kg harzburgite, 2.2 kg marlstone, 4.6 kg carbonates, 14.8 kg pebbles	58.1	49	North slope of Abel Dome	23.519	45.362	2730	2731	2786	N/A	23.514	45.368	2490	2590	N/A
20	34 kg pillow basalt, 97.8 kg basalt.	131.8	40	Southern end of East Fault	23.312	45.384	3650	3650	3760	N/A	23.313	45.376	3207	3362	N/A
21	0.1 kg basalt, 1.8 kg diabase, 10.5 kg gabbro, 4.7 kg dunite, 18.6 kg harzburgite, 0.7 kg Marlstone, 7 kg pebbles.	43.4	32	East Fault at Eve Dome	23.364	45.377	3105	3127	3195	N/A	23.361	45.371	2815	2880	N/A

Table 1. (continued)

Dredge	Contents	Wt. (kg)	Number of Pieces Logged	Location	Pinger Over			On Bottom			Off Bottom				
					Deg. N	Deg. W	Ship Depth	Ship Depth	Wire Out	MAPR Depth	Deg. N	Deg. W	Ship Depth	Wire Out	MAPR Depth
22	46 kg basalt	46.0	2	South slope of mullion structure south of Cain Dome	23.412	45.258	3394	3394	3499	N/A	23.422	45.263	2980	3019	N/A
23	Empty	0.0	0	East slope of Cain Dome	23.471	45.247	2960	2948	3015	2884	23.475	45.253	2655	2696	3640
24	2.7 kg peridotite, 0.05 kg metagabbro	2.7	12	Southern foot of Abel Dome	23.440	45.393	3451	3445	3500	3379	23.447	45.391	3175	3221	3130
25	0.15 pillow basalt, 0.1 kg basalt, 4.9 kg diabase, 24.9 kg gabbro,	30.2	30	West fault, Adam Dome	23.395	45.415	3405	3460	3497	3363	23.393	45.407	2780	2783	2706
26	10.3 kg pillow basalt, 30.5 kg basalt, 7.3 kg diabase, 10.3 kg gravel.	56.6	20	East slope, Adam Dome	23.401	45.385	3398	3410	3465	3303	23.398	45.394	2940	3010	2917
27	2.5 kg pillow basalt, 0.5 kg basalt, 64.8 kg gabbro, 31.6 dunite, 17.7 kg harzburgite, 136.7 kg gravel.	253.8	103	West Fault, northern end of Adam Dome	23.405	45.414	3540	3540	3608	3462	23.405	45.403	2966	2990	2909
28	3.3 kg gabbro, 1 kg dunite, 24.7 kg harzburgite & lherzolite, 5.5 kg marlstone, 17 kg pebbles.	51.5	39	East slope, Adam Dome	23.383	45.382	3275	3293	3346	3192	23.383	45.390	2827	2806	2727
	Total	1459	756												

[a] MAPR depth refers to the depth determined by the pressure sensor on the Miniature Autonomous Particulate Recorder (MAPR) plus 151 m as the MAPR was usually placed on the wire 151 m above the dredge (1 m above the pinger). Dredge navigation came from the Knorr GPS and Seabeam center beam records. Water depths and positions were checked against the watchkeepers notes, where the times for pinger over (best estimate of start position on-bottom) and for dredge off-bottom were logged. Small discrepancies in position and depth between the two sets of records were ignored, although the depths recorded by the watch were generally used. If the Seabeam system was off, the ship's position as recorded by the watchstander or in the ship's records was used. As water depths below the ship were not recorded in theses instances, ship depths were obtained by plotting dredge positions on the Seabeam map.

Table 2. Knorr Cruise 180, Leg 2, Rock Sample Summary[a]

Dredge/Dive	Total Dredge Weight (kg)	Number of Samples Logged	Weight of Samples Logged	Peridotite	Dunite	Gabbro	Diabase	Basalt	Polymict Breccia	Hydrothermal	Sediment
1	19.0	12	19.0	0.0	0.0	0.0	0.0	19.0			
2	8.7	21	8.3					8.3			
3	0.0	0	0.0								
4	38.8	3	38.6	36.7	0.1						1.8
5	67.3	31	67.3	64.2		3.0					0.1
6	19.7	7	19.7					17.3			2.4
7	23.6	6	23.6					23.2			0.4
8	91.9	31	91.9					91.6			0.3
9	77.4	39	77.4			16.5	6.2	49.5	5.2		
10	0.0	0	0.0								
11	71.8	7	71.3	0.7		57.7		10.1			2.8
12	6.5	16	6.5	3.9		2.6					
13	37.3	56	33.0			1.9	19.1	3.9		8.0	0.1
14	148.2	71	138.4	99.4		13.4	7.2	18.1	0.3		
15	44.5	41	44.5	13.2		1.9	28.0				1.4
16	24.3	28	24.2	0.1			0.2	8.1		3.2	12.6
17	35.0	18	33.3	33.0							0.3
18	70.6	42	64.7	24.4	1.0	1.5	4.0	33.8			
19	58.1	49	43.3	34.9		1.6					6.8
20	131.8	40	131.8					131.8			
21	43.4	32	36.4	18.6	4.7	10.5	1.8	0.1			0.7
22	46.0	2	46.0					46.0			
23	0.0	0	0.0								
24	2.7	12	2.8	2.7		0.1					
25	30.2	30	30.1			24.9	4.9	0.3			
26	56.6	20	46.3				7.3	39.0			
27	253.8	103	117.1	17.7	31.6	64.8		3.0			
28	51.5	39	34.5	24.7	1.0	3.3					5.5
Total	1459	756	1249.8	374.2	38.4	203.7	78.7	503.0	5.5	11.2	35.2
Jas 110	26.8	8	26.8					26.8			
Jas 111	80.9	21	80.9					80.7			0.2
Jas 112	405.9	119	406.0	308.9	3.6	34.9	3.0	13.5		14.4	27.65
Jas 113	217	73	216.9	165.8	1.8	42.9	5.5				0.9
Jas 114	214.4	24	214.4	130.0	4.6	24.4		53.8		0.2	1.4
Jas 116	103.6	52	103.6	15.4		7.6	10.6	62.7	7.3		
Jas 117	158.4	89	158.4			75.0	52.7	27.6			3.1
Total	1207	386	1207.0	620.1	10.0	184.8	71.8	265.1	7.3	14.6	33.3
Grand Total	2666	1142	2456.8	994.3	48.4	388.5	150.5	768.1	12.8	25.8	68.5

[a] Notes: Values in fourth column are weights in kilograms.

and crystal-plastic deformation intensity, weight, iron-manganese coating thickness, weathering, and basalt and diabase vesicularity and phenocryst content. The term weathering as used herein refers to oxidative alteration due to reaction with seawater at ambient seafloor temperature, rather than to atmospheric weathering. Crystal-plastic deformation intensity was graded from undeformed (grade 0) through clearly foliated (grade 2) to ultramylonite (grade 5). Brittle deformation was recorded from undeformed (grade 0), through brecciated by numerous cracks without clast rotation (grade 2), to reduction to >70% fine-grained matrix (grade 5). Although, as a rule, distinguishing ultramylonites from cohesive ultracataclasites cannot be done hand specimen, the ultramylonites described here occur with protomylonites and mylonites whose textures are macroscopically discernable, and are in a paragenetic-textural association that is well studied at other oceanic core complexes [e.g., *Dick et al.*, 2000; *Jaroslow et al.*, 1996]. Serpentine and soapstone deformation grades, however, are often arbitrarily assigned to crystal-plastic and brittle deformation categories because deformation mechanisms were difficult to determine.

Table 3. Summary of Sampled Gabbros[a]

	N	%	%	C-P
		*Babel and Ararat Domes**		
Kanaut Metagabbro	4	9.5	excluded	
Kanaut Oxide gabbro	4	9.5	10.5	~2.0
Kanaut Olivine gabbro	20	47.6	52.6	~1.9
Knr 180-2 Oxide gabbro	1	2.4	2.6	0.0
Knr 180-2 Olivine gabbro	13	31.0	34.2	0.8
Total	42	100.0	100.0	
All Metagabbro	4	9.5	excluded	
All Oxide gabbro	5	11.9	13.2	~1
All Olivine gabbro	33	78.6	86.8	~1.4
Total	42	100.0	100.0	~1.2
Olivine gabbro veins	5	100.0		1.0
		Cain and Abel Domes		
Metagabbro	27	37.5	excluded	1.1
Oxide gabbros	26	36.1	57.8	2.4
Olivine gabbros	19	26.4	42.2	2.3
Total	72	100.0	100.0	1.9
Metagabbro veins	53	49.5	excluded	1.4
Felsic veins	5	4.7	excluded	0.8
Oxide gabbro veins	22	20.6	44.9	2.2
Olivine gabbro veins	27	25.2	55.1	2.0
Total	107	100.0	100.0	1.7
		Adam and Eve Domes		
Metagabbros	1	0.8	excluded	0.0
Oxide gabbros	34	26.8	27.0	1.6
Olivine gabbros	45	35.4	35.7	0.9
Troctolites	47	37.0	37.3	0.4
Total	127	100.0	100.0	0.9
Metagabbro veins	3	8.8	excluded	0.0
Oxide gabbro veins	11	32.4	35.5	1.1
Olivine gabbro veins	15	44.1	48.4	0.4
Troctolites veins	5	14.7	16.1	1.8
Total	34	100.0	100.0	0.8
		All Gabbros		
Metagabbros	84	24.1	excluded	1.2
Oxide gabbro	94	26.9	35.5	1.9
Olivine gabbro	119	34.1	44.9	1.3
Troctolite	52	14.9	19.6	0.5
Total	349	100.0	100.0	1.3

[a] Notes: KANAUT data separated as descriptions used different protocols than for the Knorr 180–2 samples. N = number of samples; % = percent of samples by number; C-P = average crystal-plastic deformation intensity. In totals row, average C-P is given. Average C-P is not given for Babel and Ararat as deformation was estimated for the KANAUT samples from log descriptions, which varied in detail. The second percent column excludes metagabbros and felsic veins as metamorphism obscures the progenitors.

[32] We also assessed descriptions of 77 samples (~629 kg) from six Nautile dives on the northern wall of Kane Megamullion adjacent to Mt. Ararat and Babel Domes [*Auzende et al.*, 1993, 1994; *Ghose*, 1997; *Ghose et al.*, 1996; *Lagabrielle et al.*, 1998] (Figure 2). Sample weights were estimated from rock dimensions in the cruise report using average densities, and rock names were corrected using tables from *Ghose* [1997]. Dredge and dive lithologic proportions are shown by weight and by number of samples in pie diagrams in Figures 2 and 3. Veins and host rock were counted as separate samples, although typically no estimate of their relative weights was made; thus, fully accurate proportions of gabbros and ultramafics are given only by number of samples. When large numbers of samples are considered from many stations, the differences in proportions expressed in weight percent versus number of samples are generally insignificant. However, when small regions or small numbers of samples are considered, differences may be significant. For example, gabbro proportions by weight and by number from Cain and Abel domes in Figure 3a are different

Table 4. Summary of Sampled Peridotites[a]

	N	%	N	C-P	N	Br
			Babel and Ararat Domes			
Metaperidotites	11	25.6	2	0.25	2	0
Peridotites	32	74.4	8	0.63	8	0
Total	43	100.0	10	0.55	10	0.00
			Cain and Abel Domes			
Metaperidotites	35	9.4	18	2.3	27	1.8
Peridotites	264	71	255	1.3	253	0.5
Peridotites with Gabbro Veins	54	14.6	54	1.4	52	0.5
Plagioclase Peridotites	6	1.6	6	0.8	6	0.2
Websterite Veins	3	0.8	2	1.3	2	0.0
Dunites	9	2.4	6	0.7	7	0.3
Total	371	100.0	341	1.4	347	0.6
			Adam and Eve Domes			
Metaperidotites	5	5.6	4	0.5	4	0.0
Peridotites	32	35.9	32	0.7	32	0.4
Peridotites with Gabbro Veins	6	6.7	6	0.8	6	0.2
Plagioclase Peridotites	2	2.2	2	1.0	2	1.5
Dunites	14	15.7	2	nd	14	0.0
Dunites With Gabbro Veins	4	4.5	2	0.0	4	0.0
Plagioclase Dunites	3	3.4	3	0.0	3	0.0
Wehrlitic Dunites	18	20.2	12	0.3	18	0.0
Wehrlitic Dunite with Gabbro Veins	5	5.6	0	nd	5	0.0
Total	89	99.9	63	0.51	88	0.18
			All Peridotites			
Metaperidotites	51	10.1	24	1.83	33	1.47
Peridotites	328	65.2	295	1.21	293	0.47
Peridotites with Gabbro Veins	60	11.9	60	1.33	58	0.48
Plagioclase Peridotite	8	1.6	8	0.81	8	0.50
Dunites	23	4.6	8	0.67	21	0.10
Dunites With Gabbro Veins	4	0.8	2	0.0	4	0.0
Plagioclase Dunites	3	0.6	3	0.0	3	0.0
Wehrlitic Dunites	18	3.6	12	0.3	18	0.0
Wehrlitic Dunite with Gabbro Veins	5	1.0	0	nd	5	0.0
Websterite Veins	3	0.6	2	1.30	2	0.00
Total	503	100.0	414	1.2	445	0.5

[a] Cpx-rich peridotite in KANAUT descriptions. N = number of samples used in the percentage or average to the right.

because gabbro veins were counted as separate samples, although their volume typically is small and was not estimated. In the following sections we summarize our results, starting with the northern edge of the megamullion along the transform wall and then consider the main edifices to the south.

5. Geology of the Transform Wall

5.1. North Side of Babel Dome

[33] Although two of our dredges recovered rocks from the crest of the transform wall at Babel Dome, we rely largely on sampling and observations from the 1992 KANAUT Expedition. This expedition made six dives with the submersible Nautile (KAN 11, 12, 14–17) where the transform wall forms the northern margin of Kane Megamullion [*Auzende et al.*, 1993, 1994; *Ghose*, 1997; *Ghose et al.*, 1996]. The KANAUT scientists did an outstanding job, and our discussion below is largely based on their report [*Auzende et al.*, 1992]. However, with insights gained from mapping the core complex farther south, and with new mapping and drilling at the Atlantis Bank (SWIR) and Atlantis (MAR) oceanic core complexes, we can make new interpretations. A key difference is that greenschist facies diabase, unmetamorphosed pillow basalts, serpentinites, peridotite mylonites and often highly deformed metaperidotites found on the detachment fault surface in association with gabbro mylonite are not regarded as necessarily representative of the underlying footwall assemblage (see section 7.1).

[34] The transform wall along the northern flank of Babel Dome dips steeply (~27°), dropping some 2000 m to a depth of ~4.5 km where it disappears beneath rubble on the southern edge of the transform floor. KANAUT Dives 11 and 12, and Dive 14 from 3760 to 3325 m, traversed up sections

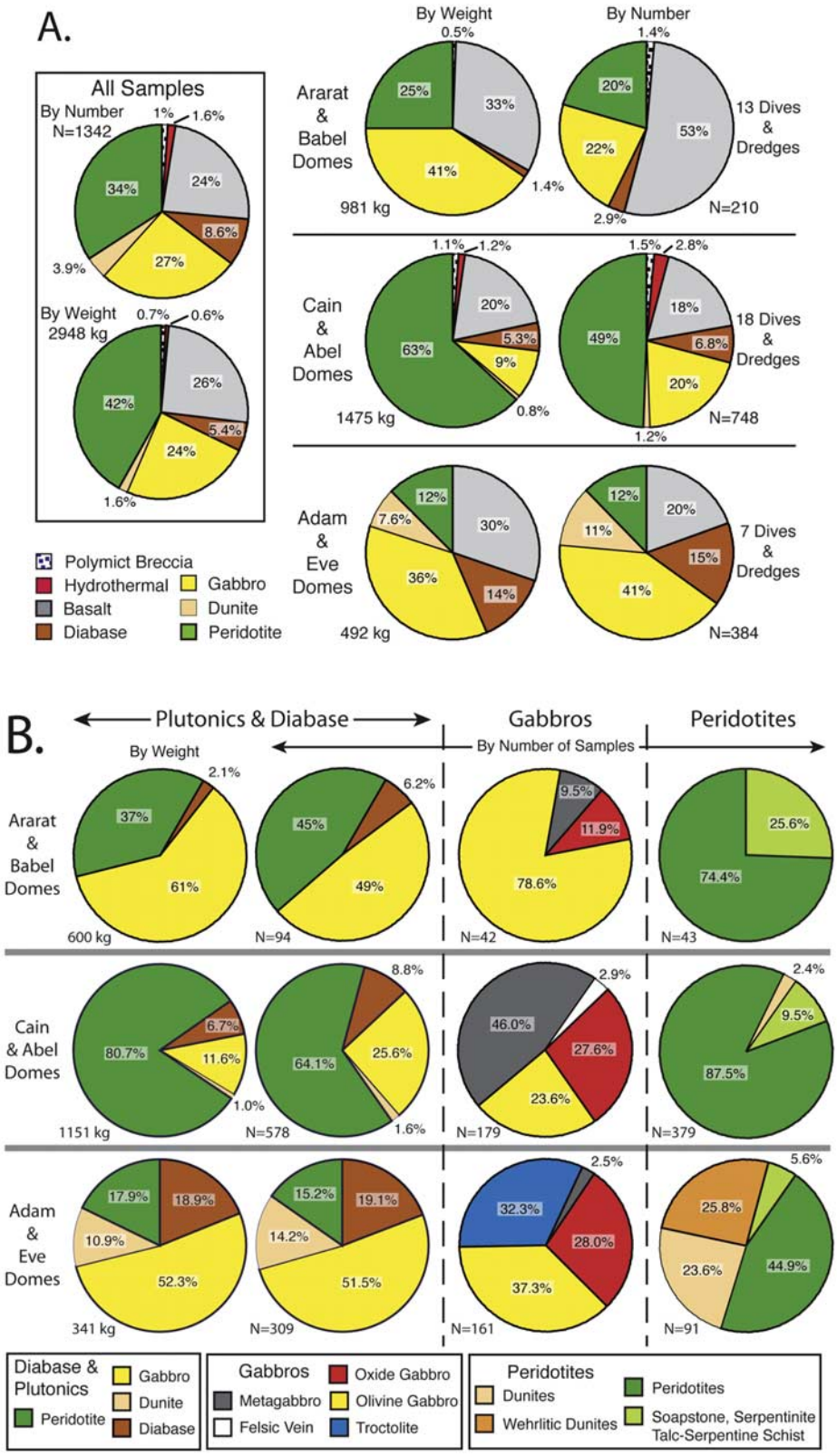

Figure 3. (a) Lithologic proportions of all rocks recovered by Knorr 180–2 Jason II dives and dredges and by the submersible Nautile during the KANAUT Expedition [*Auzende et al.*, 1993, 1994]. In both thus and Figure 3b, veins and host rocks are counted as separate samples. Lithologic proportions excluding basalt, polymict breccia, and hydrothermal rocks. Proportions are shown both by weight and by number of each rock type.

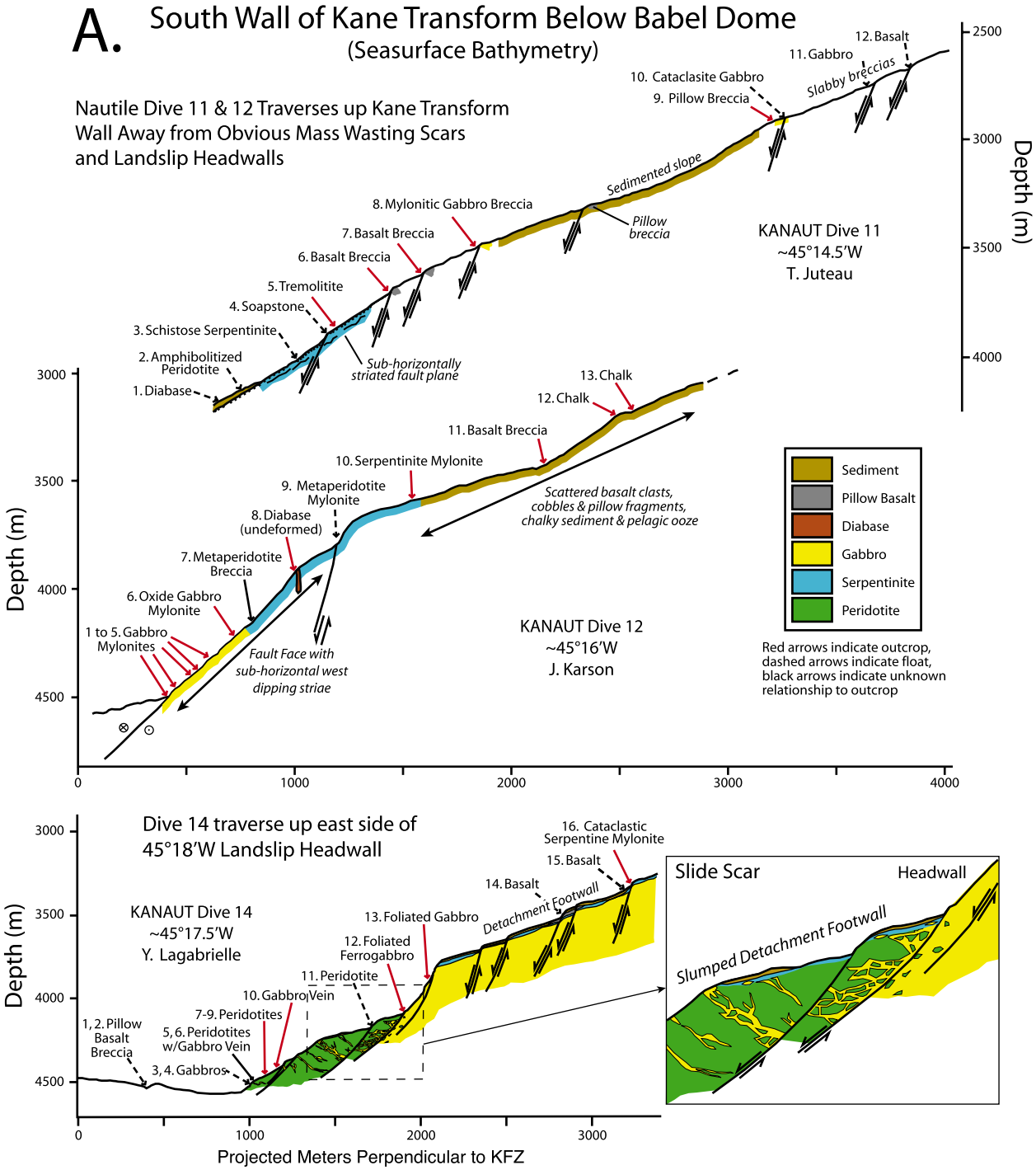

Figure 4. Nautile traverses up the southern wall of the Kane Transform bordering the Kane Megamullion. All dives are aligned with respect to one another and projected perpendicular to the strike of the Kane FZ. Interpretations differ from *Auzende et al.* [1992, 1994] as explained in the text. Diver/observer scientist is indicated below dive number on the profiles. Bathymetric profiles are from the Kanaut cruise report and were based on previously collected sea-surface bathymetry, except for Dive 16 where sample depths did not match profile depths and we used submersible depths. On the Dive 12 profile, the circled cross and dot indicate motion away from and toward the reader, respectively. Red arrows indicate samples from outcrop, black arrows indicate samples of unknown provenance, and dashed arrows indicate talus.

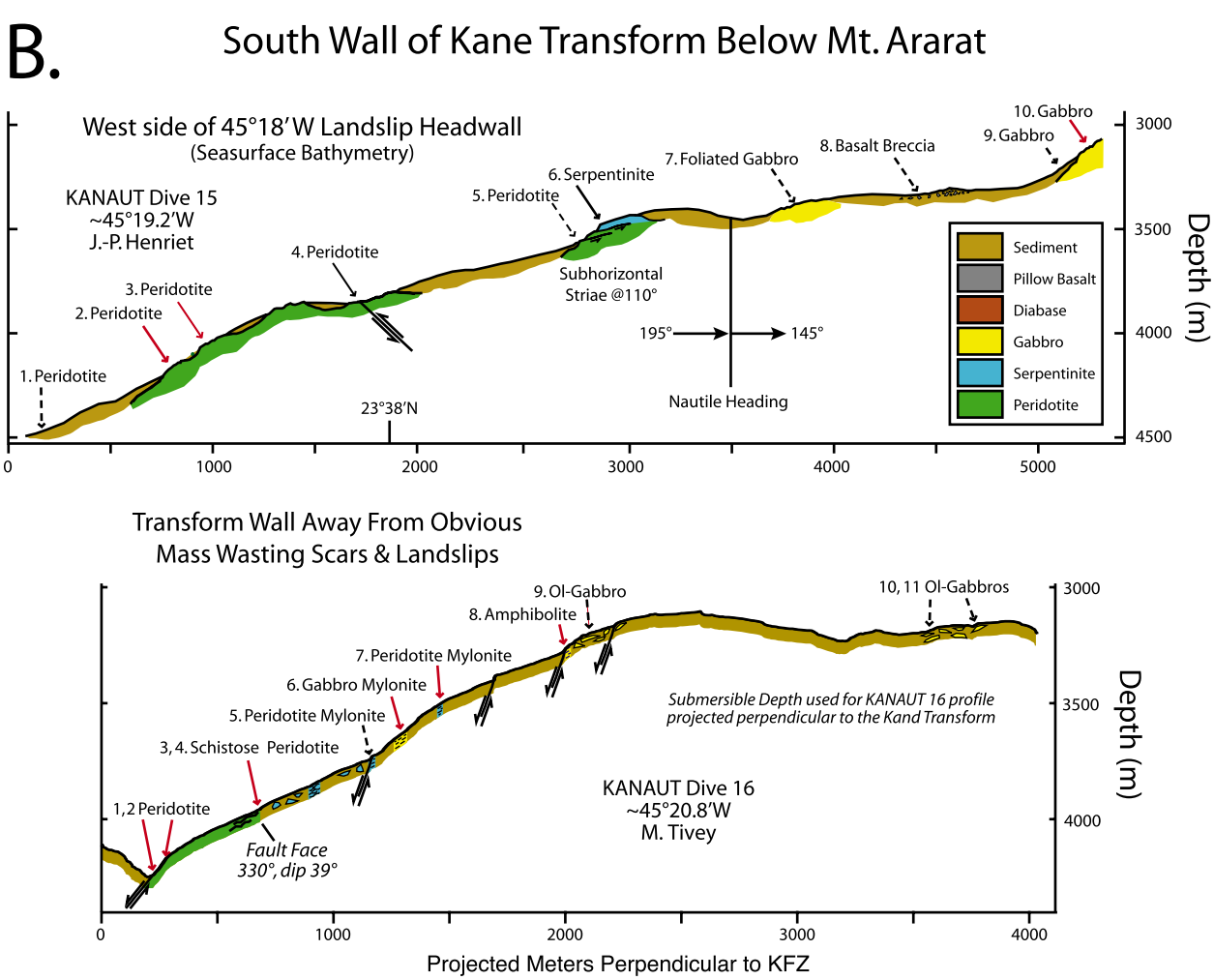

Figure 4. (continued)

where the wall was not degraded by slide scars and where remarkably smooth, planar surfaces are present [*Auzende et al.*, 1992] (Figures 2 and 4a). At the base of the slope (4200–4500 m) the wall is steep (45°–50°) and it emerges from flat or gently sloping sediment ponds. Significant portions of the surface are locally covered by debris flows, but on Dive KAN 12 the outcrops were nearly continuous on the lower slopes. The slopes locally undulate but are generally convex upward, and they become more sedimented upslope. Mostly, they expose what appears to be a single, uneroded, curviplanar fault surface. Numerous striations, mullions, and swales on the fault plane are oriented parallel to the transform [*Auzende et al.*, 1992]; thus the surface is geometrically an E-W-trending strike-slip fault. Only in one or two places were downslope lineations observed. Small scarps that appear to represent high-angle, transform-parallel normal faults locally break the fault plane; this allowed sampling beneath the fault surface or sediment, although rarely for more than several meters.

[35] Three features lead us to conclude that the transform wall is the northern extension of the megamullion detachment surface that merges downslope into the transform fault zone: (1) the gently undulating character of the fault surface, with transform-parallel slip indicators, (2) the uninterrupted union of the fault with the surface of Babel Dome at the crest of the transform wall, and (3) a fault-rock assemblage (see below) that is identical to that sampled over the main body of the core complex, as described in section 7.1.

[36] On all the dives, gentler slopes occur at shallower depths and have piles of rubble and local outcrops that expose weathered pillow basalt breccia, talus, and degraded basalt flows along with scattered blocks of gabbro, amphibolite mylonite, and schistose serpentinite. The scattered basalt

debris and degraded basalt flows are weathered but otherwise completely unaltered, contrasting with the high-temperature amphibolite and greenschist facies plutonic rocks and diabase. Thus they likely are either off-axis lavas erupted over the core complex or hanging wall debris that was stranded on the fault surface.

[37] Dive KAN 11 observed and sampled foliated, mylonitized, and amphibolitized serpentinite outcrops from 4235 m to 3730 m, and recovered a single diabase from float low on the wall (Figure 4a). From 3730 m to 3481 m, pillow-basalt rubble was scattered on a smooth, sedimented slope, while blocks of gabbro mylonite and cataclasite were interspersed with the pillows from 3496 to 2706 m. Assuming that the basalt is hanging wall debris, the dive results loosely constrain the crust-mantle boundary to lie below 3496 m where the first in situ gabbro was sampled. However, the soapstone and tremolitite sampled at 3900 m and 3885 m are common metasomatic alteration products of serpentinized peridotite associated with gabbro intrusions. Considering this, and given the likely emplacement of serpentinite along the detachment fault (see section 7.1), the main gabbro body could be covered by a thin skin of metaperidotite/serpentinite and extend down to ~3900 m.

[38] Dive KAN 12 sampled an apparent inversion of the expected stratigraphy (Figure 4a). Samples included strongly foliated gabbro mylonites from 4492 to 4322 m, an oxide gabbro mylonite at 4232 m, and upslope from 4147 to 3591 m a metaperidotite with mylonite clasts, a metaperidotite mylonite cut by an undeformed diabase dike, and then serpentinite. Upslope from the serpentinites, only one pillow basalt breccia and chalks were recovered. There are several possible explanations for this sequence: (1) the gabbros intruded the mantle at depth and then were later exhumed with the peridotite to the seafloor; (2) the peridotites represent a roof pendant in gabbros that intruded the mantle along-axis near the transform; and (3) the metaperidotites are gouge intruded along the detachment fault and thus form a skin over massive gabbro, as has been observed at Atlantis Bank [*Dick et al.*, 2001].

[39] Dive KAN 14 on the northwest corner of Babel Dome started on the transform valley floor and went up the east side of a large slide scar and related slump toe (Figure 4a). The headwall of this scar cuts deeply (~300 m) into the transform wall below the original detachment surface. At ~3760 m the dive passed up onto a relatively undisrupted smooth slope representing the undegraded surface of the transform wall. Only pillow-basalt debris was sampled on the valley floor, but the slide scar and slump toe expose significant changes in basement lithology. On the slump toe abundant outcrops and debris flows consist of massive, heavily weathered, orange porphyroclastic peridotite with gabbro veins; these were sampled on the steep slope that extends from 4481 to 4250 m and then over a gently sloping bench from 4250 to ~4125 m. The heavily weathered granular peridotites contrast sharply with deformed and metamorphosed serpentinite and mylonites found elsewhere on the undegraded detachment footwall. Massive outcrops of foliated oxide gabbro and metagabbro were found beginning at ~4092 m on the steep (~55°) slide-scar headwall. Above the headwall at ~3760 m there is an abrupt change to a 14° sedimented slope interrupted by small normal faults. Pillow basalt fragments and a schistose serpentinite were found on this slope. The regular smooth slope, scattered pillow debris, and deformed serpentinite indicate that this is again the detachment fault surface. Knorr 180–2 Dredge 9 recovered olivine gabbro, pillow basalt, basalt, and basalt breccia near the top of the transform wall on the headwall of the slide scar at 3380–2790 m, SSW of Dive KAN 14. Dredge 12 at the crest of Babel Dome (2651–2421 m), however, recovered both granular peridotite and olivine gabbro.

[40] These dives and dredges raise the question of how to interpret the position and nature of the crust-mantle boundary as exposed on the transform wall beneath Babel Dome. Although the Dive 14 serpentinite near 3325 m is probably fault gouge intruded along the detachment fault, the porphyroclastic granular peridotites sampled from 4481 to 4125 m likely represent in situ mantle outcrops. The Dredge 12 granular peridotites high on the transform wall, on the other hand, could represent several things: (1) a small undeformed block entrained in serpentinite and carried along the fault; (2) a stoped block of roof rock where gabbro intruded into the mantle near the transform, or (3) simply part of an irregular contact between a massive gabbro body that includes small plugs, dikes, and sills intruded into massive peridotite.

[41] Transform walls, as pointed out by *Francheteau et al.* [1976], do not represent simple near-vertical, kilometer-scale sections through the crust; rather they represent lateral sections that slope downward over a considerable distance to the transform valley floor (e.g., Figure 4). The simplest interpretation of

the exposures on the transform wall below Babel Dome is that a large gabbro body intruded into the mantle near the transform and net-veined the peridotite near the contact, thus creating a lateral, upslope sequence of massive peridotite that changes to net-veined peridotite and then to massive gabbro (Dive 14, Figure 4a). This kind of sequence was found vertically in ODP Hole 1268A at 14°51′S on the MAR where gabbro intruded granular peridotite [*Shipboard Scientific Party*, 2004]. In the Kane transform wall, the detachment fault appears to have cut across and exposed the boundary between the gabbros and peridotites as well as undeformed peridotite that locally overlies the intrusion in the vicinity of Dredge 12. Subsequent slope failure seems to have concentrated at the contact between the gabbro and peridotite.

5.2. North Side of Mt. Ararat

[42] Dive KAN 15 traversed up and along the west side of the slide-scar headwall opposite KAN 14, sampling heavily weathered porphyroclastic granular peridotite from 4450 m to 3446 m (Figures 2 and 4b). Unlike KAN 14 peridotites, these are largely unveined, suggesting that they are not close to a gabbro intrusion. The shallowest peridotite sample is noticeably more serpentinized than those deeper in the section. Higher up, more angular, massive outcrops yielded foliated gabbro at 3349 m, basalt rubble at 3291 m, and isotropic gabbro at 3158 and 3052 m. The character of the peridotites is consistent with massive mantle outcrops rather than fault gouge, and the crust-mantle contact apparently lies between 3446 and 3349 m.

[43] Dive KAN 16 traversed the transform wall from the base of a scarp at 4242 m and up a convex slope that forms a ridge between major slide scars to the west and the east (Figures 2 and 4b). At 3959 m a smooth, low-angle fault face strikes 330° and has an overall slope of ~25° to the north, although it locally dips 39°N. Above ~3200 m the slope levels, then undulates across a broad swale for ~1500 m where it is heavily sedimented to the end of the dive. At the deepest point, a cliff face exposes sheared and rubbly black outcrops of soft, heavily weathered peridotite. Weathered peridotite, apparently progressively more deformed upslope, was continuously sampled beginning at 4236 m. Mylonitic peridotite was sampled at 3739 m, ultramylonitic gabbro at 3632 m, and gabbro-banded peridotite mylonite at 3502 m. Amphibolite was recovered at 3268 m and isotropic olivine gabbro at 3202 m. Beyond a small rise at ~3160 m, gabbro was recovered from a small scarp at 3191 m and isotropic olivine gabbro was sampled from talus at 3162 m.

[44] The KAN 16 transect is difficult to interpret because of sediment cover. However, the smooth fault face at 3959 m and the overall convex slope with numerous peridotite and gabbro mylonites indicate an uneroded, sedimented detachment fault surface. The lack of talc schist or intense serpentinization of the peridotite mylonites makes it unlikely that these strong and dense rocks intruded significantly along the detachment fault, while the gabbro banding at 3502 m suggests a net vein complex at the periphery of an intruding gabbro body. The appearance of ultramylonitic gabbro at 3632 m, followed by the gabbro-banded peridotite mylonite at 3502 m and then by amphibolite (likely metagabbro) and isotropic gabbros above 3268 m, suggests that the crust-mantle contact, cut by the detachment fault, could be between 3502 and 3268 m.

[45] Farther west, dive KAN 17 traversed a canyon on the NW corner of Mt. Ararat. This dive went up a long gentle slope interrupted by several high-angle normal faults but crossing almost no outcrop. Gabbro was sampled in talus over the entire slope, with a single outcrop of serpentinite cut by gabbro dikes at 3412 m. No structural interpretation is possible here, but we suspect that the serpentinite could represent fault gouge in the detachment footwall.

6. Geology of the Megamullion Dome

6.1. Basalt Occurrences

[46] Overall, 26 wt.% of the rock sampled across the megamullion is pillow basalt occurring as widely scattered angular debris and debris piles. Intact, but degraded, pillow basalt flows were observed only along the north part of East Fault (Figure 3a). Only very low-grade brittle deformation is observed, and there is no evidence of ductile deformation. The basalts are generally unaltered except for often heavy seafloor weathering. Most basalts contain little if any fresh glass, particularly those scattered across the detachment surface. The basalts contrast sharply with the plutonic rocks and hypabyssal dikes and sills (section 6.2), which generally show extensive metamorphic recrystallization and are frequently highly deformed (cf. Figures 5 and 6). We interpret the scattered, loose basalts as hanging wall debris and klippe stranded on the detachment footwall.

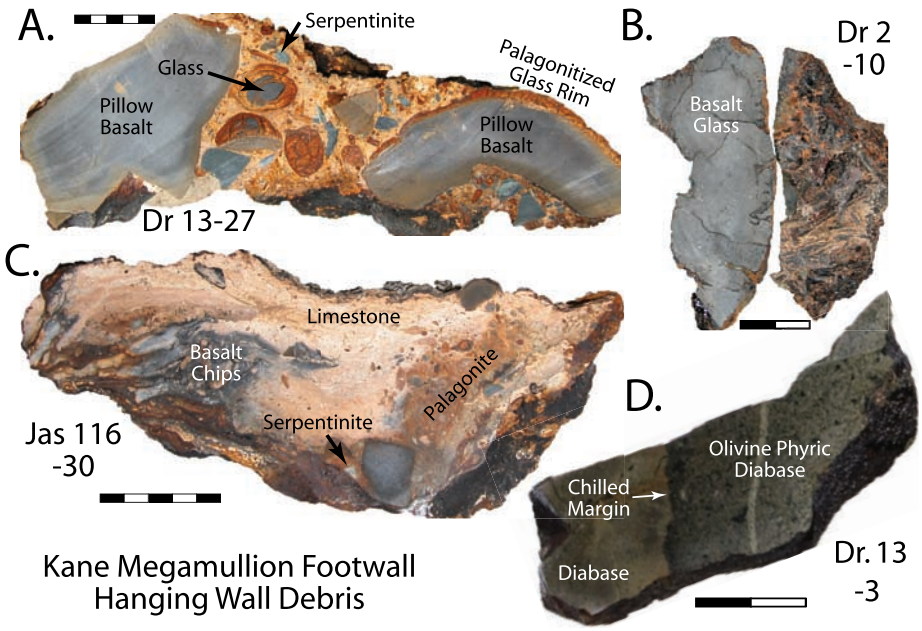

Figure 5. Knorr cruise 180–2 samples of hanging wall debris stranded on the detachment fault footwall at Kane Megamullion. (a) Dredge 13, sample 27 - carbonate cemented polymict pillow basalt-palagonite-serpentine breccia from detachment fault surface on east edge of Cain Dome near the detachment fault termination. (b) Dredge 2, sample 10 - thick, fresh glassy pillow basalt rind from possible off-axis volcanic ridge along the northern part of East Fault. (c) Jason II 116, sample 30 - deformed carbonate cemented polymict basalt-serpentine breccia from the detachment fault surface on Cain Dome. (d) Dredge 13, sample 3 - diabase dike-dike contact from detachment fault surface at the eastern edge of Cain Dome. Scale bars in centimeters.

[47] The rocks are typical mid-ocean ridge basalts. Of the 261 basalts described, 75.6% are aphyric or sparsely phyric (<2% phenocrysts) and 24.4% are phyric or highly phyric. Clinopyroxene was tentatively identified with olivine and plagioclase in 6% of the phyric samples, while 5% were olivine phyric, 25% plagioclase phyric, and 35% plagioclase-olivine phyric. Vesicularity is typically less than 2% by volume.

[48] Unmetamorphosed pillow basalt fragments cemented by carbonate, often with serpentine clasts and diabase chips are common from the detachment surface (Figure 5a). At the top of Adam Dome on Jason II Dive 117, we observed massive piles of basaltic rubble and mound-like structures of basalt debris cemented by carbonate, with no intact flow units. In some cases slumping of loose rubble left freestanding columns of cemented basalt rubble that are meters wide. Similar basaltic breccia mounds were found on Cain Dome during Dive 116, where samples of deformed carbonate cemented basalt breccia were also recovered (Figure 5c). The cemented basalt mounds and pillars presumably formed by hydrothermal flow of carbonate-rich waters up the active fault and then up through the overlying brecciated basalt, locally cementing hanging wall debris to the footwall while the surrounding uncemented rubble slid away as the footwall was exhumed.

[49] Dredging and Jason II Dives 110 and 111 along East Fault from ~23°30′N to 23°37′N (Figure 2) recovered pillow basalts with palagonitic or glassy rims (e.g., Figure 5b) and hyaloclastite breccias. Here there is a steep-sided, asymmetric ridge formed along the trace of East Fault. It slopes steeply upward from the down-dropped floor of the dome to the west and rises above the up-thrown detachment surface to the east. This ridge has a 'T' shape at 23°36′N and it appears as though volcanism may have been localized along the intersections of East Fault and a local transform parallel fault. High-resolution bathymetric mapping with ABE showed a series of broad lobes branching downslope on the west face of the ridge, consistent with a series of flow fronts. Jason observed intact but degraded pillow lava flows on the slope that continue up and over the crest of the footwall. The Kanaut dives on the transform wall show that the volcanics lie directly over massive gabbros. These volcanics could be captured from the detachment hanging wall by an east-stepping imbrication of the detachment fault,

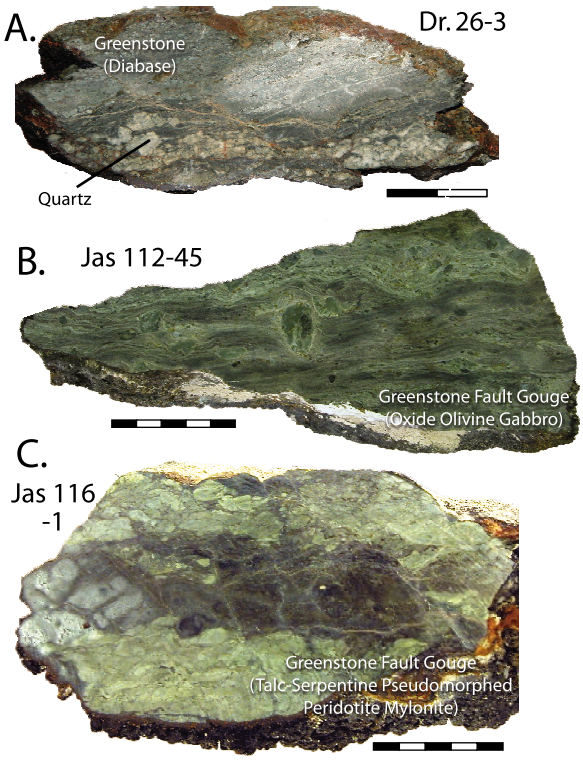

Figure 6. Fault gouges from the Kane Megamullion detachment surface. (a) Dredge 26, sample 3 - phacoidal piece of greenschist facies diabase cataclasite with fragmented quartz vein in chloritized diabase identified by XRD from the detachment fault surface on the east side of Adam Dome. (b) Jason II 112, sample 45 - oxide-olivine gabbro fault gouge with primary mineralogy replaced by chlorite, talc, and amphibole, from a slide-scar headwall where East fault cuts the detachment footwall on the west side of Cain Dome. (c) Jason II 116, sample 1 - ultramafic fault gouge consisting of peridotite mylonite and serpentine fragments replaced by talc and chlorite from the detachment fault footwall on the south side of Cain Dome. Scale bars in centimeters.

in which case they may be back-tilted to the west. However, it is equally possible that they represent off-axis constructional volcanism associated with faulting during uplift of the core complex, most likely at the paleo-inside-corner high.

[50] The morphology of two unexplored regions suggests additional off-axis volcanism (gray-shaded areas, Figure 2). One is in the area east of East Fault at 23°25′N where hummocky topography and steep-sided ridges, apparently associated with west-dipping normal faults, are present. The second is Mt. Ararat north of Abel Dome, where a volcanic carapace is suggested by the hummocky morphology. Physiographically, Mt. Ararat more closely resembles a low shield volcano than a lineated axial volcanic ridge. It is possible that intersecting faults here also localized off-axis volcanism. Kanaut Dives 16 to 17 traversed up the transform wall on the northern side of Mt. Ararat and recovered gabbro and peridotite, but did not traverse over the edifice itself. If Mt. Ararat is a volcano, then it erupted over the core complex. All these constructional features suggest that there may be a laterally significant, even if volumetrically small, component of off-axis volcanism associated with unroofing and uplift of the core complex.

6.2. Diabase

[51] Diabase was recovered in nine dredges and four dives (Figure 2), but it amounted to <6 wt.% of the rock sampled over the megamullion. Identification of diabase, as opposed to pillow basalt and sheet flows, can be done with confidence in large dredge recoveries based on greenschist facies alteration, dike-dike contacts (Figure 5d), planar chilled margins, and an absence of fresh or altered glass. While massive flows may share these characteristics, they ordinarily are intercalated with pillow lavas. Pillow basalt suites invariably have abundant fresh or altered glass. Obviously, dredges with only a few avesicular massive basalts cannot be assigned to either category, and these were cataloged simply as basalt. Little diabase was found in the north, but it was more abundant from the detachment surface across the southern two-thirds of the megamullion (Figure 3a). There is an inlier of the dike-gabbro transition at Adam Dome, but diabase was rare where we sampled slide-scar headwalls and high-angle normal fault scarps cutting beneath the detachment footwall at Cain and Abel Domes.

[52] Diabase occurred with gabbro at 11 locations, with pillow basalt at seven (exclusively with basalt in two of these), and with peridotite at 7 (Figure 2). Most diabase (69%) is fine-grained, 20% is aphanitic, and 11% is medium-grained, similar to sheeted dike complexes in ophiolites. Mineralogically, the diabase is similar to the basalts; of 106 samples described, 33% are aphyric, 35% plagioclase-olivine phyric, 24.5% plagioclase phyric, 6.6% olivine phyric, and 1% plagioclase-augite phyric. Phyric diabase averages 6.5% phenocrysts, with up to 20–30% in a few samples. Alteration is generally very heavy; 39.1% of samples have 90–100% visible alteration, 40.2% have 50–90%, 9.2% have 10–50%, and 11.5% have <10%. Most

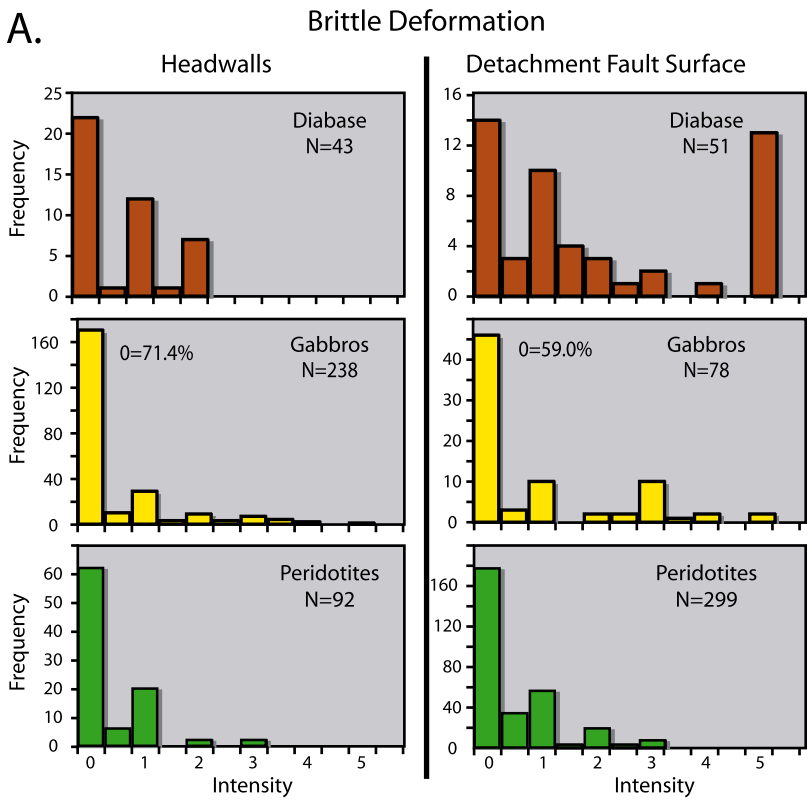

Figure 7. Semiquantitative deformation intensities from the shipboard logs based on textures in hand specimen for samples collected during Knorr Cruise 180–2. (a) Brittle deformation intensity. (b) Crystal-plastic deformation intensity. Plots labeled "Headwalls" are for samples collected by dredge or submersible from slide scars and high-angle normal fault surfaces cutting below the detachment footwall and exposing the interior of the core complex. Plots labeled "Detachment Surface" are for rocks collected directly from the detachment fault surface. Crystal-plastic deformation noted in hand specimen includes semi-brittle deformation.

samples were altered in the greenschist facies with extensive recrystallization to chlorite, actinolite and albite, while a few samples showed evidence of lower-amphibolite facies. Quartz-chlorite vein assemblages were also observed. Visible brittle deformation appears in hand specimen in 62% of the diabase samples (Figure 6a), but only 10% show evidence of crystal-plastic deformation.

[53] To see how deformation might differ between the interior of the core complex and the detachment fault zone, we grouped samples by location, i.e., samples from headwalls of large slide scars and normal faults that cut through the detachment surface versus samples from the detachment fault surface itself (Figure 7). We found little crystal-plastic deformation in diabase from either the detachment surface or the headwalls (Figure 7b). However, there is a significant difference in brittle deformation of samples from these two areas, even though the headwall/normal-fault group must have sampled slumped sections of the detachment fault surface in addition to the footwall interior (Figure 7a). The diabases show brittle deformation in 73% of the detachment-surface samples but only 49% of the headwall/normal-fault samples. Moreover, while 30% of the detachment-surface samples showed significant cataclastic deformation (grade 3 or higher; e.g., Figure 6a), none of the headwall/normal-fault samples showed this. Because our sampling in the slide scars and normal faults most likely exposes only a several-hundred-meter section beneath the detachment fault, this strongly suggests that brittle deformation was localized to within ~100 m of the detachment fault surface and possibly much less.

[54] On the south side of Cain Dome (Jason II Dive 116; Figure 2), an undeformed 30-cm-thick diabase sill was found intruding sheared soapstones and serpentine schists along the plane of the detachment fault surface where it is cut by a WNW-ESE-trending breakout. This shows that dike intrusion occurred during detachment faulting, while the

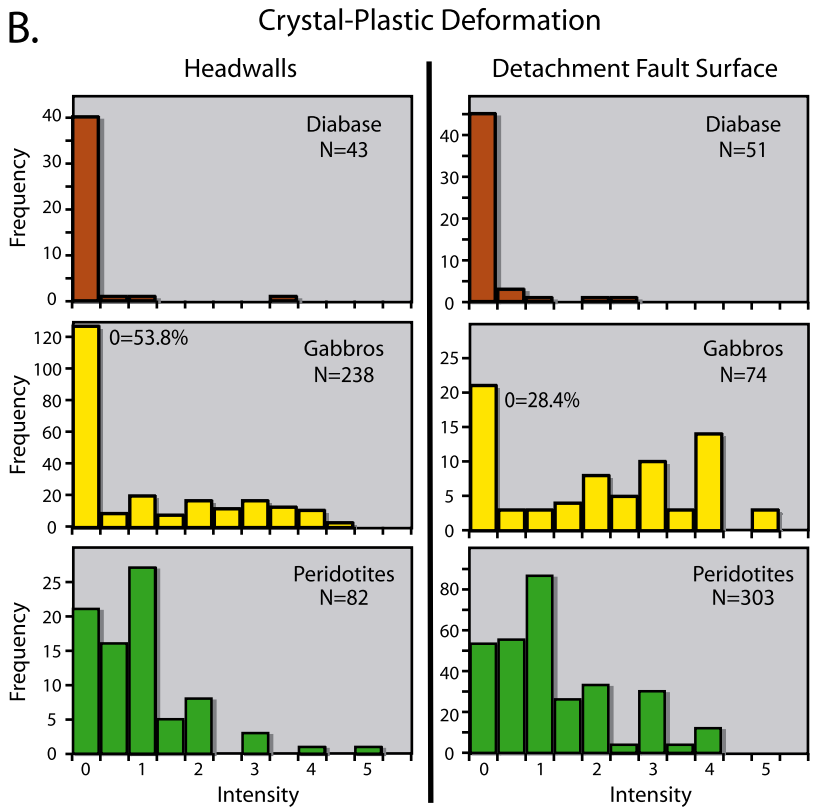

Figure 7. (continued)

lack of internal deformation shows that the dike was emplaced into highly ductile talc-serpentine schists at a shallow level.

[55] At Adam Dome, Jason II Dive 117 collected 31 diabases and 40 gabbros on two traverses up a ~700-m section on the steep (~40°) scarp formed by West Fault (Figures 8 and 9). This appears to be an inlier of the dike-gabbro transition that exposes a ~1-km section below the detachment fault surface (Figure 10). Intercalated dikes and gabbros are exposed on the southern traverse in nearly continuous, massive outcrops, and massive gabbros with a cap of pillow basalt rubble were observed on the parallel northern traverse. Gabbro or diabase was consistently sampled over long stretches, and these rocks only locally alternated in close spacing. In contrast to the gabbros, the diabase dikes are virtually 100% greenschist facies altered (Figure 9). They contain abundant chlorite and actinolite, and although many show brittle deformation they appear to lack significant crystal-plastic deformation. No significant vertical trends in alteration or deformation intensity are apparent in hand specimens. Dike dimensions were difficult to determine because the diabase occurs mostly in massive, hackly outcrops or on slickensided fault surfaces that parallel the slope. In a few cases where dike orientations could be determined reliably, they appear to strike ~N10°E and dip steeply west with widths of about half a meter. We attribute the scarcity of clearly visible dike contacts to their apparent strike (~N10°E) and their dip subparallel to the fault scarp on which they are exposed.

[56] We note that if the dikes dip as depicted in Figure 10, ~ perpendicular to the detachment surface, then the detachment fault was probably near horizontal where it rooted beneath the rift valley. This would imply that the fault had a flat-ramp-flat geometry since the dikes had to undergo a clockwise rotation as the detachment footwall unroofed the dikes and uplifted them into the rift mountains, then a counter clockwise rotation as the footwall rolled over toward the west. Finally, as West Fault developed, an additional clockwise rotation would have occurred, giving the detachment surface its present 18° eastward dip.

6.3. Gabbro

[57] Among nonbasaltic rocks form the OCC, about 40 wt.% is gabbro (Figure 3b). There is three principal varieties of gabbro, ranging from

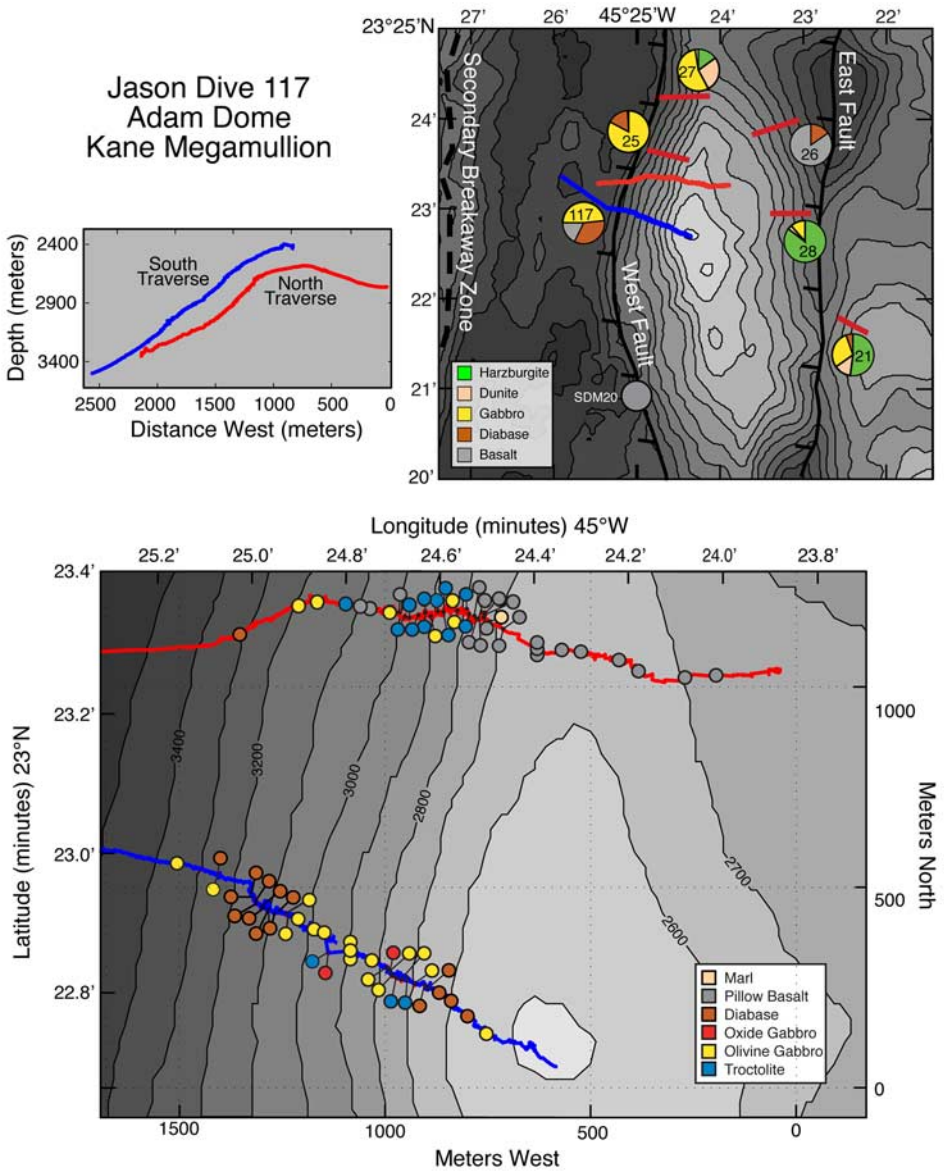

Figure 8. Tracks of two Jason II Dive 117 traverses up West Fault on the west side of Adam Dome. This fault exposes a ~1-km section below the Kane Megamullion detachment fault measured perpendicular to the back-tilted fault surface. Track where the ROV moved in mid-water from one traverse to the other has been omitted. Contour interval in both figures is 100 m.

primitive to highly evolved: (1) troctolite and troctolitic gabbro, (2) olivine gabbro and gabbro, and (3) oxide gabbro and gabbronorite (Figure 3b, Figures 11a–11c). Gabbronorite frequently contains high oxide percentages and can be difficult to distinguish from oxide gabbros in hand specimen, so all these are lumped together in our figures and discussion. Gabbros from the detachment fault surface frequently show extensive retrograde metamorphism, ranging from granulite and upper amphibolite facies down to clay alteration and complete replacement by soapstone in association with metaperidotite. Gabbros sampled from beneath the detachment surface along West and East faults, however, are often quite fresh and contain abundant relict olivine. Where igneous texture is preserved, the gabbros are mostly typical equigranular abyssal gabbros, with interlocking silicate grains varying together in grain size from microgabbro to pegmatoidal. Interstitial oxide is often abundant in oxide gabbro and gabbronorite, but it is generally negligible (<1% by volume) in the gabbros, olivine gabbros, and troctolites.

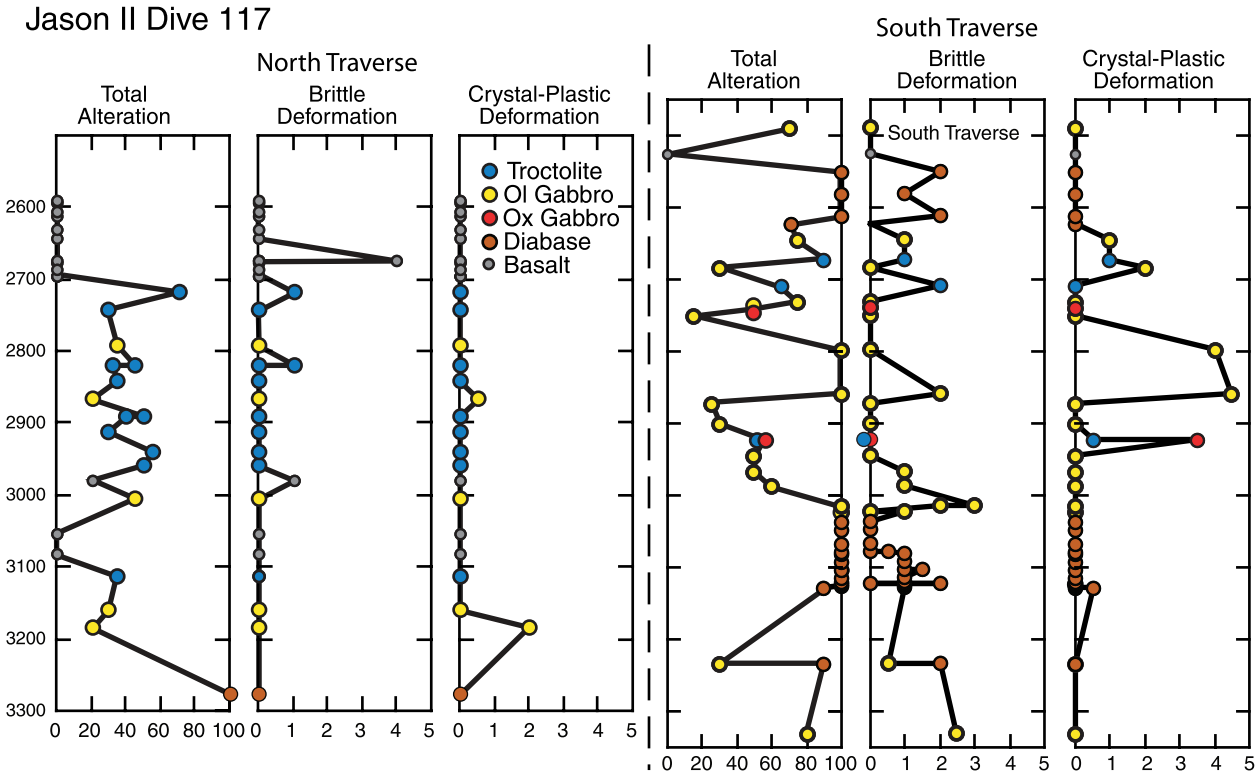

Figure 9. Seafloor sample depth versus sample alteration, brittle deformation intensity, and crystal-plastic deformation intensity for the southern and northern traverses up West Fault on the west side of Adam Dome. Data are from Knr 180–2 shipboard logs.

[58] Unlike diabase and pillow basalt, gabbros are not uniformly distributed over the core complex, and there are major differences in abundance, type, and occurrence from north to south (Table 3, Figures 2 and 3). On the transform wall and around Mt. Ararat and Babel Dome, gabbro is more abundant than peridotite, consisting largely of olivine gabbro with minor oxide gabbro (Figure 3b). However, in the central area of Cain and Abel Domes, gabbro constitutes only 12 wt.% of the plutonic rocks while peridotite is abundant. Gabbro occurs there largely as veins in peridotite (Figures 11e and 11f), with nearly equal proportions by number of oxide and olivine gabbro (Figure 3b). No troctolite was recognized in hand specimen. Rootless veins, including gabbros, are common in ophiolite mantle sections such as the Oman peridotite [e.g., *Ceuleneer et al.*, 1996; *Python and Ceuleneer*, 2003] but rarely amount to more than a few percent of the outcrop. The higher percentage of veins at Cain and Abel domes therefore likely represents net vein complexes and small intrusive bodies (~meter to kilometer scale) rather than local segregations.

[59] At Adam and Eve domes in the south, 52 wt.% of the basement rocks, excluding basalts, are gabbro, and where West Fault cuts Adam Dome these are closely associated with diabase in a putative dike-gabbro transition inlier (Figure 10). Troctolite and troctolitic gabbro constitute ~32 wt.% of the gabbros even though there is ~28 wt.% oxide gabbro (Figure 3b). These primitive gabbros were not found among samples from the domes to the north. The gabbros sampled from the west face of Adam Dome on Dive 117 and in Dredge 25 do not occur with peridotites but only with dikes, and with minor serpentinized peridotite and dunite farther to the north in Dredge 27. Thus, we conclude that they represent a large gabbro body several kilometers or more in length that intrudes northward into peridotite.

[60] Gabbros in the complete suite from the mega-mullion often show extensive high-temperature crystal-plastic deformation under granulite to lower amphibolite facies conditions, with an average crystal-plastic deformation grade of 1.3 (Table 3). Oxide gabbros are noticeably more recrystallized than olivine gabbros or troctolites, with an average crystal-plastic deformation grade of 1.9 as opposed

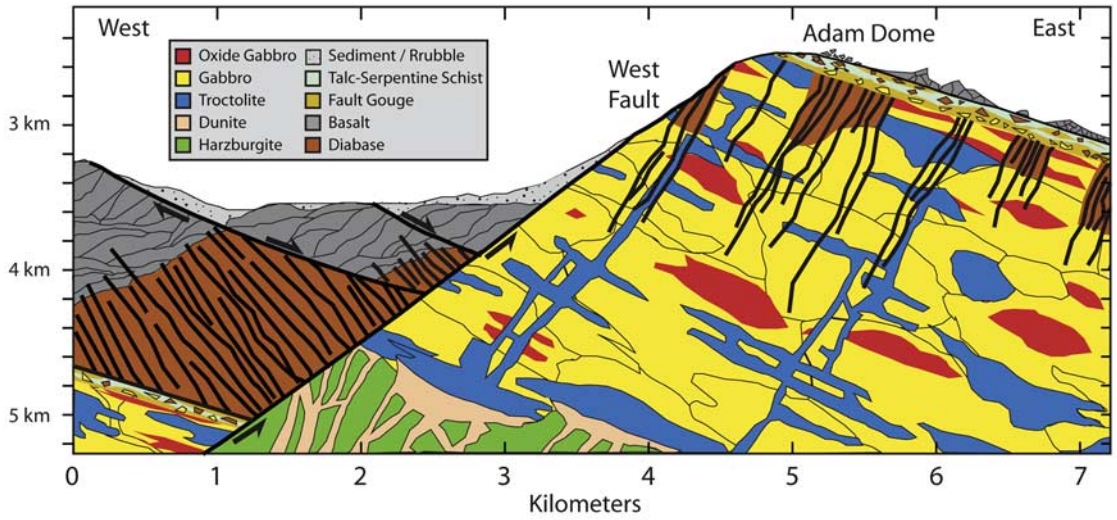

Figure 10. Bathymetric profile across Adam Dome with a schematic depiction of the possible sub-surface geology. No vertical exaggeration. Interpretation to the west of West Fault is based entirely on the seafloor morphology, which indicates an area of intact volcanic edifices that are back-tilted on inward-facing normal faults. The detachment-zone assemblage on the east slope of Adam Dome is likely only meters thick, but it is exaggerated here to depict the geological relations. Note that the fault breaking the seafloor on the left side is the same as that interpreted as the breakaway zone in Figures 2 and 8. Geometrically this is difficult if the pillow basalts and sheeted dikes are anywhere near usual thickness (1.5–2 km) for "normal" ocean crust, and it is likely that these actually are much thinner than depicted. The talc-serpentine shear zone beneath these rocks is entirely speculative.

to 1.3 for olivine gabbros and 0.5 for troctolites. This is consistent with observations at Atlantis Bank on the Southwest Indian Ridge [*Cannat*, 1991; *Cannat et al.*, 1991; *Dick et al.*, 1991a, 2000] and in the MARK area [*Agar and Lloyd*, 1997]. As is also observed in the latter regions, highly deformed oxide gabbro is often found in sharp contact with undeformed olivine gabbro, and oxide-filled cracks and tails on pyroxene porphyroclasts provide evidence that late Fe-Ti oxide-rich melts both intruded along and localized in active shear zones [*Agar and Lloyd*, 1997; *Dick et al.*, 1991a, 2000; *Natland*, 2002].

[61] Gabbros in the detachment surface have significantly more crystal-plastic deformation than those in the slide-scar headwalls and high-angle normal-fault scarps (Figure 7b). Gabbros from both areas, however, show more crystal-plastic deformation than diabase, which has virtually none. 72% of the detachment surface gabbros are deformed and 40.5% are mylonites, while only 46.2% of the headwall gabbros are deformed and 18.5% are mylonites. A similar, small difference is observed for brittle deformation of gabbros. On the detachment surface 41% of gabbros are brittlely deformed and 19.2% are cataclasites (Figure 6b), whereas 28.6% of headwall gabbros are deformed and only 5.9% are cataclasites.

6.4. Dunite

[62] A significant amount of dunite associated with gabbro and peridotite was sampled from the core complex. Notably, where gabbro and dunite occur together in a sample, the gabbro always cuts the dunite. Many dunites have contacts with peridotite, and they often occur as veins. The dunites are generally partially serpentinized, with the remaining olivine heavily weathered to orange clay. Slightly less than half the dunites contain only olivine and chrome spinel. Chrome spinel is often the only primary phase preserved because of serpentinization and weathering of olivine, and it sometimes occurs in segregations similar to those in podiform dunites in ophiolites. Locally abundant wehrlitic dunites (<5% Cpx) and minor plagioclase dunite were also found. These rocks contain interstitial plagioclase and clinopyroxene that are interpreted to be the products of intercumulus crystallization within dunite residues during melt migration through the rock.

[63] Dunites are not uniformly distributed over the core complex (Figures 2 and 3b, Table 4); they are rare north of 23°25′N but are common in the vicinity of Adam and Eve Domes. None were found at Babel Dome or on the transform wall at the north edge of the megamullion. In terms of frequency, at Cain and Abel Domes only 2.4% of the peridotites

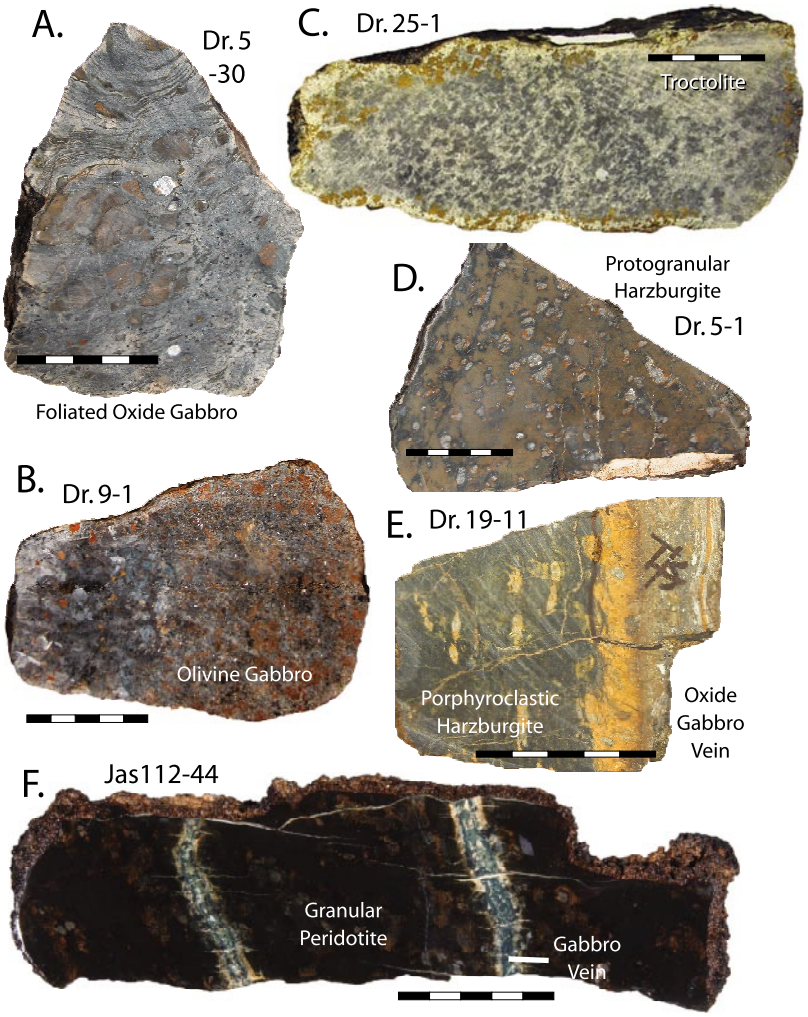

Figure 11. Samples of basement lithologies from below detachment shear zone. (a) Dredge 5, sample 30 - oxide gabbro mylonite cut at a high angle to foliation, from slide-scar headwall along East Fault on west side of Cain Dome. (b) Dredge 9, sample 1 - olivine gabbro with coarse-medium grained sutured igneous contact, from the slide scar headwall at the northwest corner of Babel Dome. (c) Dredge 25, sample 1 - granular troctolite dredged with diabase from West Fault at Adam Dome. (d) Dredge 5, sample 1 - partially serpentinized and oxidized weathered granular peridotite from slide-scar headwall on East Fault at Cain Dome. (e) Dredge 19, sample 11 - harzburgite protomylonite with a mylonitized oxide-olivine gabbro vein from the detachment footwall on the north side of Abel Dome. (f) Jason II 112, sample 44 - partially serpentinized protogranular harzburgite with talc-chlorite pseudomorphed gabbro veins, from slide-scar headwall along East Fault at Cain Dome. Scale bars in centimeters.

(nine samples) are dunite (Figure 3b). At Adam and Eve Domes, however, 44 dunites were found in the three peridotite-bearing dredges, compared to only nine dunites in all of the 14 dredges containing peridotite to the north. Overall, half of the mantle rocks collected around Adam and Eve Domes are dunite. More than half of these are wehrlitic dunite, and 6.8% is plagioclase dunite. Such rocks are not recognized at all to the north and are generally atypical of dunites from transform faults [*Dick*, 1989].

6.5. Peridotite

[64] Peridotite is the most abundant rock sampled from Kane Megamullion, constituting 34% of all samples by number and 42% by weight (Figure 3a). It is most abundant around Cain and Abel Domes, occurring in massive outcrops in slide scars and high-angle faults that cut into the domes as well as scattered occurrences over the detachment surface. Peridotite is also common at Babel Dome and on the transform wall, where it occurs as metaperidotite, mylonite, serpentinite, and talc-serpentine schist. Such rocks are common-

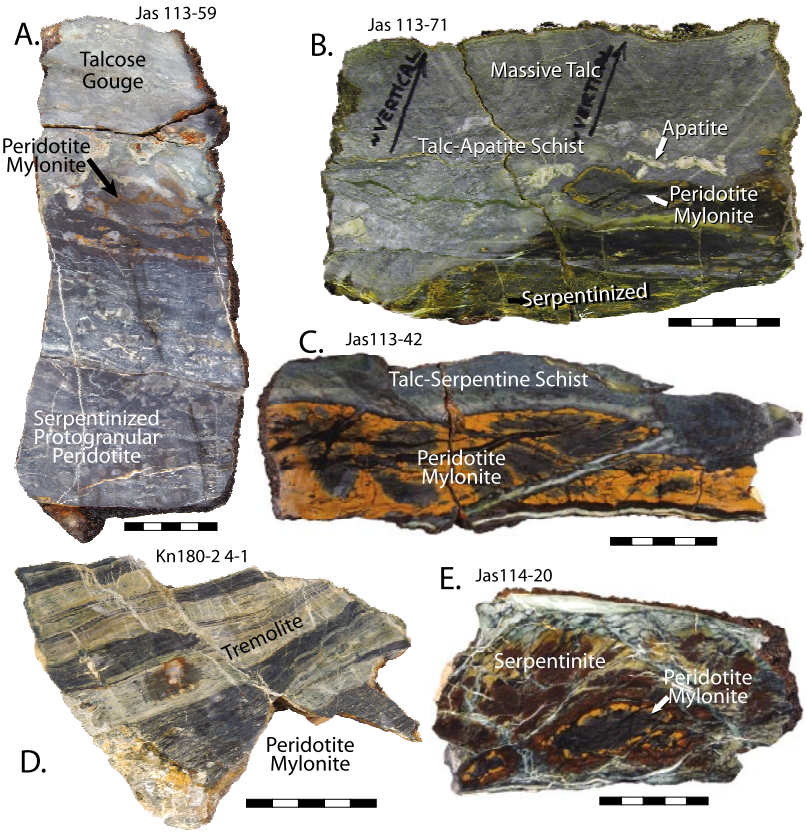

Figure 12. Samples from the detachment shear zone. (a) Jason II 113, sample 59 - peridotite mylonite overlying protogranular to porphyroclastic peridotite in contact with overlying talcose fault gouge with deformed chloritized gabbro along the contact; sampled from near the detachment fault surface at 2521 m in a slide scar along East Fault on the west side of Cain Dome. (b) Jason II 113, sample 71 - deformed talc-chlorite-apatite schist intruding peridotite mylonite; sampled at 2524 m on the west side of Cain Dome. (c) Jason II 113, sample 42 - talc serpentine schist in contact with relatively fresh peridotite mylonite showing local oxidation of olivine due to weathering, from the west side of Cain Dome. (d) Dredge 4, sample 1 - cross-faulted peridotite mylonite showing a small core of slightly oxidized peridotite with alternating mylonite bands replaced by talc-tremolite (white) and talc-serpentine (dark), from East Fault, west side of Cain Dome. (e) Jason II 114, sample 20 - fresh peridotite mylonite with oxidized rim enclosed in a sheared phacoid of talc-serpentine schist; sampled from an area of platy outcrop in slide-scar headwall at 2518 m near the detachment surface on the southeast side of Abel Dome. Scale bars in centimeters.

ly associated with detachment shear zones, so many of these may be serpentinite intrusions along the fault and thus not representative of the underlying bedrock geology. To the south around Adam and Eve Domes, peridotite occurs at three of six sample locations (Figure 2) but is subordinate to dunite and gabbro, and excluding basalts, it is less than 18 wt. % of the rocks (Figure 3b).

[65] Overall, in hand specimen peridotites appear largely to be highly depleted harzburgite tectonites, with only minor, locally occurring lherzolite or plagioclase-bearing peridotite. The great majority of all the peridotites are typical granular porphyroclastic or protogranular tectonites (Figures 11d and 11f). Abundant 3–7 mm enstatite grains with accessory chrome spinel occur in a black to light green, partially serpentinized matrix or in a matrix heavily discolored to orange clay by olivine weathering. Samples from below the detachment surface on slide-scar headwalls and high-angle fault scarps (e.g., Jason II Dives 112–114, and 117, Kanaut Dives 14 and 15, and Dredges 4, 5, 12, 17, 21 and 27) are largely massive, granular, partially serpentinized tectonites.

[66] In contrast to samples from beneath the detachment footwall, peridotites from the fault surface, or near it (e.g., Jason II Dive 116 and Dredges 11, 14, 15, 18, 19, 24 and 28), include abundant highly altered and deformed metaperidotites. These range from high-temperature mylonites (e.g., ~600°–1000°C [*Jaroslow et al.*, 1996]) (Figures 12c, 12d, and 12e), through talc, talc-tremolite, talc-serpen-

tine schists, and sheared serpentinites (Figure 12), to fault gouges of serpentinite, soapstone, and mylonite fragments altered to clay minerals (Figures 6c and 12a). There is often a clear paragenetic sequence found in peridotites from or near the detachment surface (Figure 12). This begins with high-temperature recrystallization and the formation of a narrow (~10 cm) mylonite zone, followed by formation and intrusion of massive talc schist. Static serpentinization then partially pseudomorphed the mylonite and adjacent granular peridotite, while ongoing deformation was accommodated by the talc schist (Figure 12a). These samples are also frequently associated with highly deformed and retrogressively altered gabbros (granulite to zeolite facies).

[67] The primary protogranular to porphyroclastic peridotite fabrics are characteristic of abyssal and ophiolitic peridotite massifs, and they reflect high-temperature solid-state mantle flow and emplacement to shallow depth beneath the crust. The anticipated deformation grade in the absence of detachment faulting is a crystal-plastic deformation intensity of 0 to 2, usually averaging somewhere between those values; only crystal-plastic deformation higher than grade 2 can be related to shallow-level faulting. As shown in Figure 7b, both overall deformation intensity and the number of mylonitic samples with crystal-plastic deformation >2 are higher for the detachment surface than for samples from East and West faults and within slide scars. This is noteworthy because the latter populations include samples taken near tops of scarps and thus within or near the detachment shear zone, and they also include slumped material from that zone. The dichotomy of crystal-plastic deformation in the peridotites mirrors that in the gabbros (Figure 7b). However, there is little difference recorded in brittle deformation (Figure 7a), largely because under brittle-deformation conditions peridotite alters to talc and serpentine. These deform easily through mechanisms that can be described as either plastic or brittle, and therefore their assignment in deformation statistics is rather arbitrary.

7. Discussion

7.1. Detachment Fault Assemblages

[68] Rocks from fault zones should be used with great care in interpreting the geology of the underlying basement. In particular, in an oceanic setting any rock that exhibits cataclasis and retrograde greenschist-facies alteration on a fault that has slipped for more than a few kilometers likely represents fault gouge of entirely ambiguous provenance. Oceanic detachment faults in particular have a long and complex history. They initiate at high temperatures under granulite or even hyper-solidus conditions [*Agar and Lloyd*, 1997; *Dick et al.*, 1991a]. Displacement is initially accommodated by plastic deformation that involves microscopic processes like recrystallization, dislocation glide and diffusion creep, and a fault zone centimeters to meters thick develops, as can be clearly seen in many of the peridotites sampled near the detachment surface at Kane Megamullion (e.g., Figure 12). Deformation is heterogeneous rather than homogeneous, and this leads to the deformation zone migrating in space and time, developing complex imbrications, and widening considerably.

[69] The best-documented oceanic example of this is the Atlantis Bank OCC, a 400-km^2 gabbro massif exposed beneath a single, domed fault surface that extends ~20 km in the spreading direction on the Southwest Indian Ridge. The zone of high-temperature crystal-plastic deformation is >500 m thick, and it includes rocks deformed from hyper-solidus conditions through granulite facies to middle amphibolite facies [*Cannat et al.*, 1991; *Dick et al.*, 1991a, 2000; *Stakes et al.*, 1991]. This zone localized late penetrative melt and volatile flow from crystallizing intrusions and eventually from seawater circulation [*Dick et al.*, 2000; *Kelley and Früh-Green*, 2001], resulting in penetrative alteration and formation of amphibolite gneiss [*Dick et al.*, 1991a, 2000; *Matsumoto et al.*, 2002; *Mével et al.*, 1991; *Stakes et al.*, 1991]. With continued slip and decreasing temperature as the footwall was exhumed, the fault zone localized to a narrow, brittle deformation plane and a new fault zone assemblage developed, consisting of gouge, breccias, and schists between rigid plates of recrystallized rock in the footwall and hanging wall. Ongoing hydrothermal circulation produced alteration in the greenschist facies, continuing down through the zeolite facies until the footwall reached the seafloor [*Arai et al.*, 2001; *Dick et al.*, 2001; *Miranda et al.*, 2002]. Thus such faults, often with 20 km or more of heave, record a complex deformation history under varying P-T-Strain conditions even before one considers that the faults can localize both alteration and igneous intrusion.

[70] Where detachment faults cut across the contact between mantle peridotite and intruded gabbro, for example at weakly magmatic ridge-transform intersections, the situation becomes even more complex. At relatively shallow depths (1–2 km), seawater can

percolate down a fault, hydrate the mantle in the shear zone, and produce serpentine and talc-serpentine schist [e.g., *Boschi et al.*, 2006]. These rocks are weak and highly mobile [e.g., *Moore and Lockner*, 2007], and are notorious for migrating long distances along faults and lubricating them [*Byerlee and Brace*, 1968; *Dengo and Logan*, 1981; *Hirauchi*, 2004, 2005, 2006a, 2006b]. Serpentinites and talc-serpentine schists can thus intrude laterally along a detachment fault to be emplaced beneath the rift-valley floor between footwall gabbros and hanging wall diabase and basalt, and the exhumed footwall can have a thin skin of highly deformed serpentinite and talc-serpentine schists. These metaperidotites commonly entrain high-temperature mylonite blocks that represent the earliest stages of fault nucleation (Figures 12b, 12c, and 12e). The faults can also localize igneous intrusions, as is shown by gabbro veins in serpentinized peridotite mylonites (e.g., Figure 12a) and by undeformed diabase intruding talc schist found in the footwall near the detachment fault surface at Kane Megamullion. Thus, none of the rocks in a talc-serpentine rich shear zone are necessarily representative of the underlying footwall rocks.

[71] In a different tectonic setting 30 km south of the Kane transform, serpentinites and metaperidotites were dredged on the back-tilted detachment surface that comprises the east side of Adam Dome, while only diabase and gabbro are exposed where West Fault cuts deep into its interior (Figure 8). This is consistent with the detachment fault crossing from the Adam and Eve gabbros and dikes into the adjacent, massive Cain and Abel peridotites, from which serpentinites may have been mobilized along the shear zone. The Atlantis Bank OCC provides another example of the mobility of serpentinite and talc-serpentine schists. A 1-m thick sheet of talc-serpentine schist exposed on the detachment fault surface there overlies 500 m of oxide gabbro exposed in a slide-scar headwall [*Dick et al.*, 2001]. This thin schist extends upslope from the top of the headwall over a distance of 7.5 km; it covers $\sim$15 km^2 of the detachment footwall before the underlying massive gabbro remerges at shallow levels because of extensive erosion of the fault surface [*Arai et al.*, 2001], only 5.2 km from the 1505 m of gabbro drilled in Hole 735B. Similarly, drilling at the Atlantis Massif OCC on the MAR [*Blackman et al.*, 2006] shows that a talc-serpentine skin locally overlies 1415 m of gabbro in the detachment footwall; this is only $\sim$5 km from massive peridotite outcrops that are veined by small gabbro bodies on the adjacent transform wall. At the Mt. Mike OCC north of the Fifteen-Twenty FZ on the MAR, a submersible dive also found serpentinized peridotite on the detachment surface, where later drilling penetrated 209 m of gabbro in the footwall [*Shipboard Scientific Party*, 2004].

[72] Considering the mobility of serpentinite and talc-serpentine schists, the presence of these rocks together with entrained peridotite mylonites on the north slope of Babel Dome is a good indicator that the detachment-fault shear zone lies along the transform wall there. The local occurrence of ultramafic schists overlying massive gabbros also indicates that the shear zone passed laterally across the contact where gabbro intrudes the mantle.

7.2. How Representative of Basement Are Our Samples?

[73] As discussed above, our interpretation of true basement lithology relies heavily on sampling headwalls of major slide scars and late high-angle faults that cut the detachment fault at Kane Megamullion. The broader sampling of rocks from the detachment surface itself (Figure 2) undoubtedly includes displaced rocks that are not representative of the underlying basement. Even so, there is a strong correspondence between overall lithologic patterns and the RMBA gravity field over the megamullion [*Maia and Gente*, 1998] (Figures 13 and 14). Earlier work by *Tucholke and Lin* [1994] showed that peridotite with gabbroic intrusions and a thin basaltic cover was common in areas of high RMBA at inside corners of ridge-axis discontinuities. In our study area, *Cannat et al.* [1995b] found a similar correlation near and along the MAR axis from 22° to 24°N, particularly at the 23°10′ discontinuity which marks the southern end of the spreading segment encompassing Kane Megamullion. These results are consistent with seismic observations of thin crust and attenuated layer 3 at segment ends [*Mutter and Mutter*, 1993; *Purdy and Detrick*, 1986; *Tolstoy et al.*, 1993]. As seen in Figure 14, there is elevated RMBA at Cain and Abel Domes on the central part of Kane Megamullion where we sampled largely peridotite. To the north and south where we find evidence for gabbro plutons, the RMBA is reduced, but along the trace of the 23°10′ discontinuity where peridotites were sampled it is again elevated. The lowest RMBA gravity anomaly is observed over the fossil hanging wall just east of the detachment termination where surface morphology and limited sampling indicates that volcanic crust is present. Thus the gravity field supports the general geologic

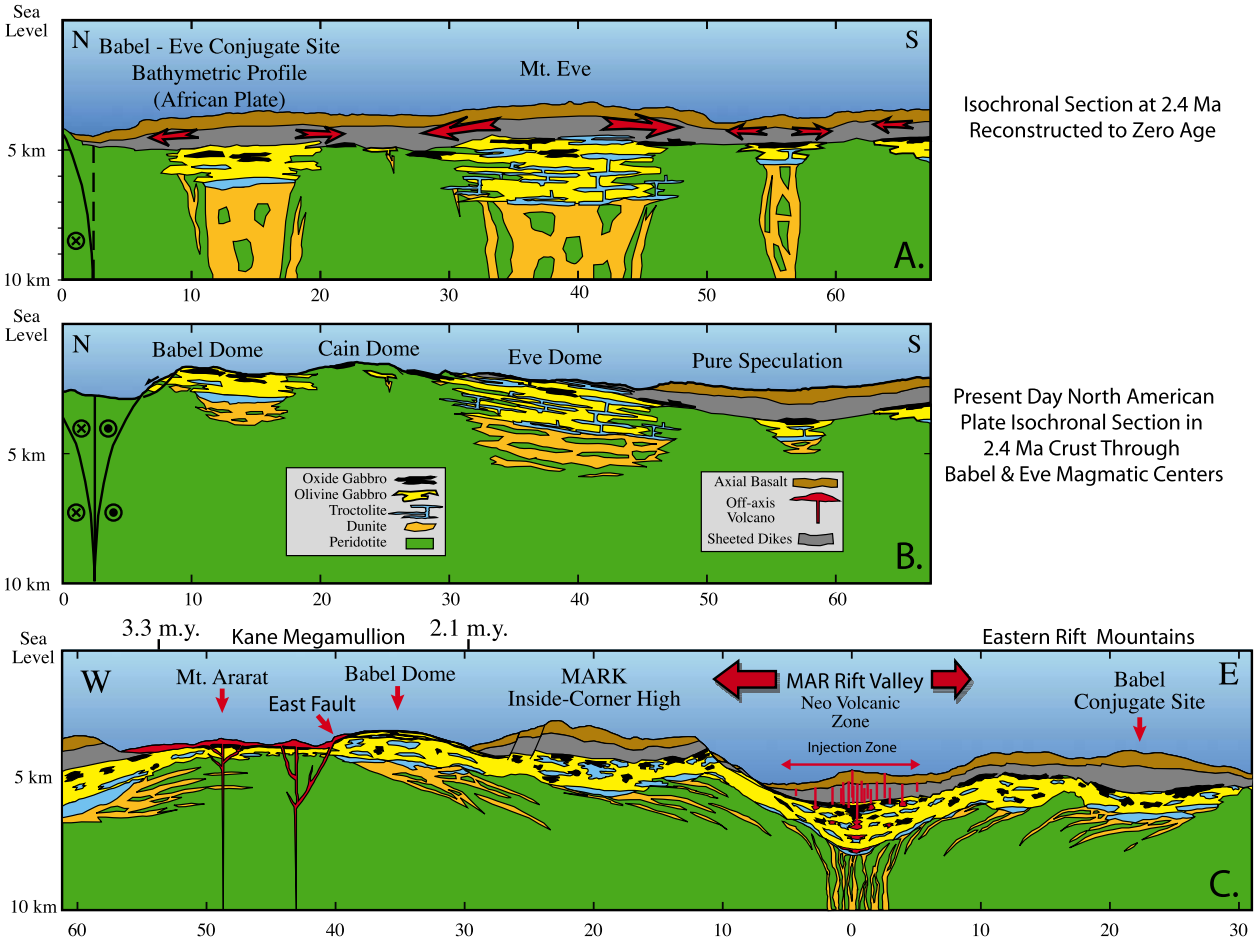

Figure 13. Schematic sketches showing the inferred geology of the Kane core complex. A. Reconstructed, zero-age, isochron-parallel section through Babel and Eve domes, based on a ~N-S bathymetric profile across the ancient volcanic carapace preserved on the African plate in 2.4 Ma crust (between anomalies 2A and 2r). Arrows indicate lateral melt transport at crustal levels. B. Isochron-parallel section in 2.4 Ma crust through the present-day Kane Megamullion on the North American plate. The transform fault is shown as a flower structure, consistent with tracing the transform-parallel, lineated detachment surface of the Kane Megamullion down to the floor of the transform; the circled x and dot indicate motion away from and toward the reader, respectively. C. Present-day ~E-W profile through Mt. Ararat and Babel Domes near the Kane transform, continuing across the MAR rift valley in the MARK area. Actual profile azimuths are parallel and perpendicular to the transform, as shown in Figures 2 and 10.

relations that we have described, as depicted in the schematic diagrams of Figure 13.

7.3. Direct Evidence for Focused Melt Flow at Kane Megamullion

[74] On the basis of the abundance of troctolite and dunite at Adam and Eve Domes, and their near absence across the core complex farther north, melt flow from the mantle appears to have been focused to a relatively narrow, ~10-km-wide zone ~25 km south of the Kane FZ. Experimental studies and microphenocrysts in primitive MORBs show that the sequence of crystallization at lower crustal and shallow mantle pressures is olivine, followed by olivine and plagioclase, and then olivine, plagioclase and clinopyroxene together. Thus, a parental magma will successively crystallize dunite (Ol ± spinel), troctolite (Ol + Pl ± Sp), and then olivine gabbro (Ol + Pl + Cpx), followed by oxide gabbro at about 60–70% crystallization. The troctolites from Adam and Eve Dome, in particular, have forsteritic olivine [*Lissenberg and Dick*, 2006] indicating they crystallized from liquids close to equilibrium with mantle olivine, as expected for primitive magmas directly intruded from the mantle.

[75] Troctolites and troctolitic gabbro are rarely found on transform walls, which raises the problem of the "missing" primitive cumulates needed to

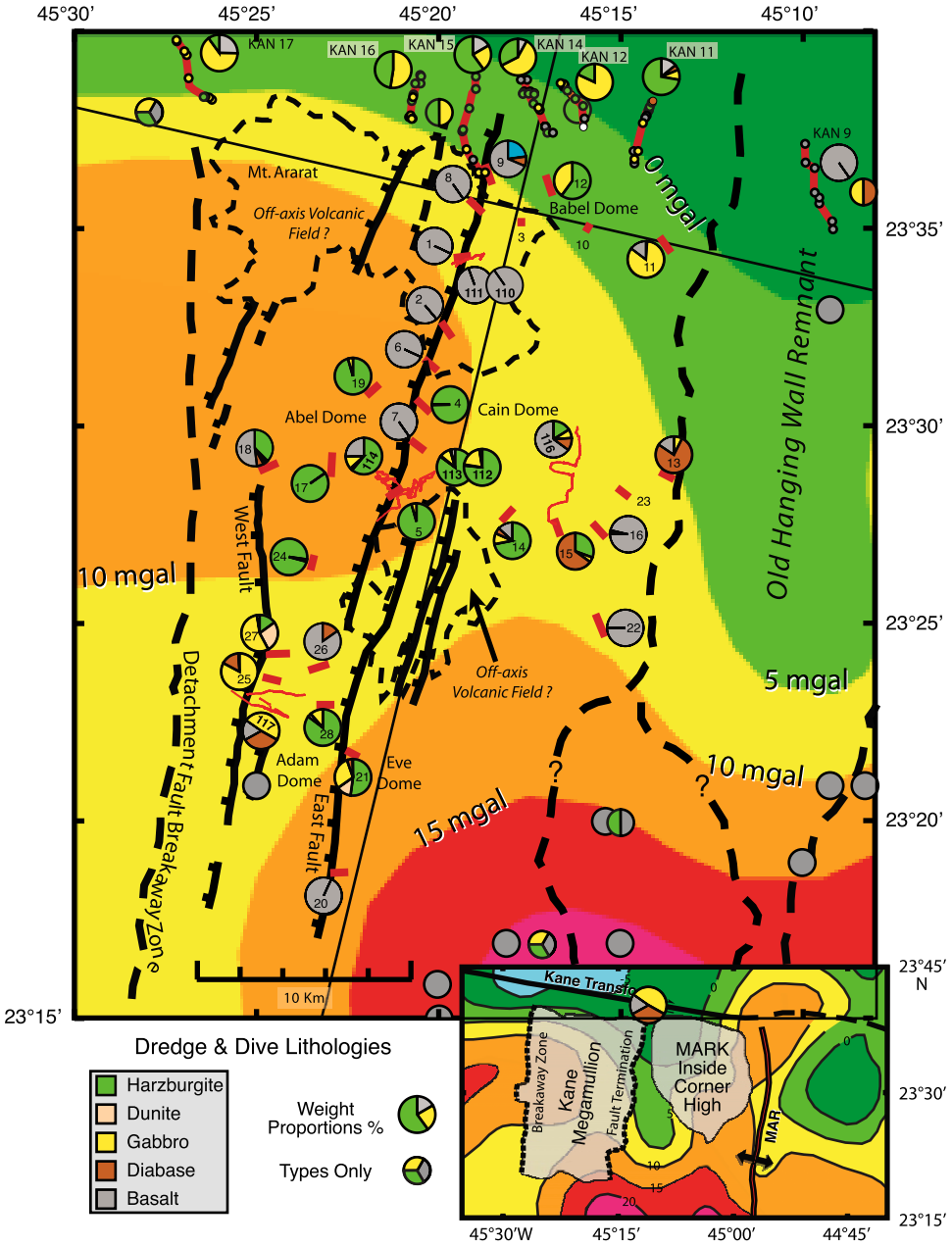

Figure 14. Residual mantle Bouguer anomaly computed using passive flow model from *Maia and Gente* [1998]. Major structures, areas of inferred off-axis volcanism, and the location and contents of dredges and dives at the Kane Megamullion are shown. Thin black lines locate the cross sections in Figure 13. Thin black lines show the positions of the Figure 13 cross sections (which extend beyond the limits of this figure).

mass balance mid-ocean ridge basalts (generally moderately differentiated) back to the composition of likely parent magmas [*Dick et al.*, 2000]. There is considerable speculation, fueled by ODP Leg 209, that the location of such cumulates is in the mantle [*Coogan et al.*, 2001; *Shipboard Scientific Party*, 2004]. At Adam and Eve domes, however, these rocks occur in massive outcrops intercalated with sheeted dikes (Figure 8). Primitive troctolite there occurs together with roughly equal proportions of olivine gabbro (>5% modal olivine) and oxide gabbro (>1% Fe-Ti oxide) (Figure 3b). Olivine gabbro is the most common abyssal gabbro, generally equivalent to more differentiated MORB erupted at rift valleys, while oxide gabbros usually do not have eruptive equivalents [e.g., *Bloomer et al.*, 1989; *Dick et al.*, 1991a]. The proportions of troctolite, olivine gabbro, and oxide

gabbro at Adam and Eve domes are roughly appropriate for in situ crystallization of parental mantle melt, thus marking the southern part of the Kane core complex as a past location for direct intrusion of magma from the mantle.

[76] The close association of harzburgite, dunite, and troctolite at Adam and Eve domes also shows that this was a major zone of late-stage melt transport through the mantle to the crust. Dunites associated with peridotite tectonites largely represent the remains of melt transport channels through the mantle, while, as discussed above, additional dunite may form preceding troctolite by direct precipitation from primary melts. All melts precipitate olivine and dissolve pyroxene as they ascend in the mantle, following the reaction Pyroxene + $Melt_1$ = Olivine + $Melt_2$ as the phase field of olivine expands and that of enstatite and diopside decreases with decreasing pressure [*Kushiro*, 1968; *O'Hara*, 1968]. In the upwelling asthenosphere, melt mass increases as it flows up through the mantle, and where there is sufficient melt, continuous reaction exhausts pyroxene and produces dunite. Thus dunite forms due to focused upward melt flow [*Boudier and Nicolas*, 1972; *Cassard et al.*, 1981; *Ceuleneer and Nicolas*, 1985; *Dick*, 1977; *Dick and Kelemen*, 1991; *Kelemen and Dick*, 1995; *Kelemen et al.*, 1997; *Lago et al.*, 1982; *Leblanc et al.*, 1980; *Nicolas*, 1986; *Quick*, 1981, 1982]. This process continues as melts traverse the lithosphere, even as melt mass decreases, because the thermodynamic driving force remains, and the heat of dissolution and precipitation of pyroxene and olivine are nearly equal [*Kelemen*, 1990].

[77] An elevated volcanic edifice is present in conjugate crust of the same age on the African plate (Figure 1a, box 2; Figure 13a). The shallowest part of this edifice is in the same along-isochron position as Adam and Eve domes. It deepens markedly to the north in positions corresponding to the conjugate Abel, Cain, and Babel Domes, and it also deepens to a lesser extent to the south. Thus all the necessary elements are present to demonstrate melt flow from the mantle to the crust at a focused magmatic center: a prominent volcanic high, primitive troctolites, and abundant dunites. Melt from this center likely was intruded laterally to form the crust to the north and south along-axis (Figure 13a).

7.4. Cain and Abel Peridotite Massif and a Dike-Mantle Transition

[78] In the area of Cain and Abel Domes, basement appears to consist of massive, porphyroclastic peridotite veined by differentiated melts. The abundant diabase and pillow basalt debris sampled from the surface of the megamullion indicates that a dike and pillow-basalt sequence overlay the peridotite, although it was largely removed in the hanging wall. The scarcity of diabase within the footwall suggests that the detachment fault in this area rooted at or through the base of a "dike-mantle" transition. If a large gabbro pluton had been present, the fault most likely would have rooted near or through the dike-gabbro transition, as at Adam Dome and at Atlantis Bank on the Southwest Indian Ridge, and abundant gabbro would be present in the footwall. Furthermore, if the detachment rooted even lower, i.e., through a gabbro-peridotite transition, we would expect that gabbro would be more prominently represented in debris scattered across the megamullion footwall.

[79] The scarcity of dunite among the peridotites at Cain and Abel domes (Figure 3b) also suggests that there was little vertical delivery of primary melt through the shallow mantle there. This is further supported by the scarcity of troctolite and by the abundance of oxide gabbro in vein assemblages in the peridotites. Oxide gabbro (or ferrogabbro) represents a highly evolved basaltic liquid that has previously undergone 70–80% fractional crystallization from parental MORB [e.g., *le Roex et al.*, 1982].

[80] Many Cain and Abel Dome gabbros are highly deformed, consistent with initial intrusion into, and then localized deformaiton in the detachment shear zone beneath the rift valley and possibly in related faults beneath the detachment surface (Table 3, Figures 6b, 11a, and 12a). Gabbro veins in the peridotites consistently localize late deformation, as was also common in the net vein complexes cored in ODP Leg 209 peridotites peripheral to gabbro intrusions [*Shipboard Scientific Party*, 2004].

[81] The presence of moderately to highly evolved gabbro veins over large areas where peridotite is the dominant rock and primitive gabbro is rare might indicate they were intruded from differentiating magma bodies that lay at greater depths or laterally along strike from Babel or Eve domes. Seismic-velocity tomography models across this area show a high-velocity zone that lies beneath

the crest of Cain Dome and continues east to the detachment termination, and this has been interpreted as a large gabbro body emplaced into the detachment footwall (J. C. Canales et al., manuscript submitted to *Geochemistry, Geophysics, Geosystems*, 2008). This gabbro obviously would be younger than that beneath Adam or Eve Domes, assuming a similar origin and emplacement history. If it were originally emplaced at some depth in the shallow mantle, then a net vein complex of oxide and olivine gabbro might be emplaced in the overlying mantle section, which would then be exhumed to the seafloor in the western Cain peridotite section before exhumation of the main gabbro body farther to the east. It is equally possible, however, that the eastern gabbro body was emplaced directly at a shallow level in the crust. The lack of serpentinized peridotite screens in the dike-gabbro sequence on the west face of Adam Dome, however, argues that initial intrusion of the gabbro body there was at crustal levels. If the gabbro body inferred from seismics to the east in Cain Dome has a similar origin, then the most likely explanation for the irregular patchwork of small gabbro intrusions and veins within the Abel and western Cain peridotites is contemporaneous along-axis intrusion of moderately to highly differentiated melts from magmatic centers located to the north and/or south.

7.5. Magmatic Activity at the Ridge-Transform Intersection

[82] At the northern end of Kane Megamullion, gabbro bodies intrude the mantle near the transform and underlie Babel Dome and Mt. Ararat (Figures 4 and 13; see section 5). Their maximum dimensions are difficult to determine due to the presence of the Mt. Ararat volcanics and fault zone assemblages that mask their extent. We can make some estimates at the transform wall, although it should be kept in mind that the orientation of the crust-mantle contact is unknown, and that transforms represent lateral, not vertical sections through the crust. The inferred location of the crust-mantle boundary along the transform wall suggests a significant change in magmatic activity in the vicinity of East Fault (Figure 13c). West of the fault, the contact appears to be shallow, ~3300–3500 m, whereas to the east of the fault it ranges from a lateral intrusive contact at ~4100 m (KAN 14) to minimum depths of ~4500 m (KAN 12) and then possibly shoals to somewhere between ~3900 and 3500 m (KAN 11) (Figure 2). If the depth on the transform wall over which gabbros are exposed bears any relationship to their actual vertical dimension, then the gabbros may be ≥2 km thick beneath Babel Dome. The dives also suggest that the Babel pluton extends a minimum of 7 km to the east of East Fault. There are fewer constraints on the N–S dimension, but gabbros in Dredges 11 and 12 suggest intrusion over at least 5 km in that direction (Figure 2). High velocities in seismic tomography models (Canales et al., submitted manuscript, 2008) suggest that a gabbro layer may be beneath the eastern portion of Cain Dome. Below Mt. Ararat, the gabbro appears to be highly attenuated, less than 500 m thick, based on Kanaut Dives 15 and 16. Farther west, gabbro was sampled in talus over all of Kanaut Dive 17, but the total wall relief was only ~800 m, so the dive provides little constraint on the maximum size of the gabbro body.

[83] The apparently large gabbro pluton and thick crust below Babel Dome contrast with the presumed thin plutonic section below Mt. Ararat, and these features suggest that magmatism became significantly more robust beginning near East Fault (Figure 2). This interpretation, however, hinges on the assumption that the detachment fault that exposed the plutonics consistently rooted at, or through, the dike-gabbro transition and not deeper. For example, if the detachment rooted well below the dike-gabbro transition during exhumation of the Mt. Ararat area (thus explaining a thin gabbro/dike section there), then the conjugate (i.e., the hanging wall) crust should show a relatively thick, normal crustal section. We can assess this by looking at the seafloor morphology of the conjugate crust on the African plate. A prominent, hooked volcanic ridge is developed there at anomaly 2r, and an older, prominent fossil nodal basin is present at anomaly 2An (Figure 1a). These "magmatic" and "amagmatic" features correlate with Babel Dome and Mt. Ararat, respectively (Figure 13c). The relatively amagmatic character of the conjugate to Mt. Ararat indicates that the detachment did not root at unusually great depths when those parcels of crust were emplaced. Furthermore, the volcanic ridge conjugate to Babel Dome argues for subsequent, increased magmatism. Thus it is likely that the detachment fault consistently rooted at the dike-gabbro transition and that our interpretation of increased magmatism east of East Fault is valid.

[84] The Babel Dome pluton presents something of a puzzle. The scarcity of primitive gabbros and the lack of dunite seem to argue that not much melt was delivered directly from the mantle there.

Where then did the melt originate? If the Adam and Eve magmatic center continued to be active during exhumation of the younger part of the megamullion, melt may have intruded northward along fissures and "pooled" adjacent to the old cold transform wall. However, if this were the case, it has not left a very prominent record in the intervening Cain and Abel peridotites. A second possibility is that melt was delivered through the overlying crust in the hanging wall and then channeled downward into the footwall to form the large, deep gabbro pluton, although this seems highly unlikely. The best explanation, then, is the simplest: that melt was delivered more or less vertically to Babel Dome from the underlying mantle, such that the expected dunites and primitive gabbros lie well below the dome and thus farther south than the transform wall.

[85] As noted above, the variations in magmatism inferred from the gabbros emplaced along the transform wall beneath Mt. Ararat and Babel Dome is also seen in the volcanic carapace preserved along the fracture zone trace to the east (see also section 3.3). Waxing and waning magmatism near a transform fault is also seen at Atlantis Bank on the Southwest Indian Ridge. There a 400-km^2-gabbro massif laterally intrudes the mantle near the Atlantis II Transform, [*Dick et al.*, 2001, 1999b]. The contact between gabbro and massive granular peridotite first appears at the crest of the transform wall and then migrates some 7 km closer to the transform as magmatism waxed over a 2.3 ma period. Thus, as at the Kane and Atlantis II fracture zones, transform walls may expose only massive peridotite, peridotite net-veined by small gabbro intrusions presumably peripheral to a large gabbro body, or massive gabbro; consistent with waxing and waning of melt flow from the mantle.

7.6. Melt Transport and Crustal Accretion at Slow-Spreading Ridges

[86] We note that the Babel gabbro massif is in younger lithosphere than that at Adam and Eve Domes, and thus it likely reflects a separate episode of magmatism that initiated later. It is also possible that farther east of the section drawn in Figure 13b a more continuous gabbro layer extends southward beneath Cain Dome. This is consistent with a sharp west to east increase in seismic velocity beneath Cain Dome that suggests an eastward transition from serpentinized peridotite to gabbro (Canales et al., submitted manuscript, 2008). This could represent either greatly increased magma input to the Babel magmatic center with time, or possibly formation of a new magmatic center beneath Cain Dome that merged with that to the north to form a relatively continuous gabbro layer. The broad swales separating Cain Dome from domes to the north and south suggest significant along isochron variability in crustal stratigraphy, consistent with the latter hypothesis.

[87] In this paper we have shown an example of shallow mantle melt flow focusing to a narrow region beneath a second-order, slow-spreading ridge segment. It is clear, however, that the position of major magmatic centers fed by that flow, and the melt fluxes involved, vary both in time and space along the segment. Thus, melt flow most likely is not generally focused simply to the midpoint of magmatic segment as previously suggested [e.g., *Whitehead et al.*, 1984]. This may explain the lack of any descriptions of regular distribution of dunites in mantle sections of large ophiolite massifs that would reflect long-term (millions of years) melt focusing to a single locus in the shallow mantle beneath a ridge.

7.7. Comparison to Ophiolites: Mantle Flow at Slow Versus Fast Spreading Ridges

[88] "Intact" ophiolites such as Troodos, Bay of Islands, and Oman preserve large sections of mantle tectonite and gabbro that in principle should allow us to make comparisons to Kane Megamullion. In general, however, the tectonic setting of ophiolites is debated, and most ophiolites are attributed on geochemical grounds to "supra-subduction zone" environments including back-arc basins. These ophiolites are crystalline thrust sheets that lack a natural, underlying decollément zone. The internal strength of such thrust sheets is too weak to support them in the absence of a lubricating zone at their base [*Hubbert and Rubey*, 1959]. This problem is resolved in regions of unusually high heat flow such as in back-arc basins and fast spreading mid-ocean ridges where a shallow brittle-ductile transition can serve as the decollément zone [*Armstrong and Dick*, 1974]. However, this makes it likely that most ophiolites represent ridges that have very thin lithosphere. Thus, geochemical characteristics aside, it is difficult to identify a possible ophiolite section of slow-spreading ocean crust and mantle with any degree of confidence.

[89] Despite these uncertainties, it is useful to compare our results with a well-known ophiolite section. The Oman ophiolite, although generally

believed to have been modified in an arc environment [e.g., *Alabaster et al.*, 1982], is generally taken as the type example of fossil fast spreading ocean crust [e.g., *Nicolas*, 1989]. Moreover, Oman is possibly the only place where mapping has proceeded to the point that zones of focused mantle flow can be identified with confidence. The mapping has described mantle diapirs defined by flow structures that are broadly consistent with the spreading direction deduced from the orientations of sheeted dikes in the overlying crustal section [e.g., *Nicolas*, 1989]. Mafic veins [*Ceuleneer et al.*, 1996; *Python and Ceuleneer*, 2003] and tabular dunite bodies [*Braun and Kelemen*, 2002] in the peridotite also parallel this orientation. The mapped vein distribution provides direct evidence for transport of primitive melts represented by troctolite and olivine gabbro; these are focused along an 80-km-long corridor centered on the Maqsad mantle diapir and are roughly parallel to the paleo-spreading axis [*Ceuleneer et al.*, 1996; *Python and Ceuleneer*, 2003]. This contrasts sharply with the far more restricted ~10 km zone of focused melt flow centered about Adam and Eve Domes at Kane Megamullion. The dichotomy of these observations is consistent with the proposition that mantle and melt flow beneath slow-spreading ridges is highly three-dimensional, while such flow at fast spreading ridges is broadly two-dimensional [*Lin and Phipps Morgan*, 1992].

7.8. Where Are the Sheeted Dikes?

[90] Several authors have noted a deficiency of diabase exposed on transform walls and rift valley walls, relative to the hypothetical Penrose model for ocean crust. This led to the suggestion that a uniform sheeted-dike layer may be absent at slow-spreading ridges, reflecting an erratic magma supply or heterogeneous accretion across rift valleys, and that structurally complex ocean crust without a simple layered structure may be typical of many slow-spreading ridges [*Karson*, 1998]. This seems to conflict with seismic refraction results that predict ~1.5 km of sheeted dikes and a simple layered structure beneath much of the Atlantic [*Houtz and Ewing*, 1979], although recent work suggests that much of the shallow crustal layering could be due to depth-dependent alteration [*Christeson et al.*, 2007]. In part, however, the apparent conflict may stem from a failure to recognize diabase in dredge hauls because many investigators work under the assumption that such rocks generally have medium grain size. In fact, inspection of sheeted dike complexes on land shows that medium-grained diabase is subordinate to fine- and very-fine-grained diabase. At Kane Megamullion, it is clear that there are numerous dike rocks, the majority of which are fine grained (see section 6.2).

[91] As previously discussed, uneroded OCCs often expose a thin layer (meters thick) of cataclastic rocks that are intruded by gabbro, diabase, and talc-serpentine schist and contain entrained higher-temperature debris from the hanging wall and footwall. Although these may be misleading as to the nature of the underlying basement, they provide valuable evidence of what was in the hanging wall. At Kane Megamullion, abundant diabase sampled across the detachment footwall at Cain and Abel domes provides evidence of an overlying dike complex, while a scarcity of gabbro and diabase within the footwall suggests that a gabbroic layer 3 was intermittent or absent. At Babel Dome, only one of three dredges contains diabase, and this might suggest either that the detachment fault rooted well below the dike-gabbro transition or that a sheeted dike layer was absent. Given our small, possibly nonrepresentative sample, however, no firm conclusions can be drawn.

[92] The common occurrences of diabase scattered across the surface of Kane Megamullion, the presence of large inliers of the dike-gabbro transition at Adam Dome, and the presence of similar inliers at numerous locations at Atlantis Bank OCC [*Dick et al.*, 2001] all show that detachment faults that form OCCs commonly root through the dike-gabbro transition. Wherever this occurs, most of the sheeted dikes will be removed with the hanging wall, and the footwall will be dominated by gabbros and peridotites. This, in large part, probably accounts for the absence of diabase in tectonic windows at slow- and ultraslow-spreading ocean ridges.

7.9. Plutonic Growth Faults

[93] The large-throw, long-lived normal faults that form OCC's have been termed ''detachment faults'' based on analogy to faults that form continental metamorphic core complexes of similar scale and morphology [e.g., *Cann et al.*, 1997; *Karson*, 1999; *Tucholke et al.*, 1996, 1998]. These faults, however, differ from continental core complexes in several significant ways. At ridge-transform intersections they represent the integrated expression of extension and corner-flow at the plate boundary where they are a continuation of the active transform fault. They also constitute a focused narrow plate boundary during core com-

plex emplacement, rather than a diffuse or widespread zone of plate extension. Instead extension across the rift valley is concentrated along the active fault trace at the base of the rift valley wall rather than in the center of the axial valley.

[94] Most critically, unlike continental core complexes, detachment faults at oceanic core complexes are non-conservative. During more magmatic periods melt may be added at any depth in the overlying hanging wall, up to and including the seafloor. However, even during relatively avolcanic periods, when little or no growth of the upper plate occurs, melt and/or rising asthenosphere are continuously added to the base of the footwall as seafloor spreading continues. Thus, for example, spreading may occur largely by the emplacement and growth of gabbroic intrusions in the footwall, with significantly less addition to the overlying volcanic section. This can result in highly asymmetric seafloor spreading, as is the case at Kane Megamullion (section 3.2). At the Atlantis Bank gabbro massif on the Southwest Indian Ridge, spreading in the direction of core complex emplacement was at more than twice the rate of spreading in the opposite direction [*Dick et al.*, 1991b; *Hosford et al.*, 1999; *Williams*, 2007]. Although we have used the general term "detachment fault" here, the above considerations show that long-lived normal faults that form oceanic core complexes should be regarded as a special class of detachment fault due to their nonconservative nature. We propose here that they be termed plutonic growth faults.

7.10. Off-Axis Volcanism

[95] If the East Fault volcanics erupted off-axis, they probably were not emplaced far from the rift axis due to lithospheric cooling with age. A possible mechanism for emplacement is related to stress distribution in the megamullion as it was exhumed. If we consider the footwall to be a bending "beam," then its lower part was in compression and its upper part was in extension as it rolled over [*Manning and Bartley*, 1994]. This stress differential should force any melt at depth in the footwall toward the surface and could result in surficial volcanism along active faults [*Tucholke et al.*, 2001].

8. Conclusions

[96] The MARK area of the Mid-Atlantic Ridge has been considered to be a classic representative of a normal, slow-spreading magmatic ridge segment, both in terms of geochemistry [*Bryan et al.*, 1981] and in terms of regional seismic structure [*Purdy et al.*, 1978]. Within this spreading segment, long-lived slip on the detachment fault that formed Kane Megamullion exposed much of the plutonic foundation of the crust between about 3.3 and 2.1 Ma. Our studies of this foundation show major features that do not fit the Penrose model for "normal" ocean crust, the traditional seismic models, or alternates such as the "gabbro-pudding" model for slow-spreading ridges. Our principal conclusions are as follows.

[97] 1. For the first time, we directly document focused melt delivery through the shallow mantle to a narrow region (~10 km) within a slow-spreading ridge segment. This region (Adam and Eve Domes) is in the southern part of Kane Megamullion and somewhat south of the center of the enclosing spreading segment (Figure 1b). Adam and Eve domes are characterized by the presence a full gabbro suite including primitive troctolite intruded by sheeted dikes with abundant spatially associated dunite. Crust of the same age on the conjugate ridge flank exhibits a robust, elevated volcanic ridge system that correlates with this locus of magmatism and becomes more subdued and deeper away from it.

[98] 2. The zone of focused melt supply is flanked to the north by an elevated region (Cain and Abel Domes) of comparable lateral scale that appears to be weakly magmatic. It consists primarily of porphyroclastic to protogranular peridotite tectonites with evolved gabbro and oxide gabbro vein assemblages and scattered diabase, but there is little evidence for any vertical melt transport through the mantle. This region correlates with a zone of elevated RMBA gravity (i.e., thinner crust). On the basis of the internal geology of the footwall and on hanging wall debris scattered over the footwall surface, the detachment fault appears to have rooted in a mantle-dike transition.

[99] 3. At the north end of Kane Megamullion (Babel Dome), a large ($\geq$~5–7 km) pluton containing olivine gabbro and minor oxide gabbro was intruded into the mantle adjacent to Kane transform. This, together with the physiography of volcanic crust of the same age on the conjugate plate, indicates a period of robust volcanism near the transform. It is likely that the pluton was connected to an underlying melt source in the mantle, although we lack direct evidence to dem-

onstrate this other than a corresponding local axial volcanic high preserved on the conjugate crust.

[100] 4. Our results document at least two major, apparently independent magmatic centers that are offset in space and time within a single second-order spreading segment. This observation is consistent with waxing and waning of volcanism with time, as well as with along-isochron variations in robustness of volcanic ridges, both of which are recorded in the volcanic carapace preserved in the rift mountains of the conjugate crust. Magmatic cycles occur on timescales of hundreds of thousands to millions of years and at space scales of tens of kilometers beneath a single ridge segment, rather than being focused at a single central point. This is consistent with plate-driven flow that engenders local, stochastically distributed transient instabilities at depth in the partially molten mantle beneath longer segments. Fixed boundaries, such as large offset fracture zones, or relatively short segment lengths, however, may help to focus melt transport to the same location.

[101] 5. Possible off-axis volcanism is documented along portions of high-angle, isochron-parallel faults that may have occurred along or at the crest of the rift-valley wall during exhumation of the megamullion. As proposed by *Tucholke et al.* [2001], this may occur because melt contained within the footwall can be forced to the surface by differential stress between the lower (compressional) and upper (tensional) parts of the bending footwall as it was exhumed. Such off-axis volcanism, although likely volumetrically small, may be more common than previously thought, at least on the deforming footwalls of large-offset detachment faults.

[102] 6. Long-lived oceanic detachment faults differ significantly from those that form continental core complexes. At ridge-transform intersections they merge with the active transform fault and are a direct expression of corner flow and exhumation of deep lithosphere at the plate boundary. Mid-ocean ridge detachment faults are non-conservative and can be best described as plutonic growth faults. Unlike normal growth faults where mass is added continuously to the surface of the faulted terrain, plutonic growth faults accrete mass from rising asthenosphere or intruding melts at the base of the footwall. This occurs even when the overlying hanging wall may accrete little or no new material, and it is an important mechanism whereby "tectonic extension" is accommodated at slow-spreading ridges. Viewed from the perspective of rocks exposed only at the seafloor, this is "amagmatic accretion." We note, however, that if this accretion includes significant intrusion of gabbros into the footwall, it is hardly "amagmatic" or solely "tectonic."

[103] 7. There is remarkable geologic diversity at Kane Megamullion that documents robust, large-scale (~10 km) variability in melt source, transport, accumulation, and composition within a single second-order ridge segment. These variations are more dramatic than previously anticipated in early models for melt focusing at ridges [e.g., *Dick*, 1989; *Whitehead et al.*, 1984]. Although our results document crustal architecture that is different from existing models, with not one, but at least two principal magmatic centers within a spreading segment, in our view the other models remain valid for specific tectonic settings [see also *Dick et al.*, 2006]. For fast spreading crust, there is little evidence to challenge the Penrose ophiolite model. Toward the slow-spreading end of the spectrum, the *Cannat* [1993] model, in which lower crust is a mixture of gabbro plugs and peridotite screens, explains the geology of a substantial region of magma-poor MAR crust near the Fifteen-Twenty FZ. In environments that are even more magma-limited, such as the ultraslow-spreading Gakkel Ridge and Southwest Indian Ridge, the crystalline basement at nearly amagmatic spreading segments appears to be massive mantle peridotite accompanied by only scattered basalt and rare gabbro [*Dick et al.*, 2003; *Michael et al.*, 2003]. Finally, crust formed at mid-ocean ridges near mantle hot spots (e.g., Iceland) must differ significantly from all of these environments. We conclude that the structure of the ocean crust is far more variable than previously thought, and changes dramatically with spreading rate, ridge geometry, mantle temperature, composition, and melt productivity of the mantle [e.g., *Dick et al.*, 2006].

Acknowledgments

[104] We gratefully acknowledge the hard work and contributions of the Knorr Cruise 180 Leg 2 scientific party and the Jason II ROV and ABE AUV groups. In particular, we note insightful comments and contributions of Mike Cheadle, who makes an excellent metamorphic petrologist. Tivey participated in the Kanaut Expedition at the kind invitation of Jean-Marie Auzende and Ifremer, and he thanks the scientific party for their insights and the chief scientist for access to the cruise data. We particularly acknowledge the cruise report prepared by the Kanaut scientific party, without whose observations much of our analysis would not be possible. We apologize in advance for any ill-informed reinterpretations they might find

particularly annoying. Invaluable information on the Kanaut dive results was obtained from the thesis of Indraneel Ghose; although cited in the text, we wish to draw particular attention to this document, available through interlibrary loan, and to the contribution of Mathilde Cannat, the Directrice de thèse who brought this work to our attention. We also thank Pablo Canales, who made his seismic-velocity tomography models at Kane Megamullion freely available to us, and Clare Williams for sharing her insights drawn from analysis of rock magnetics and surface and near-bottom magnetics at Kane megamullion. Johan Lissenberg provided helpful discussions and shared mineral data on Kane Megamullion gabbros. Margaret Sulanowska provided photography and XRD analysis. Georges Ceuleneer and Rob Pockalny provided helpful comments that greatly improved the manuscript. NSF Grants OCE-0118445, OCE-0624408 and OCE-0621660 supported this research. B. Tucholke was also supported by the Henry Bryant Bigelow Chair in Oceanography at Woods Hole Oceanographic Institution.

References

Agar, S. M., and G. E. Lloyd (1997), Deformation of Fe-Ti oxides in gabbroic shear zones from the MARK area, *Proc. Ocean Drill. Program Sci. Results*, *153*, 123–135.

Agar, S. M., J. F. Casey, and P. D. Kempton (1997), Textural, geochemical and isotopic variations in gabbroic shear zones from the MARK area, Mid-Atlantic Ridge, *Proc. Ocean Drill. Program Sci. Results*, *153*, 99–122.

Alabaster, T., J. A. Pearce, and J. Malpas (1982), The volcanic stratigraphy and petrogenesis of the Oman Ophiolite Complex, *Contrib. Mineral. Petrol.*, *81*, 168–183, doi:10.1007/BF00371294.

Arai, S., H. J. B. Dick, and the MODE 2000 Scientific Party (2001), *Cruise Report MODE 2000 (Kairei/Kaiko KR00–06) Investigation of Atlantis Bank and the SW Indian Ridge from 57°E to 62°E*, 337 pp., Jpn. Mar. Sci. and Technol. Cent., Yokosuka, Japan.

Armstrong, R. L., and H. J. B. Dick (1974), A model for the development of thin overthrust sheets of crystalline rock, *Geology*, *2*, 35–40, doi:10.1130/0091-7613(1974)2<35:AMFTDO>2.0.CO;2.

Auzende, J.-M., J. Honnorez, Y. Lagabrielle, J. Malavieille, V. Mamaloukas-Frangoulis, and C. Mével (1989a), Direct observation of a section through slow-spreading oceanic crust, *Nature*, *337*, 726–729, doi:10.1038/337726a0.

Auzende, J.-M., J. Honnorez, Y. Lagabrielle, J. Malavieille, V. Mamaloukas-Frangoulis, and C. Mével (1989b), L'intersection entre la Zone de Fracture Vema et la dorsale médio-Atlantique: Résultats préliminaires del la campagne Vemanaute, *C. R. Acad. Sci. Paris*, *309*, 1341–1348.

Auzende, J.-M., M. Cannat, M. P. Gente, P. J.-P. Henriet, T. Juteau, J. Karson, Y. Lagabrielle, C. Mével, and M. Tivey (1992), Rapport de la Campagne Kanaut du Nautille sur le N/O Nadir, 15 Novembre – 16 Decembre 1992, 426 pp. Ifremer, Brest.

Auzende, J.-M., M. Cannat, M. P. Gente, J.-P. Henriet, T. Juteau, J. Karson, Y. Lagabrielle, C. Mével, and M. Tivey (1993), Affleurements des roches profondes de la croûte océanique et du manteau sur le mur sud de la fracture Kane (Atlantique central): Observations par submersible, *C. R. Acad. Sci. Paris*, *317*, 1641–1648.

Auzende, J.-M., M. Cannat, M. P. Gente, J.-P. Henriet, T. Juteau, J. Karson, Y. Lagabrielle, C. Mével, and M. Tivey (1994), Observation of sections of oceanic crust and mantle cropping out on the southern wall of Kane FZ (N. Atlantic), *Terra Nova*, *6*, 143–148, doi:10.1111/j.1365-3121.1994.tb00647.x.

Blackman, D. K., B. Ildefonse, B. E. John, Y. Ohara, C. J. MacLeod, and Expedition 304/305 Scientists (2006), *Proc. Integr. Ocean Drill. Program, 304–305*, doi:10.2204/iodp.proc.304305.302006.

Bloomer, S. H., J. H. Natland, and R. L. Fisher (1989), Mineral relationships in gabbroic rocks from fracture zones of Indian Ocean ridges: evidence for extensive fractionation, parental diversity and boundary-layer recrystallization, in *Magmatism in the Ocean Basins*, edited by A. D. Saunders and M. J. Norry, *Geol. Soc. Am. Spec. Publ.*, *42*, 107–124.

Bonatti, E., and M. Seyler (1987), Crustal underplating and evolution in the Red Sea Rift: Uplifted gabbro/gneiss crustal complexes on Zabargad and Brothers Islands, *J. Geophys. Res.*, *92*, 12,803–12,812.

Bonatti, E., A. Peyve, P. Kepezhinskas, N. Kurentsova, M. Seyler, S. Skolotnev, and G. Udintsev (1992), Upper mantle heterogeneity below the Mid-Atlantic Ridge, 0°–15°N, *J. Geophys. Res.*, *97*, 4461–4476.

Boschi, C., G. L. Frueh-Green, A. G. Delacour, D. S. Kelley, and J. A. Karson (2006), Mass transfer and fluid flow during detachment faulting and development of an oceanic core complex, Atlantis Massif (MAR 30°N), *Geochem. Geophys. Geosyst.*, *7*, Q01004, doi:10.1029/2005GC001074.

Boudier, F., and A. Nicolas (1972), Fusion partielle gabbroique dans la lherzolite de Lanzo, *Bull. Suisse Mineral. Petrogr.*, *52*, 39–56.

Braun, M. G., and P. B. Kelemen (2002), Dunite distribution in the Oman Ophiolite: Implications for melt flux through porous dunite conduits, *Geochem. Geophys. Geosyst.*, *3*(11), 8603, doi:10.1029/2001GC000289.

Bryan, W. B., G. Thompson, and J. N. Ludden (1981), Compositional variation in normal MORB from 22°–25°N: Mid-Atlantic Ridge and Kane Fracture Zone, *J. Geophys. Res.*, *86*, 11,815–11,836.

Byerlee, J. D., and W. F. Brace (1968), Stick slip, stable sliding, and earthquakes; effect of rock type, pressure, strain rate, and stiffness, *J. Geophys. Res.*, *73*, 6031–6037.

Cann, J. R., D. K. Blackman, D. K. Smith, E. McAllister, B. Janssen, S. Mello, E. Avgerinos, A. R. Pascoe, and J. Escartin (1997), Corrugated slip surfaces formed at ridge-transform intersections on the Mid-Atlantic Ridge, *Nature*, *385*, 329–332, doi:10.1038/385329a0.

Cannat, M. (1991), Plastic deformation at an oceanic spreading ridge: A microstructural study of the Site 735 gabbros (Southwest Indian Ocean), *Proc. Ocean Drill. Program Sci. Results*, *118*, 399–408.

Cannat, M. (1993), Emplacement of mantle rocks in the seafloor at mid-ocean ridges, *J. Geophys. Res.*, *98*, 4163–4172, doi:10.1029/92JB02221.

Cannat, M. (1996), How thick is the magmatic crust at slow-spreading oceanic ridges, *J. Geophys. Res.*, *101*, 2847–2857.

Cannat, M., C. Mevel, and D. Stakes (1991), Normal ductile shear zones at an oceanic spreading ridge: Tectonic evolution of Site 735 gabbros (southwest Indian Ocean), *Proc. Ocean Drill. Program Sci. Results*, *118*, 415–430.

Cannat, M., D. Bideau, and H. Bougault (1992), Serpentinized peridotites and gabbros in the Mid-Atlantic Ridge axial valley at 15°37′N and 16°52′N, *Earth Planet. Sci. Lett.*, *109*, 87–106, doi:10.1016/0012-821X(92)90076-8.

Cannat, M., , J. A. Karson, and D. J. Miller (Eds.) (1995a), *Proceedings of Ocean Drill. Program, Initial Reports*, 798 pp., Ocean Drilling Program, College Station, Tex.

Cannat, M., et al. (1995b), Thin crust, ultramafic exposures, and rugged faulting patterns at the Mid-Atlantic Ridge (22°–24°N), *Geology*, *23*, 49–52, doi:10.1130/0091-7613(1995)023<0049:TCUEAR>2.3.CO;2.

Cannat, M., G. Ceuleneer, and J. Fletcher (1997a), Localization of ductile strain and the magmatic evolution of gabbroic rocks drilled at the Mid-Atlantic Ridge (23°N), *Proc. Ocean Drill. Program Sci. Results*, *153*, 77–98.

Cannat, M., Y. Lagabrielle, H. Bougault, J. Casey, N. de Coutures, L. Dmitriev, and Y. Fouquet (1997b), Ultramafic and gabbroic exposures at the Mid-Atlantic Ridge: Geologic mapping in the 15°N region, *Tectonophysics*, *279*, 193–213.

Casey, J. F., M. G. Braun, T. Fujiwara, T. Matsumoto, P. B. Kelemen, and the Scientific Party (1998), Megamullions along the Mid-Atlantic Ridge between 14 and 16N: Results of Leg 1, JAMSTEC/WHOI Mode 98 survey, *Eos Trans. AGU*, *79*, Fall Meet. Suppl., F920.

Cassard, D., A. Nicolas, M. Rabinovitch, J. Moutte, M. Leblanc, and A. Prinzhofer (1981), Structural classification of chromite pods in Southern New Caledonia, *Econ. Geol.*, *76*, 805–831.

Ceuleneer, G., and A. Nicolas (1985), Structures in podiform chromite from the Maqsad district (Sumail ophiolite, Oman), *Mineralium Deposita*, *20*, 177–185, doi:10.1007/BF00204562.

Ceuleneer, G., M. Monnereau, and I. Amri (1996), Thermal structure of a fossil mantle diapir inferred from the distribution of mafic cumulates, *Nature*, *379*, 149–153, doi:10.1038/379149a0.

Christeson, G. L., K. D. McIntosh, and J. A. Karson (2007), Inconsistent correlation of seismic layer 2A and lava layer thickness in oceanic crust, *Nature*, *445*, 418–421, doi:10.1038/nature05517.

Conference Participants (1973), Penrose Field Conference: Ophiolites, *Geotimes*, *17*, 24–26.

Coogan, L., C. J. McCleod, H. J. B. Dick, S. J. Edwards, A. Kvassnes, J. H. Natland, P. T. Robinson, G. Thompson, and M. J. O'Hara (2001), Whole rock geochemistry of gabbros from the Southwest Indian Ridge: Constraints on geochemical fractionations between the upper and lower crust and magma chamber processes at (very) slow-spreading ridges, *Chem. Geol.*, *178*, 1–22, doi:10.1016/S0009-2541(00)00424-1.

Cormier, M.-H., and R. S. Detrick (1984), Anomalously thin crust in oceanic fracture zones: New seismic constraints from the Kane Fracture Zone, *J. Geophys. Res.*, *89*, 10,249–10,266.

DeMets, C., R. G. Gordon, D. F. Argus, and S. Stein (1990), Current plate motions, *Geophys. J. Int.*, *101*, 425–478, doi:10.1111/j.1365-246X.1990.tb06579.x.

Dengo, C. A., and J. M. Logan (1981), Implications of the mechanical and frictional behavior of serpentinite to seismogenic faulting, *J. Geophys. Res.*, *86*, 10,771–10,782.

Detrick, R. S., M.-H. Cormier, R. A. Prince, D. W. Forsyth, and E. L. Ambos (1982), Seismic constraints on the crustal structure within the Vema fracture zone, *J. Geophys. Res.*, *87*, 10,599–10,612.

Detrick, R. S., J. Collins, R. Stephen, and S. Swift (1993a), In situ evidence for the nature of the seismic layer 2/3 boundary in oceanic crust, *Nature*, *370*(1994), 288–290.

Detrick, R. S., R. S. White, and G. M. Purdy (1993b), Crustal structure on North Atlantic fracture zones, *Rev. Geophys.*, *31*, 439–458, doi:10.1029/93RG01952.

Dick, H. J. B. (1977), Evidence of partial melting in the Josephine Peridotite, in *Magma Genesis*, edited by H. J. B. Dick, pp. 59–62, Oreg. Dept. of Geol. and Mineral Indust., Portland, Ore.

Dick, H. J. B. (1989), Abyssal peridotites, very slow-spreading ridges and ocean ridge magmatism, in *Magmatism in the Ocean Basins*, edited by A. D. Saunders and M. J. Norry, *Geol. Soc. Am. Spec. Publ.*, *42*, 71–105.

Dick, H. J. B., and P. B. Kelemen (1991), Chromian spinel as a petrogenetic indicator of magmagenesis in shallow mantle rocks, *Eos Trans. AGU*, *72*, Fall Meet. Suppl., F142.

Dick, H. J. B., S. Arai, J. G. Hirth, B. J. John, and Kr-06 Scientific Party (2001), A subhorizontal cross-section through the crust mantle boundary at the SW Indian Ridge, *Geophys. Res. Abstr.*, *3*. (Available at http://www.copernicus.org/EGS/egsga/nice01/programme/abstracts/aai3777.pdf)

Dick, H. J. B., G. Thompson, and W. B. Bryan (1981), Low-angle faulting and steady-state emplacement of plutonic rocks at ridge-transform intersections, *Eos Trans. AGU*, *62*, Fall Meet. Suppl., F406.

Dick, H. J. B., R. L. Fisher, and W. B. Bryan (1984), Mineralogic variability of the uppermost mantle along mid-ocean ridges, *Earth Planet. Sci. Lett.*, *69*, 88–106.

Dick, H. J. B., P. S. Meyer, S. Bloomer, S. Kirby, D. Stakes, and C. Mawer (1991a), Lithostratigraphic evolution of an in-situ section of oceanic layer 3, *Proc. Ocean Drill. Program: Sci. Results*, *118*, 439–540.

Dick, H. J. B., H. Schouten, P. S. Meyer, D. G. Gallo, H. Bergh, R. Tyce, P. Patriat, K. T. M. Johnson, J. Snow, and A. Fisher (1991b), Tectonic evolution of the Atlantis II Fracture Zone, *Proc. Ocean Drill. Program Sci. Results*, *118*, 359–398.

Dick, H. J. B., J. H. Natland, and D. J. Miller (Eds.) (1999a), *Proceedings of Ocean Drilling Program, Initial Reports (CD-ROM)*, Ocean Drill. Progr., College Station, Tex.

Dick, H. J. B., H. Schouten, B. John, H. Kinoshita, J. H. Natland, C. J. MacLeod, and J. G. Hirth (1999b), Evidence for a "melt lens" equivalent in the lower crust at an ultra-slow-spreading ridge, *Eos Trans. AGU*, *80*, Fall Meet. Suppl., F956.

Dick, H. J. B., et al. (2000), A Long In-Situ Section of the Lower Ocean Crust: Results of ODP Leg 176 Drilling at the Southwest Indian Ridge, *Earth Planet. Sci.*, *179*, 31–51, doi:10.1016/S0012-821X(00)00102-3.

Dick, H. J. B., J. Lin, and H. Schouten (2003), An ultraslow-spreading class of ocean ridge, *Nature*, *426*, 405–412, doi:10.1038/nature02128.

Dick, H. J. B., J. H. Natland, and B. Ildefonse (2006), Past and future impact of deep drilling in the oceanic crust and mantle, *Oceanography (Wash. D.C.)*, *19*, 72–80.

Escartin, J., and M. Cannat (1999), Ultramafic exposures and the gravity signature of the lithosphere near the Fifteen-Twenty Fracture Zone (Mid-Atlantic Ridge, 14°–16.5°N), *Earth Planet. Sci. Lett.*, *171*, 411–424, doi:10.1016/S0012-821X(99)00169-7.

Fox, P. J., E. Schreiber, H. Rowlett, and K. McCamy (1976), The geology of the Oceanographer Fracture Zone: A model for fracture zones, *J. Geophys. Res.*, *81*, 4117–4128.

Fox, P. J., et al. (1985), The geology of the Oceanographer Transform: The transform domain, *Mar. Geophys. Res.*, *7*, 329–358, doi:10.1007/BF00316773.

Francheteau, J., P. Choukroune, R. Hekinian, X. Le Pichon, and H. D. Needham (1976), Oceanic fracture zones do not provide deep sections in the crust, *Can. J. Earth Sci.*, *13*, 1223–1235.

Fujimoto, H., N. Seama, J. Lin, T. Matsumoto, T. Tanaka, and K. Fujioka (1996), Gravity anomalies of the Mid-Atlantic Ridge north of the Kane fracture zone, *Geophys. Res. Lett.*, *23*, 3431–3434.

Fujimoto, H., C. Mevel, M. Cannat, K. Fujioka, T. Gamo, C. R. German, U. Muench, S. Ohta, L. M. Parson, and R. C. Searle (1998), Preliminary Results from the First Submersible Dives on the Southwest Indian Ridge, *Eos Trans. AGU*, *79*, Fall Meet. Suppl., F893.

Gao, D., J. A. Karson, J. R. Delaney, and F. N. Speiss (1998), Computer-aided interpretation of side-looking sonar images from the eastern intersection of the Mid-Atlantic Ridge with the Kane Transform, *J. Geophys. Res.*, *103*, 20,997–21,014.

Gente, P., R. A. Pockalny, C. Durand, C. Deplus, M. Maia, G. Ceuleneer, C. Mével, M. Cannat, and C. Laverne (1995), Characteristics and evolution of the segmentation of the Mid-Atlantic Ridge between 20°N and 24°N during the last 10 million years, *Earth Planet. Sci. Lett.*, *129*, 55–71, doi:10.1016/0012-821X(94)00233-O.

Ghose, I. (1997), Fusion du manteau et cristallisation des roches gabbroiques pres de faille tranformante Kane (Océan Atlantique), Ph.D. thesis, 226 pp, Univ. de Paris VII, Paris, France.

Ghose, I., M. Cannat, and M. Seyler (1996), Transform fault effect on mantle melting in the MARK area (Mid-Atlantic Ridge south of the Kane Transform), *Geology*, *24*, 1139–1142, doi:10.1130/0091-7613(1996)024<1139:TFEOMM>2.3.CO;2.

Grindlay, N. R., P. J. Fox, and K. C. MacDonald (1991), Second-order ridge axis discontinuities in the south Atlantic: Morphology, structure and evolution, *Mar. Geophys. Res.*, *13*, 21–49, doi:10.1007/BF02428194.

Hirauchi, K. (2004), Structural Analysis of Serpentinite in the Jikkoku Pass Area, Northwestern Kanto Mountains, Central Japan, *Eos Trans. AGU*, *85*(47), Fall Meet. Suppl., Abstract T51A–0443.

Hirauchi, K. (2005), Serpentine minerals and their textural changes on solid intrusion tectonics of the Kurosegawa Belt in the northwestern Kanto Mountains, central Japan, *Eos Trans. AGU*, *86*(52), Fall Meet. Suppl., Abstract V51B–1480.

Hirauchi, K. (2006a), Identification of tectonically controlled serpentinite intrusion: Examples from Franciscan serpentinites, Gorda, California, *Eos Trans. AGU*, *87*(52), Fall Meet. Suppl., Abstract T31C–0463.

Hirauchi, K. (2006b), Serpentinite textural evolution related to tectonically controlled solid-state intrusion along the Kurosegawa Belt, northwestern Kanto Mountains, central Japan, *I. Arc*, *15*, 156–164, doi:10.1111/j.1440-1738.2006.00521.x.

Hosford, A., M. Tivey, and T. Matsumoto (1999), The spreading history, segmentation, and crustal structure of the Atlantis Segment, Southwest Indian Ridge, *Eos Trans. AGU*, *80*(46), Fall Meet. Suppl., F956.

Houtz, R., and J. I. Ewing (1979), Acoustic stratigraphy and structure of the oceanic crust, in *Deep Drilling Results in the Atlantic Ocean: Ocean Crust*, edited by M. Talwani et al., pp. 1–14, AGU, Washington, D. C.

Hubbert, M. K., and W. W. Rubey (1959), Mechanics of fluid-filled porous solids and its application to overthrust faulting (Part) 1 of Role of fluid pressure in mechanics of overthrust faulting, *Geol. Soc. Am. Bull.*, *70*, 115–166, doi:10.1130/0016-7606(1959)70[115:ROFPIM]2.0.CO;2.

Jaroslow, G. E., G. Hirth, and H. J. B. Dick (1996), Abyssal peridotite mylonites: implications for grain-size sensitive flow and strain localization in the oceanic lithosphere, *Tectonophysics*, *256*, 17–37, doi:10.1016/0040-1951(95)00163-8.

Karson, J. A. (1990), Seafloor spreading on the Mid-Atlantic Ridge: Implications for the structure of ophiolites and oceanic lithosphere produced in slow-spreading environments, in *Ophiolites: Oceanic Crustal Analogues*, edited by J. Malpas, E. M. Moores, A. Panyiotou, and C. Xenophontos, pp. 547–555, Geol. Surv. Dept., Nicosia, Cyprus.

Karson, J. A. (1998), Internal structure of oceanic lithosphere: A perspective from tectonic windows, in *Faulting and Magmatism at Mid-Ocean Ridges*, edited by W. Buck, P. T. Delaney, J. A. Karson, and Y. Lagabrielle, pp. 177–218, AGU, Washington, D. C.

Karson, J. A. (1999), Geological investigation of a lineated massif at the Kane Transform Fault: implications for oceanic core complexes, *Phil. Trans. R. Soc. London, Ser. A*, *357*, 713–740, doi:10.1098/rsta.1999.0350.

Karson, J. A., and H. J. B. Dick (1983), Tectonics of ridge-transform intersections at the Kane Fracture Zone, *Mar. Geophys. Res.*, *6*, 51–98, doi:10.1007/BF00300398.

Karson, J. A., and H. J. B. Dick (1984), Deformed and metamorphosed oceanic crust on the Mid-Atlantic Ridge, *Contrib. 5648*, pp. 279–301, Woods Hole Oceanogr. Inst., Woods Hole, Mass.

Karson, J. A., and P. J. Fox (1986), Geological and geophysical investigation of the Mid-Cayman Spreading Centre: Seismic velocity measurements and implications for the constitution of layer 3, *Geophys. J. R. Astron. Soc.*, *85*, 389–411.

Karson, J. A., and R. M. Lawrence (1997), Tectonic setting of serpentinite exposures on the western median valley wall of the MARK Area in the vicinity of Site 920, *Proc. Ocean Drill. Program Sci. Results*, *179*, 5–22.

Karson, J. A., and P. A. Rona (1990), Block-tilting, transfer faults, and structural control of magmatic and hydrothermal processes in the TAG area, Mid-Atlantic Ridge 26°N, *Geol. Soc. Am. Bull.*, *102*, 1635–1645, doi:10.1130/0016-7606(1990)102<1635:BTTFAS>2.3.CO;2.

Karson, J. A., and A. T. Winters (1992), Along-axis variations in tectonic extension and accommodation zones in the MARK Area, Mid-Atlantic Ridge 23°N latitude, in *Ophiolites and their Modern Oceanic Analogues*, edited by L. M. Parson, B. J. Murton, and P. Browing, *Geol. Soc. Spec. Publ.*, *60*, 107–116.

Karson, J. A., et al. (1984), The geology of the oceanographer transform: The ridge-transform intersection, *Mar. Geophys. Res.*, *6*, 109–141, doi:10.1007/BF00285956.

Karson, J. A., J. R. Delaney, F. N. Speiss, S. D. Hurst, B. Lawhead, S. Bigger, D. D. Naidoo, and P. Gente (1992), Deep-Tow operations at the eastern intersection of the Mid-Atlantic Ridge and the Kane Fracture Zone, *Eos Trans. AGU*, *73*, Fall Meet. Suppl., F552.

Karson, J. A., M. Cannat, J. Miller, and D. Elthon (Eds.) (1997), *Proceedings of Ocean Drilling Program, Science Results*, 577 pp., Ocean Drill. Progr., College Station, Tex.

Karsten, J., et al. (1999), The northern Chile Ridge revealed: Preliminary cruise report of PANORAMA Expedition Leg 04, *InterRidge News*, *8*, 15–21.

Kelemen, P. B. (1990), Reaction between ultramafic rock and fractionating basaltic magma II. Experimental investigation of reaction between olivine tholeiite and harzburgite at 1150–1050°C and 5 kb, *J. Petrol.*, *31*, 99–134.

Kelemen, P. B., and H. J. B. Dick (1995), Focused melt flow and localized deformation in the upper mantle: Juxtaposition of replacive dunite and ductile shear zones in the Josephine peridotite, SW Oregon, *J. Geophys. Res.*, *100*, 423–438, doi:10.1029/94JB02063.

Kelemen, P. B., G. Hirth, N. Shimizu, M. Speigelman, and H. Dick (1997), A review of melt migration processes in the adiabatically upwelling mantle beneath oceanic spreading ridges, *Phil. Trans. R. Soc. London, Ser. A*, *355*, 283–318.

Kelley, D. S., and G. Früh-Green (2001), Volatile lines of descent in submarine plutonic environments: insights from stable isotopes and fluid inclusion analyses, *Geochim. Cosmochim. Acta*, *65*, 3325–3346, doi:10.1016/S0016-7037(01)00667-6.

Klein, E. M., and C. H. Langmuir (1987), Global correlations of ocean ridge basalt chemistry with axial depth and crustal thickness, *J. Geophys. Res.*, *92*, 8089–8115.

Kuo, B.-Y., and D. W. Forsyth (1988), Gravity anomalies of the ridge-transform system in the South Atlantic between 31 and 34.5°S: Upwelling centers and variations in crustal thickness, *Mar. Geophys. Res.*, *10*, 205–232, doi:10.1007/BF00310065.

Kushiro, I. (1968), Compositions of magmas formed by partial zone melting of the earth's upper mantle, *J. Geophys. Res.*, *73*, 619–634.

Lagabrielle, Y., V. Mamaloukas-Frangoulis, M. Cannat, J.-M. Auzende, J. Honnorez, C. Mével, and E. Bonatti (1992), Vema Fracture Zone (Central Atlantic): Tectonic and magmatic evolution of the Median Ridge and the Eastern Ridge-Transform Intersection Domain, *J. Geophys. Res.*, *97*, 17,331–17,351.

Lagabrielle, Y., D. Bideau, M. Cannat, J. A. Karson, and C. Mével (1998), Ultramafic-mafic plutonic rocks suites exposed along the Mid-Atlantic Ridge (10°N–30°N): Symmetrical-asymmetrical distribution and implications for seafloor spreading processes, in *Faulting and Magmatism at Mid-Ocean Ridges*, edited by W. Buck, P. T. Delaney, J. A. Karson, and Y. Lagabrielle, pp. 153–176, AGU, Washington, D. C.

Lago, B. L., M. Rabinowicz, and A. Nicolas (1982), Podiform chromite ore bodies: A genetic model, *J. Petrol.*, *23*, 103–125.

Leblanc, M., C. Dupuy, D. Cassard, J. Moutte, A. Nicolas, A. Prinzhoffer, M. Rabinovitch, and P. Routhier (1980), Essai sur la genese des corps podiformes de chromitite dans les peridotites ophiolitiques: Etude des chromites de Nouvelle-Caledonie et comparaison avec celles de Mediterranee orientale, *Proc. Int. Ophiolite Symp. Cyprus*, *1979*, 691–695.

le Roex, A. P., H. J. B. Dick, A. M. Reid, and A. J. Erlank (1982), Ferrobasalts from the Spiess Ridge segment of the Southwest Indian Ridge, *Earth Planet. Sci. Lett.*, *60*, 437–451, doi:10.1016/0012-821X(82)90079-6.

Lin, J., and J. Phipps Morgan (1992), The spreading rate dependence of three-dimensional mid-ocean ridge gravity structure, *Geophys. Res. Lett.*, *19*, 13–16.

Lissenberg, J., and H. Dick (2006), Melt-rock reaction in oceanic gabbros and its implications for the genesis of mid-ocean ridge basalt, *Eos Trans. AGU*, *87*(52), Fall Meet. Suppl., Abstract V23E–0695.

Maia, P., and P. Gente (1998), Three dimensional gravity and bathymetric analysis of the mid-Atlantic ridge between 20°N and 24°N: flow geometry and temporal evolution of the segmentation, *J. Geophys. Res.*, *103*, 951–974.

Mamaloukas-Frangoulis, V., J.-M. Auzende, D. Bideau, E. Bonatti, M. Cannat, J. Honnorez, Y. Lagabrielle, J. Malavielle, C. Mével, and H. D. Needham (1991), In situ study of the eastern ridge transform intersection of the Vema Fracture Zone, *Tectonophysics*, *190*, 55–71, doi:10.1016/0040-1951(91)90354-U.

Manning, A. H., and J. M. Bartley (1994), Postmylonitic deformation in the Raft River metamorphic core complex, northwestern Utah: Evidence of a rolling hinge, *Tectonics*, *13*, 596–612.

Matsumoto, T., H. J. B. Dick, and A. B. C. D. E. Cruise (2002), In-situ observation of the lower crust and upper mantle lithology in Atlantis Bank, SWIR: Results from ABCDE Cruise, *Eos Trans. AGU*, *83*(47), Fall Meet. Suppl., Abstract T11A–1239.

Mével, C., M. Cannat, P. Gente, E. Marion, J. M. Auzende, and J. A. Karson (1991), Emplacement of deep crustal and mantle rocks on the west wall of the MARK area (Mid-Atlantic Ridge, 23°N), *Tectonophysics*, *190*, 31–53, doi:10.1016/0040-1951(91)90353-T.

Michael, P. J., C. H. Langmuir, H. J. B. Dick, J. E. Snow, S. L. Goldstein, D. W. Graham, K. Lehnert, G. Kurras, R. Mühe, and H. N. Edmonds (2003), Magmatic and amagmatic seafloor spreading at the slowest mid-ocean ridge: Gakkel Ridge, Arctic Ocean, *Nature*, *423*, 956–961, doi:10.1038/nature01704.

Miranda, E. A., B. E. John, G. Hirth, and H. Dick (2002), Structural development of an oceanic detachment fault system, Atlantis Bank, Southwest Indian Ridge, *Eos Trans. AGU*, *83*(47), Fall Meet. Suppl., Abstract T11A–1234.

Mitchell, N. C., and S. Allerton (1998), Detachment faults at mid-ocean ridges garner interest, *Eos Trans. AGU*, *79*(10), 127, doi:10.1029/98EO00095.

Moore, D. E., and D. A. Lockner (2007), Comparative deformation behavior of minerals in serpentinized ultramafic rock: Application to the slab-mantle interface in subduction zones, *Int. Geol. Rev.*, *49*, 401–415, doi:10.2747/0020-6814.49.5.401.

Morris, E., and R. S. Detrick (1991), Three-dimensional analysis of gravity anomalies in the MARK area, Mid-Atlantic Ridge 23 degrees N, *J. Geophys. Res.*, *96*, 4355–4366, doi:10.1029/90JB02173.

Muller, M. R., C. J. Robinson, T. A. Minshull, R. S. White, and M. J. Bickle (1997), Thin crust beneath ocean drilling program borehole 735B at the Southwest Indian Ridge?, *Earth Planet. Sci. Lett.*, *148*, 93–107, doi:10.1016/S0012-821X(97)00030-7.

Mutter, C. Z., and J. C. Mutter (1993), Variations in thickness of layer 3 dominate oceanic crustal structure, *Earth Planet. Sci. Lett.*, *117*, 295–317, doi:10.1016/0012-821X(93)90134-U.

Natland, J. H. (2002), Magnetic susceptibility as an index of lithology and composition of gabbros, ODP Leg 176, Hole 735B, Southwest Indian Ridge, *Proc. Ocean Drill. Program Sci. Results*, *176*, 69.

Natland, J. H., and H. J. B. Dick (2001), Formation of the lower ocean crust and the crystallization of gabbroic cumulates at a very slow-spreading ridge, *J. Volcanol. Geotherm. Res.*, *110*, 191–233, doi:10.1016/S0377-0273(01)00211-6.

Natland, J. H., H. J. B. Dick, D. J. Miller, and R. P. Von Herzen (Eds.) (2002), *Proceedings of Ocean Drilling Program, Scientific Results* [CD-ROM], Ocean Drill. Program, College Station, Tex.

Nicolas, A. (1986), A melt extraction model based on structural studies in mantle peridotites, *J. Petrol.*, *27*, 999–1022.

Nicolas, A. (1989), *Structures of Ophiolites and Dynamics of Oceanic Lithosphere*, 367 pp., Springer, New York.

O'Hara, M. J. (1968), Are oceanic basalts primary magma?, *Nature*, *220*, 683–686, doi:10.1038/220683a0.

Ohara, Y., T. Yoshida, Y. Kato, and S. Kasuga (2001), Giant megamullion in the Parece Vela backarc basin, *Mar. Geophys. Res.*, *22*, 47–61, doi:10.1023/A:1004818225642.

Okino, K., K. Matusuda, D. M. Christie, Y. Nogi, and K. Koizumi (2004), Development of an oceanic detachment and asymmetric spreading at the Australian-Antarctic Discordance, *Geochem. Geophys. Geosyst.*, *5*, Q12012, doi:10.1029/2004GC000793.

OTTER (Oceanographer Tectonic Research Team) (1984), The geology of the Oceanographer Transform: the ridge-trans-

form intersection, *Mar. Geophys. Res.*, *6*, 109–141, doi:10.1007/BF00285956.
Pockalny, R. A., R. S. Detrick, and P. J. Fox (1988), Morphology and tectonics of the Kane Transform from sea beam bathymetry data, *J. Geophys. Res.*, *93*, 3179–3193.
Pockalny, R. A., A. Smith, and P. Gente (1995), Spatial and temporal variability of crustal magnetization of a slowly spreading ridge; Mid-Atlantic Ridge (20 degrees–24 degrees N), *Mar. Geophys. Res.*, *17*, 301–320, doi:10.1007/BF01203467.
Purdy, G. M., and R. S. Detrick (1986), Crustal structure of the Mid-Atlantic Ridge at 23°N from seismic refraction studies, *J. Geophys. Res.*, *91*, 3739–3762.
Purdy, G. M., and J. Ewing (1986), Seismic structure of the ocean crust, in *The Western North Atlantic Region*, edited by P. R. Vogt and B. E. Tucholke, p. 100, Geol. Soc. of Am., Boulder, Colo.
Purdy, G. M., P. D. Rabinowitz, and H. Schouten (1978), The Mid-Atlantic Ridge at 23°N: Bathymetry and magnetics, *Init. Rep. Deep Sea Drilling Proj.*, *XLV*, 119–128.
Python, M., and G. Ceuleneer (2003), Nature and distribution of dykes and related melt migration structures in the mantle section of the Oman Ophiolite, *Geochem. Geophys. Geosyst.*, *4*(7), 8612, doi:10.1029/2002GC000354.
Quick, J. E. (1981), Petrology and petrogenesis of the Trinity Peridotite, an upper mantle diapir in the Eastern Klamath Mountains, Northern California, *J. Geophys. Res.*, *86*, 11,837–11,863.
Quick, J. E. (1982), The origin and significance of large, tabular dunite bodies in the Trinity Peridotite, Northern California, *Contrib. Mineral. Petrol.*, *78*, 413–422, doi:10.1007/BF00375203.
Reston, T. J., W. Weinrebe, I. Grevemeyer, E. R. Flueh, N. C. Mitchell, L. Kirstein, C. Kopp, and H. Kopp (2002), A rifted inside corner massif on the Mid-Atlantic Ridge at 5°S, *Earth Planet. Sci. Lett.*, *200*, 255–269, doi:10.1016/S0012-821X(02)00636-2.
Schulz, N. J., R. S. Detrick, and S. P. Miller (1988), Two- and three-dimensional inversions of magnetic anomalies in the MARK Area (Mid-Atlantic Ridge 23°N, *Mar. Geophys. Res.*, *10*, 41–57, doi:10.1007/BF02424660.
Searle, R. C., P. Patriat, G. Pouliquen, C. Mevel, K. Tamaki, and FUJI Scientific Team (1998), TOBI Sidescan imagery and magnetics of the Southwest Indian Ridge III: Detailed history and tectonic style of seafloor spreading and detachment faulting, 0–3 Ma, 63°30E–63°56′E (FUJI box 3), *Eos Trans. AGU*, *79*, Fall Meet. Suppl., F855.
Shipboard Scientific Party (1999), Leg 179 summary, in *Proceedings of Ocean Drilling Program, Initial Reports*, vol. 179, edited by T. L. Pettigrew, J. F. Casey, and D. J. Miller, pp. 1–26, Ocean Drill. Program, College Station, Tex.
Shipboard Scientific Party (2004), Leg 209 Summary, in *Proceedings of Ocean Drilling Program, Initial Reports*, vol. 209, edited by P. B. Kelemen, E. Kikawa, and D. J. Miller, pp. 1–139, Ocean Drill. Program, College Station, Tex.
Stakes, D., C. Mével, M. Cannat, and T. Chaput (1991), Metamorphic stratigraphy of Hole 735B, *Proc. Ocean Drill. Program Sci. Results*, *118*, 153–180.
Stroup, J. B., and P. J. Fox (1981), Geologic investigations in the Cayman Trough: Evidence for thin oceanic crust along the Mid-Cayman Rise, *J. Geol.*, *89*, 395–420.
Tolstoy, M., A. J. Harding, and J. A. Orcutt (1993), Crustal thickness on the Mid-Atlantic Ridge: Bull's-eye gravity anomalies and focused accretion, *Science*, *262*, 726–729, doi:10.1126/science.262.5134.726.
Tucholke, B. E., and J. Lin (1994), A geological model for the structure of ridge segments in slow-spreading ocean crust, *J. Geophys. Res.*, *99*, 11,937–11,958, doi:10.1029/94JB00338.
Tucholke, B. E., and H. Schouten (1988), Kane Fracture Zone, *Mar. Geophys. Res.*, *10*, 1–39, doi:10.1007/BF02424659.
Tucholke, B. E., J. Lin, and M. C. Kleinrock (1996), Mullions, megamullions, and metamorphic core complexes on the Mid-Atlantic Ridge, *Eos Trans. AGU*, *77*, Fall Meet. Suppl., F724.
Tucholke, B. E., J. Lin, and M. C. Kleinrock (1998), Megamullions and mullion structure defining oceanic metamorphic core complexes on the Mid-Atlantic Ridge, *J. Geophys. Res.*, *103*, 9857–9866.
Tucholke, B. E., K. Fujioka, T. Ishitara, G. Hirth, and M. Kinoshita (2001), Submersible study of an oceanic megamullion in the central North Atlantic, *J. Geophys. Res.*, *106*, 16,145–16,161, doi:10.1029/2001JB000373.
White, R. S., R. S. Detrick, M. C. Sinha, and M. H. Cormier (1984), Anomalous seismic crustal structure of oceanic fracture zones, *Geophys. J. R. Astron. Soc.*, *79*, 779–798.
White, R. S., D. McKenzie, and R. K. Onions (1992), Oceanic crustal thickness from seismic measurements and rare earth element inversions, *J. Geophys. Res.*, *97*, 19,683–19,715, doi:10.1029/92JB01749.
Whitehead, J. A., Jr., H. J. B. Dick, and H. Schouten (1984), A mechanism for magmatic accretion under spreading centres, *Nature*, *312*, 146–148, doi:10.1038/312146a0.
Williams, C. M. (2007), Oceanic lithosphere magnetization: Marine magnetic investigations of crustal accretion and tectonic processes in mid-ocean ridge environments, Ph.D. thesis, 285 pp, Mass. Inst. of Technol., Woods Hole Oceanogr. Inst., Woods Hole, Mass.